Baharak Sajjadi*, Wei-Yin Chen and Nosa O. Egiebor[a]

A comprehensive review on physical activation of biochar for energy and environmental applications

https://doi.org/10.1515/revce-2017-0113
Received November 26, 2017; accepted May 7, 2018

Abstract: Biochar is a solid by-product of thermochemical conversion of biomass to bio-oil and syngas. It has a carbonaceous skeleton, a small amount of heteroatom functional groups, mineral matter, and water. Biochar's unique physicochemical structures lead to many valuable properties of important technological applications, including its sorption capacity. Indeed, biochar's wide range of applications include carbon sequestration, reduction in greenhouse gas emissions, waste management, renewable energy generation, soil amendment, and environmental remediation. Aside from these applications, new scientific insights and technological concepts have continued to emerge in the last decade. Consequently, a systematic update of current knowledge regarding the complex nature of biochar, the scientific and technological impacts, and operational costs of different activation strategies are highly desirable for transforming biochar applications into industrial scales. This communication presents a comprehensive review of physical activation/modification strategies and their effects on the physicochemical properties of biochar and its applications in environment-related fields. Physical activation applied to the activation of biochar is discussed under three different categories: I) gaseous modification by steam, carbon dioxide, air, or ozone; II) thermal modification by conventional heating and microwave irradiation; and III) recently developed modification methods using ultrasound waves, plasma, and electrochemical methods. The activation results are discussed in terms of different physicochemical properties of biochar, such as surface area; micropore, mesopore, and total pore volume; surface functionality; burn-off; ash content; organic compound content; polarity; and aromaticity index. Due to the rapid increase in the application of biochar as adsorbents, the synergistic and antagonistic effects of activation processes on the desired application are also covered.

Keywords: biochar; electrochemical activation; gaseous activation; physical activation; plasma activation; thermal activation; ultrasound activation.

1 Introduction

Biochar, a low-cost carbon-rich material, is produced from the thermal decomposition of (waste) biomass, such as wood chips, manure, and crop residue in the absence of oxygen or under oxygen-limited conditions. Biochar (BC) is also a solid byproduct in the production of high-energy-density fuels, including bio-oil and biogas. Raw chars produced from the pyrolysis of biomass, coal, and lignite in an inert gas contain clusters of four to six parallel graphene and graphitic oxide sheets that comprise the backbone of these materials (Figure 1), as illustrated in Franklin (1951) and Hammes and Schmidt (2009).

Thermochemical conversion of biomass in anoxic or oxygen-limited conditions results in the production of a mixture of solid (BC), liquid (bio-oil), and gas (syngas) (Mohan et al. 2006). Not only the distribution (volume fraction) of these phases but also their properties depend on the process conditions as well as the biomass source. Hence, different thermal decomposition processes have been defined and employed so far, as summarized in Table 1. The lowest range of temperature (200–300°C) belongs to the torrefaction, also named as mild pyrolysis, which is normally used to improve biomass properties rather than BC production (Tumuluru et al. 2011, Chen et al. 2015). In other words, the solid produced by torrefaction still contains some volatile organic compounds and hence has the properties between BC and raw biomass. In pyrolysis, biomass is heated up to temperatures generally between 300 and 800°C, in which

[a]Formerly with Chemical Engineering Department, School of Engineering, University of Mississippi, 134 Anderson Hall, Oxford, MS 38677-1848, USA
***Corresponding author: Baharak Sajjadi,** Department of Chemical Engineering, University of Mississippi, University, MS 38677, USA, e-mail: bsajjadi@olemiss.edu
Wei-Yin Chen: Department of Chemical Engineering, University of Mississippi, University, MS 38677, USA
Nosa O. Egiebor: Environmental Resources Engineering Department, College of Environmental Science and Forestry (ESF), 206 Bray Hall, Syracuse, NY 13210, USA

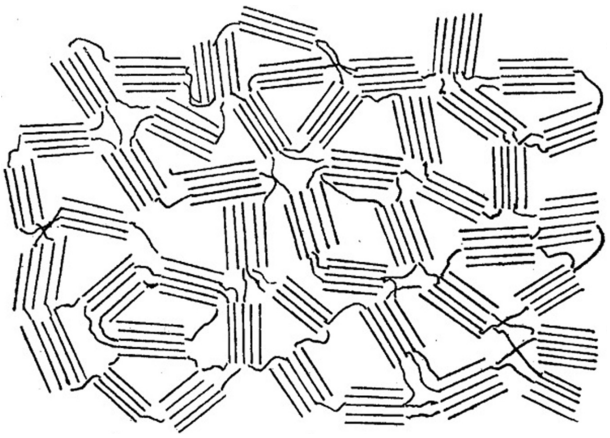

Figure 1: Postulated structures of chars derived from nongraphitic coal (Franklin 1951), copyright license no. 4307130512402, The Royal Society.

the maximum temperature, heating rate, and residence time determine the desired procedure (slow, fast, and flash pyrolysis). The highest quantity of BC is produced through slow and flash pyrolysis, while condensable liquid makes the major product of fast pyrolysis. Gasification needs the highest temperature and a limited quantity of oxygen. In this process, biomass is partially burnt and most of the organic materials are converted to syngas along with small fractions of BC. The wet pyrolysis of the biomass-water mixture under elevated pressure at temperatures between 180 and 400°C is also named as hydrothermal carbonization. Most of the organic materials in this process are converted to solid particles (hydrochar) and liquid (bio-oil mixed with water), while the amount of gas produced is very small.

1.1 BC characteristics

1.1.1 Elemental content

BCs usually contain carbon (C) (40–70%), oxygen (O) (10–45%), hydrogen (H) (1–5%), nitrogen (N) (0–3%), sulfur (S) (<1%), and other trace elements. The O/C value represents the quantity of superficial polar functional groups and the hydrophilicity of BC, whereas the H/C value indicates the aromatization of the organic structure (Fang et al. 2014, Han et al. 2017). During pyrolysis, under increasing temperature, the higher degree of carbonization reduces the atomic ratios of H/C, O/C, and N/C, followed by a reduction in the abundances of carboxylic, hydroxyl, and amino groups. Different elements of BC are (usually) determined by dry combustion,

Table 1: Typical thermal processes and product properties for biochar production.

Conversion type	Operating temperature	Process duration	Heating rate	Product distribution			Solid proximate analysis				Reference
				Solid	Liquid	Gas	Moisture	VM	Ash	Fixed C	
Torrefaction (no oxygen)	200–300	10–120 min	<1	30–85	0	10–60	0–1	50–89	0.5–10	13–50	Bach et al. (2016), Chen et al. (2017), Spokas et al. (2012), Bamdad et al. (2017)
Slow pyrolysis (carbonization) (no oxygen)	300–700	Hours–days	1–100	15–40	20–55	15–60	0–5	5–20	2–10	40–90	Rajapaksha et al. (2016), Gogoi et al. (2017), Qambrani et al. (2017), Zhang et al. (2017), Spokas et al. (2012), Bamdad et al. (2017)
Fast pyrolysis (no oxygen)	450–550	<1 min	>1000	10–35	50–70	5–30	0–5	40	30	40–60	Cha et al. (2016), Qambrani et al. (2017), Spokas et al. (2012), Bamdad et al. (2017)
Flash pyrolysis (no oxygen)	300–800	<2 s	>1000	12–40	–	60–70	0–5	5–26	0–40	40–60	Cha et al. (2016), Qambrani et al. (2017), Spokas et al. (2012), Bamdad et al. (2017)
Gasification (partial oxidization)	800–1200	10 s to 1 min	Variable	0–10	5	85–100	n/a	n/a	n/a	n/a	Cha et al. (2016), Qambrani et al. (2017), Spokas et al. (2012), Bamdad et al. (2017)
Hydrothermal carbonization	180–400	1–16 h	n/a	50–80	5–40	2–10	10–40	50–90	5–15	4–10	Cha et al. (2016), Qambrani et al. (2017), You et al. (2017), Spokas et al. (2012), Bamdad et al. (2017)
Microwave assisted pyrolysis	250–600	3 min–4 h	n/a	20–30	0–20	50–70	10–25	20–30	20–25	50–60	Wahi et al. (2017), Spokas et al. (2012), Bamdad et al. (2017)

in which elements such as carbon, hydrogen, nitrogen, and oxygen are converted to simple gasses of CO_2, H_2O, N_2, and CO, respectively. The product gasses are then separated under steady-state conditions and measured as a function of thermal conductivity. The remaining fraction of BC is made of ash that contains Na, Mg, K, Ca, P, and other mineral elements. Mineral elements play key roles in the treatment of wastewater, especially those containing metal compounds (Tan et al. 2017). Depending on biomass feedstock, different quantities of mineral compounds exist in BCs. For example, poultry litter- and swine manure-based BCs generally contain higher K contents (1.6–5.9%) than do BCs from other materials (Komiyama et al. 2013). Apart from feedstock, the concentrations of mineral components are influenced by pyrolysis temperature. BCs produced at higher temperatures are enriched in mineral compounds (Rafiq et al. 2016). However, water-soluble concentrations of mineral components behave differently from their total concentrations. Generally, water-soluble concentrations of mineral compounds increase with synthesis temperature up to 200°C, but a further increase in temperature decreases this portion of mineral compounds, which is due to the increased crystallization (Li et al. 2017).

1.1.2 Functional groups

The properties of BC and the reaction mechanisms of the charring processes are closely related to functional groups, mainly oxygen-containing groups (Tables 2 and 3). The oxygen complexes include carboxylic, hydroxyl, phenolic (hydroxyl), carbonyl, lactone, carboxylic acid anhydride, and cyclic peroxide groups (see, e.g. Cookson 1978 and Figure 2). These surface oxides may exist in the original biomass or be formed either during the pyrolysis or the subsequent activation stage that involves oxidation.

Table 2: Surface functional groups and the corresponding products on temperature-programmed desorption (Chen et al. 2008, Marsh et al. 1997).

Surface functional group	TPD products
Carbonyl	CO
Quinone	CO
Ether	CO
Carboxylic anhydride	CO, CO_2
Lactone	CO_2
Carboxylic acid	CO_2, H_2O
Phenol	CO, H_2O
Intercalated oxygen	CO

Moreover, carboxyl and hydroxyl groups also form salts with metallic cations such as K^+, Na^+, Ca^{+2}, and Mg^{+2} in BC. These salts enhance the BC alkalinity and contribute to the soil cation exchange capacity (Yuan et al. 2011, Xu et al. 2012) when BC is applied as a soil amendment.

The surface oxides can be quantified by titration method (Boehm 1966, 2002), temperature-programmed desorption (TPD) (Calo and Hall 1991), FTIR-PAS, or Fourier transform mid-infrared photoacoustic spectroscopy (Yuan et al. 2011, Xu et al. 2012), and X-ray photoelectron spectroscopy (XPS) (Boehm 1966). In the widely used selective titration method of Boehm, four bases of different strengths, $NaHCO_3$, Na_2CO_3, NaOH, and $NaOC_2H_5$, are used to neutralize oxygen functional groups of different acidities. $NaHCO_3$ neutralizes carboxylic acid functionalities; Na_2CO_3 neutralizes both carboxylic acids and lactones; NaOH neutralizes carboxylic acids, lactones, and phenols; and the groups reacting with $NaOC_2H_5$ but not with NaOH are suggested to be carbonyl (Derry 2001). Desorption of CO, CO_2, and H_2O from char at various temperatures during TPD is another major approach in characterizing surface functional groups (see Tables 2 and 3, and also Cookson 1978, Marsh et al. 1997). While extensive TPD work has been devoted to the characterization of surface oxide below 1000°C, Chen et al. (2008) reported the existence of abundant "stable" surface oxide above 1000°C. Chars oxidized at 1000°C with less than 0.3 s residence time shows CO desorption peaks during TPD at three distinct temperatures: 730, 1280, and 1560°C. The peaks at 730°C are mainly caused by incomplete devolatilization. The peaks at 1280°C mainly represent desorption of stable surface oxides and incomplete devolatilization. Increasing the gas phase oxidants notably increases the amount of stable surface oxides. The broad peaks between 1400 and 1650°C are attributed to the reactions of oxidants decomposed from minerals and carbon in the char.

Oxygen- and nitrogen-containing functional groups on AC have been considered as the major active sites for adsorption (Biniak et al. 1999, Hulicova-Jurcakova et al. 2009, Marsh and Reinoso 2006). Mattson and Mark (Mark and Mattson 1971) and Cookson (1978) reviewed the contributions of surface oxides on BC adsorption behaviors. The unpaired electrons of oxygen (such as carbonyls) and nitrogen enhance the adsorption of polar and polarizable species, through Lewis acid-base (or electron acceptor-donor) interactions. For instance, acidic surface oxides attract water and reduce the adsorption of nonpolar paraffin and many aromatic compounds. However, if acidic oxides on the carbon surface can form stronger hydrogen bonds with other compounds rather than with water, the compound can displace water from the acidic sites.

Table 3: Major surface functional groups in biochar structure as identified by FTIR spectra.

Peaks (cm^{-1})	Chemical bonds	Vibration	Composition
3100–3800	Alcohol/phenol O-H stretch	Stretching	H_2O or alcohols
2800–3000	Alkyl C-H stretch	Stretching	CH_4, alkyl structure
2380–2100	C=O i.e. carbonyl bond group	Stretching	
1700–1760	C=O stretch	Stretching	Aldehyde, ketone, ester, carboxylic acid
1400–1660	C=C stretch	Stretching	Aromatics
1300–1400	Phenol O-H bending	Bending	
1080–1300	C-O stretching C-O-C groups and aryl ethers; phenolic C-O associated with lignin	Stretching Bending	Alkanes, alcohols, phenols, ethers, lipid
980–1080	C-O-C stretching; phosphines and phosphine oxides	Stretching	
550–800	Aromatic C-H bending	Bending	Aromatic

References: Qian et al. (2015), Ahmed et al. (2016), Işıtan et al. (2016), Qambrani et al. (2017).

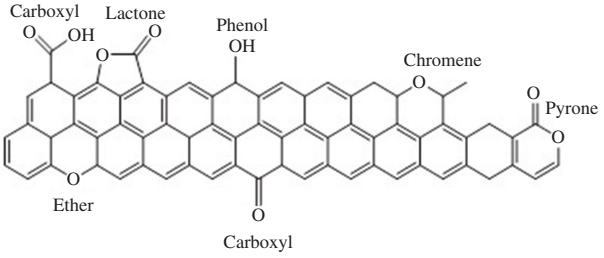

Figure 2: Representative surface functional groups on carbonaceous materials.

Surface acidity is commonly determined by the zeta potential in electrophoretic mobility measurement (e.g. Corapcioglu and Huang 1987, Chiang et al. 2002b). Pyrolysis temperature has profound impacts on the surface functional groups and the properties of BCs (e.g. Cookson 1978). Carbons produced at high temperatures, or the H-type, tend to be hydrophobic, adsorb acids in water, and exhibit positive charges in the electrophoretic mobility measurement. On the contrary, carbons produced at low temperatures, or the L-type, tend to be hydrophilic, adsorb bases in water, and exhibit negative charges in the electrophoretic mobility measurement. These properties have fundamental importance on the behaviors of activated carbon.

1.1.3 Surface charge and pH

Surface charge and pH are the other important characteristics of BCs. The analysis between functional groups, pyrolysis temperature, and BC properties demonstrated that BC pH increases with pyrolysis temperature. In other words, high-temperature pyrolysis produces alkaline BCs, whereas low-temperature pyrolysis yields acidic BCs. Two reasons suggest this phenomenon: first, the loss of acidic functional groups during pyrolysis at high temperatures, and second, the increase in ash content with temperature. Both the loss of acidic groups and high contents of alkali and alkaline earth metals in ash give alkaline characteristic to BC (Jung and Kim 2014). Surface charge is the difference between the electrical potential of the inner and outer surface of a particle in a solution. The net surface charge density is easily measured by acid-base titration (Lützenkirchen et al. 2012). The surface charge of a particle is strongly affected by the solution pH. The point of zero charge (pH_{PZC}) refers to the pH at which the net charge of BC surface is zero. When solution pH is lower than pH_{PZC}, the BC is positively charged, and when solution pH is higher than pH_{PZC}, the BC is negatively charged. In the former, BC binds metal anions such as $HCrO_4^-$ and $HAsO_4^{2-}$, while in the latter, it binds to metal cations such as Hg_2^+, Pb_2^+, and Cd_2^+. It should be noted that the quantity of oxygen-containing groups that can be negatively charged is reduced at higher temperatures, increasing the surface charge. Klüpfel et al. (2014) demonstrated that BC produced from pyrolysis in temperatures from 400 to 700°C possessed the potentiality to donate or accept up to 2 mmol electrons per gram. The electron accepting moieties increase with temperature. The authors therefore proposed environmental engineering applications (as redox-active organic phases) that required controlled electron transfer redox reactions. Saquing et al. (2016) recently reported such redox reactions to facilitate abiotic and microbial transformation. In their work, chemically or biotically reduced BC served as an electron donor to reduce nitrate to N_2 while air-oxidized BC served as an electron acceptor facilitating acetate oxidation. On the basis of nitrate reduction and acetate oxidation, the bioavailable (to the bacterium *Geobacter metallireducens*, GS-15) electron storage capacities of the BC were estimated

to be 0.87 and 0.85 mmol e-/g, respectively, comparable to the capacities of a natural organic electron acceptor and donor such as humic acid (HA).

1.1.4 Surface area and porosity

Surface area and porosity as the major physical properties directly affect the sorption capacity. Gas adsorption analysis is commonly used for porosity and surface area measurements. In this process, solid material is exposed to vapors or gases at a variety of conditions. Analysis of either the weight uptake or the sample volume provides information regarding the physical characteristics of the solid, including skeletal density, porosity, total pore volume, and pore size distribution. Nitrogen and carbon dioxide are generally employed as the probe molecules.

Surface area and porosity are influenced by BC feedstock, pyrolysis temperature, and the activation process (Figure 3). The dehydration process due to water loss during pyrolysis generates pores of different sizes, which can be categorized into three levels, namely, nano (<0.9 nm), micro (<2 nm), and macro (>50 nm). Regardless of their charges or polarity, BC with a small pore size cannot trap large sorbate. Larger pore size and the subsequent larger surface area are obtained at higher pyrolysis temperatures. In terms of the effect of feedstock compositions, microporous structures have mainly been observed in BCs produced from cellulose-enriched biomass (e.g. husks), while biomass with a high quantity of lignin (e.g. bamboo and coconut shell) yields a predominantly macroporous-structured BC. Moreover, the surface area and porosity of biosolid and manure BC are much smaller than those of plant BC, which is due to the lower C content of animal-waste-derived BCs compared with plant-derived BC (Qiu et al. 2014). Aside from this, BC origin significantly affects the surface morphology of BC, its subsequent application, and its efficiency. Scanning electron microscopy and electron dispersive X-ray analysis techniques provide us a direct way to observe the surface structure of BC (Feng et al. 2017a,b). Surface area,

Figure 3: Growing of micropores and mesopores under steam activation process.

aromatic carbonaceous skeleton, mineral compounds, surface charge, and various polar functional groups are the key physicochemical characteristics of BC. The application and efficiency of BC (soil amendment, contaminant adsorption, CO_2 capture, etc.) depend on its origin and thermal history; however, it is often limited by the functional groups. Hence, BC produced from pyrogenic processes is often activated to form functional groups on it or to increase its specific surface area, pore fraction, and pore size distribution. Physical and chemical activation are the two common modification methods prior to use of BC. The objective of this review is to provide a comprehensive, updated view on the physical activations of BC through gaseous modification by H_2O, CO_2, air, and O_3; thermal modification by conventional heating and microwave irradiation; and the most recent methods involving ultrasound, plasma, and electrochemical modifications. Our review on the chemical activation and modification of BC will soon appear as a sequel.

2 Physical activation of BC

Physical activations of carbonaceous materials include a sequence of processes (Marsh and Reinoso 2006). The two most important steps in these processes are carbonization and activation. Partial carbonization (pyrolysis) of biomass and complete carbonization of BC are usually conducted in an inert gas atmosphere with temperatures between 600 and 900°C. In commercial and laboratory production, raw BC is often produced in flue gas or oxygen-limited gas. Carbonization removes the noncarbon species and produces a BC with a high percentage of carbon. Raw BC is then activated with the primary objective of increasing the internal surface area via partial gasification of the carbon skeleton. This objective is usually achieved by applying thermal treatment in a partial oxidizing medium (e.g. steam, CO_2, ozone, and limited air) or an inert agent (He or N_2). These methods are simple but energy intensive since they normally need high temperature. Hence, activation by microwave, ultrasound irradiation, plasma treatment, and electrochemical modification methods has recently emerged to improve BC characteristics such as adsorption capacity at a reasonable cost.

2.1 Gaseous activation

In physical activation using an oxidizing agent, also named as "gaseous activation," BC is exposed to a desired

volume of either steam, ozone, carbon dioxide, or air at temperatures usually above 700°C. These oxidizing agents penetrate into the internal structure of char and gasify the carbon atoms, which results in opening and widening of inaccessible pores (Dalai and Azargohar 2007). BCs activated in such oxidizing environments not only have higher internal surface areas but also abundance of oxygen functional groups that often serve as active sites for adsorption. The mechanisms of these activation methods are investigated in the next sections. Note that in all reactions, a free active carbon site and a surface complex are designated by C_f and C(n), respectively, where n is the type of complex.

$C_f + H_2O \rightarrow C(O) + H_2$	$\Delta H_r^0 = 131\ kj \cdot mol^{-1}$	Chemisorption	(1)
$C(O) \rightarrow CO + C_f$	–	Scavenging of surface oxide by CC	(2)
$CO(g) + C(O) + CO_2(g) + C_f$	–	Carbon gasificatio	(3)
$CO + H_2O \rightarrow CO_2 + H_2$	$\Delta H_r^0 = -41\ kj \cdot mol^{-1}$	Shift reaction	(4)
$C_f + 2H_2O \rightarrow CO_2 + 2H_2$	–	Carbon gasification by water	(5)
$C_f + CO_2 \rightarrow 2CO$	$\Delta H_r^0 = 171\ kj \cdot mol^{-1}$	Carbon gasification by carbon dioxide	(6)
$C_f + 2H_2 \rightarrow CH_4$	$\Delta H_r^0 = -74.5\ kj \cdot mol^{-1}$	Carbon gasification by hydrogen	(7)
$CH_4 + H_2O \rightarrow CO + 3H_2$	$\Delta H_r^0 = 208\ kj \cdot mol^{-1}$	Carbon gasification by hydrogen	(8)

2.1.1 Steam activation

Compared with the other activating gases, steam and carbon dioxide are the most commonly used ones for either pyrolysis of biomass or physical activation of BC. It should be noted that steam and CO_2 can also be used during pyrolysis of biomass. The presence of steam or CO_2 in the pyrolysis of biomass increases the rate of thermal conversion of biomass by means of two hierarchical steps: i) homogeneous and ii) heterogeneous. The homogeneous reaction between volatile organic compounds from pyrolysis and steam or CO_2 reduces the amount of tar formed during pyrolysis, thereby increasing the production of syngas at high temperatures. The heterogeneous reaction between the surface of the biomass and the gasifying agent increases the pyrolysis atmosphere and affects the chemical functional groups on BC surface. Also, this process can be applied to produce a high-quality bio-oil from fast pyrolysis of biomass (Lee et al. 2017).

In terms of activation of BC, steam or CO_2 can be injected either at the end of the pyrolysis process or a separated activation can be applied to the synthesized BC. The smaller size of water molecule compared with CO_2 facilitates the activation by using steam. Unlike air activation, the reaction between steam and carbon is an endothermic process, which is easier to control and is better suited for gasifying carbons with high surface activity. Thus, BC in this process is normally imposed to superheated steam (800–900°C) for 30 min to 3 h (Demiral et al. 2011, Girgis et al. 2011, Han et al. 2013). The overall reaction between carbon and steam includes chemisorption of water, carbon gasification, water shift, and gasification by steam, CO_2, and hydrogen. The generally accepted mechanism of BC activation using steam is described in reactions 1–8 (R1–R8) as below (Lussier et al. 1998):

The process starts with the exchange of oxygen from the water molecule to the carbon surface to create a surface oxide (R1), which may be devolved as CO (R2). CO may increase the rate of gasification by scavenging the surface oxide to produce CO_2 (R3). The process is followed by a water-gas shift reaction in which water vapor is broken down to CO_2 and hydrogen gas (R4), which may activate the surface by R6 or R7, respectively. The heterogeneous and endothermic gas-solid reactions (R1 and R6) play a key role in noncondensable gas formation, while the equilibrium of gaseous homogeneous reactions (R4 and R8) defines the final composition of noncondensable gases (Sattar et al. 2014, Ferreira et al. 2017). On the other hand, H_2 can inhibit carbon gasification. Huttinger (Hermann and Hüttinger 1986) introduced three possible mechanisms by which hydrogen may inhibit the steam gasification:

$C_f + \frac{1}{2}H_2 \leftrightarrow C(H)$	Dissociative hydrogen adsorption	(9)
$C(O) + H_2 \rightarrow C_f + H_2O$	Reverse oxygen exchange	(10)

$C_f + H_2 \leftrightarrow C(H)_2$ Scavenging of surface oxide by H_2 (11)

Through the aforementioned reactions, the produced hydrogen reacts with the carbon surface and block and deactivate the active sites, yielding a surface hydrogen complex (R9–11) (Lussier et al. 1998). It should be noted that hydrogen adsorbed onto carbon surfaces requires temperatures up to 1500°C to completely desorb. More details about the hydrogen sorption on graphite at elevated temperatures are available in Redmond and Walker (1960).

The procedure of pore formation in steam activation is closely and mainly related to the water-gas shift reactions and the depletion of carbon (Rajapaksha et al. 2015). Steam activation also improves the porous structure of BC by removing the trapped products (e.g. some acids, aldehydes, ketones, or particular constituents of the biomass; Santos et al. 2015) as a result of incomplete combustion during pyrolysis. Thus, unlike carbon dioxide, which forms and widens micropores, steam develops both micropores and mesopores and produces a wider range of pore size distribution (Dalai and Azargohar 2007, Feng et al. 2018).

Three parameters, including activation temperature (T), the mass ratio of steam to char (S/C), and activation time (t), play the key roles in steam activation. In general, the volume/radius of pores and surface area increase with steam temperature and treatment time, due to further removal of carbon atoms from the carbon surface (Table 4). The trend of increments is more significant at higher temperatures. It has also been reported that high-temperature steam activation mostly compensates the negative effect of low-temperature pyrolysis on BC porosity and its surface area (Kołtowski et al. 2016). For instance, specific surface area (SSA) enhancement is up to almost 6 times its initial value at a lower temperature, while it reaches 76 times its value in the original BC at higher steam temperature. However, reduction in surface area has also been observed in some cases activated with low-temperature steam (Rajapaksha et al. 2015). The greatest reactivity of H_2O-activated BC was observed in activating temperatures from 700 to 800°C as per Table 4 and Feng et al. (2017b,c). In such temperatures, the changes in BC structures (i.e. aromatic structure and surface oxygen-containing groups) and the alkali and alkaline earth metallic (AAEM) species in BC would contribute to the reactivity of H_2O-activated BC (H_2O-ABC). In short, the reactivity of BC depends on the balance between the accumulation of AAEM species, which has catalytic effects, and the BC structure. Highly condensed/graphitized aromatic structures have lower activity. By increasing the temperature under H_2O activation up to 700°C, the accumulation of AAEM species (even clusters) on the surface, along with the removal of carbonaceous matter, increases the BC reactivity. The highest content of AAEM along with the well-developed structures of BC is observed at 800°C. In temperatures between 700 and 800°C, the H radicals penetrate deep into the BC structure to initiate/enhance the ring condensation reactions; meanwhile, the AAEM species agglomerate and enlarge their particle size. Reactivity then decreases with a further increase in activation temperature under H_2O due to the effect of temperature on physical structure. At temperatures above 800–850°C during activation with H_2O, the small aromatic ring structures are gradually consumed; hence, BC becomes more ordered so that less reactive structures are generated. It should also be noted that AAEM species improve O-containing groups at the beginning of gasification and they are gradually consumed as the carbon conversion increases, resulting in a decrease in reactivity. Although a higher temperature of steam (up to 800°C) demonstrates positive results on the physicochemical properties of BC, a longer duration of activation (>45–60 min depends on the BC origin) with steam imposes negative effects on those characteristics. In longer duration at high temperatures, which would allow faster and more gasification to occur, overactivation can happen. In such situation, pores are developed, while on the other hand, walls begin to collapse, and thus, pore sizes exceed the desired size for adsorption. In short, micropores are converted to mesopores and macropores and the volume fraction of micropores decreases (Fan et al. 2004). Longer duration also leads to a lower total surface area and higher ash content in BC. In terms of steam flow at low temperatures, no significant improvement on pore size distribution has been reported by a higher steam flow. The increase in steam flow yields more water vapor on the particles' outer surface, resulting in mass loss and/or the creation of macropores. The reason is that the steam on the internal portions of the carbon is diluted by the inhibiting factors produced by gasification (CO and H_2), thus leaving the highest concentrations of pure steam on the external surface of the particle, which would lead to external gasification rather than internal. This is known as dilution theory (Martín-Gullón et al. 1996, Arriagada et al. 1997). However, an increase in the volume of mesopores with the steam flow is observed at higher temperatures. This observation was explained by Rodríguez-Reinoso et al. (1995) by noting that at higher temperatures, where the gas-water shift is less efficient, the inhibiting effect of hydrogen is less effective. Thus, an increase in the oxidant concentration would yield an increase in oxidation without a significant effect on hydrogen inhibition.

Table 4: Effects of steam modification on physicochemical properties of biochar (numbers in parentheses refer to activated biochar).

Biochar source	Pyrolysis temperature (°C), time (h)	Steam temperature (°C), time (h)	pH	S_{BET} (m^2/g)	S_{micro} (m^2/g)	V_{micro} ($cm^3\ g^{-1}$)	V_{meso} ($cm^3\ g^{-1}$)	$V_{P\ (total)}$ ($cm^3\ g^{-1}$)	Ash	R_p (nm)	C	H	N	O	Reference
Burcucumber plants	300, 2	300, 0.75	10.8 (11.1)	2.28 (0.85)	–	–	–	0.006 (0.004)	13.5 (25.4)	3.6 (3.1)	66.0 (68.1)	5.55 (5.11)	5.08 (5.1)	23.1 (21.4)	Rajapaksha et al. (2015)
Burcucumber plants	700, 2	700, 0.75	12.32 (11.7)	2.31 (7.10)	–	–	–	0.008 (0.038)	43.7 (70.7)	6.8 (8.4)	69.4 (50.5)	1.3 (1.7)	4.6 (2.5)	24.5 (44.9)	Rajapaksha et al. (2015)
Wheat straw	650, 1.3	800, –	9.9 (8.8)	26.3 (246)	10.8 (140)	0.0046 (0.06)	–	0.026 (0.159)	–	1.95 (1.0)	–	–	–	–	Kołtowski et al. (2016)
Coconut	650, 1.3	800, –	8 (7.2)	3.1 (627)	2.3 (472)	0.0087 (0.21)	–	0.0009 (0.336)	–	0.6 (0.85)	–	–	–	–	Kołtowski et al. (2016)
Willow	650, 1.3	800, 1	9.1 (8.2)	11.4 (840)	4.5 (509)	0.0016 (0.22)	–	0.006 (0.576)	7.7 (20.5)	1.08 (1.09	69.9 (56.9)	2.08 (0.59)	1.13 (0.37)	19.1 (21.7)	Kołtowski et al. (2017a)
Broiler litter manure	350, 1	800, 0.75	–	59 (335)	0 (276)	0 (0.134)	–	–	–	–	45.6 (30.4)	4 (1.14)	4.5 (1.85)	–	Uchimiya et al. (2010)
Broiler litter manure	700, 1	800, 0.75	–	94 (335)	41 (278)	0.018 (0.136)	–	–	–	–	46 (29.1)	1.42 (1.14)	2.8 (1.72)	–	Uchimiya et al. (2010)
Broiler litter	700, –	800, 0.25–0.75		↑↓ with time	↓ with time	↓ with time	–	–	–	–	–	–	–	–	Lima and Marshall (2005)
		Flow: 1–5 ml/min		↑↓ with time	↓ with flow	↓ with flow									
Broiler cake	700, –	800, 0.25–1		↑↓ with time	↓ with time	↓ with time	–	–	–	–	–	–	–	–	Lima and Marshall (2005)
		Flow: 1–5 ml/min		↑↓ with time	↓ with flow	↓ with flow									
Rice husk	700, 2	700, 0.75	9.9 (9.5)	52 (223)	–	–	–	0.04 (0.08)	39.2 (45.6)	4.8 (14.9)	–	–	–		Herath et al. (2016)
Tea waste	300, 2	300, 0.75	7.9 (8.6)	2.3 (1.5)	–	–	–	0.006 (0.004)	5.7 (6.4)	1.14↑	70.0 (71.5)	5.2 (4.75)	5 (5.5)	19.6 (18.2)	Rajapaksha et al. (2014)
Tea waste	700, 2	700, 0.75	11 (10.5)	342 (576)	–	–	–	0.022 (0.109)	10.9 (16.7)	1.08↑	85 (82.4)	1.98 (2.06)	3.92 (3.89)	8.9 (11.6)	Rajapaksha et al. (2014)
Giant Miscanthus	500, 1	800, –	–	181 (322)	–	–	–	–	–	–	80.9 (82.1)	2.8 (2.67)	0.29 (0.31)	12.2 (11.0)	Shim et al. (2015)
Porphyra tenera	500, 1	700, 1	–	ND (22)	–	–	–	ND (0.01)	21.3 (30.7)	ND (12.9)	74.7 (89)	3.0 (1.8)	9.1 (6.6)	9.0 (1.3)	Park et al. (2016)
Enteromorpha compressa	500, 1	700, 1	–	ND (52)	–	–	–	ND (0.021)	43.3 (60)	ND (1.61)	57.6 (79.8)	2.6 (1.6)	5.6 (5.2)	22.4 (0.4)	Kim et al. (2016)
Oat hulls	500, 1.5S	450, 2	–	4.8 (625)	–	↓	↑	–	0 (39.7)[a]	–	–	–	–	–	Fan et al. (2004)
Corn stover	500, 1.5S	450, 1	–	5.8 (442)	–	↓	↑	–	0 (30.5)[a]	–	–	–	–	–	Fan et al. (2004)
		450, 2		5.8 (311)					0 (40.2)[a]						
Olive bagasse	500, –	900, 0.75	–	0.009 (1106)	0.006 (659)	(0.40)	(0.2055)	0.0033 (0.61)	–	–	–	–	–	–	Demiral et al. (2011)
		900, 1		0.009 (915)	0.006 (608)	(0.37)	(0.1011)	0.0033 (0.47)							
Switchgrass	500, 1	800, 0.75	–	3.62 (167.8)	ND (92.3)	ND (0.145)	0.022 (15.41)	–	–	86.5 (15.4)	–	–	–	–	Han et al. (2013)
Hardwood	500, 1	800, 0.75	–	119 (343.9)	67 (318.4)	0.03 (0.0151)	0.046 (15.49)	–	–	17.6 (15.5)	–	–	–	–	Han et al. (2013)
Softwood	500, 1	800, 0.75	–	94.7 (383.7)	63.6 (340)	0.033 (0.196)	0.023 (15.42)	–	–	15.5 (15.42)	–	–	–	–	Han et al. (2013)
Peanut hulls	500, 2	850, 2	7.65 (9)	162 (600)	74 (452)	0.029 (0.181)	0.094 (0.188)	0.158 (0.427)	7.9 (11.6)	25 (14) Å	–	–	–	–	Girgis et al. (2011)
Cottonseed hulls	500, 2	850, 2	7.3 (9.12)	132 (226)	7 (200)	0.008 (0.079)	0.081 (0.084)	0.120 (0.187)	7.3 (10.4)	18 (46) Å	–	–	–	–	Girgis et al. (2011)
Broad Bean hulls	500, 2	850, 2	7.25 (8.76)	105 (225)	29 (107)	0.012 (0.036)	0.084 (0.091)	0.132 (0.156)	9.6 (15.2)	25 (14) Å	–	–	–	–	Girgis et al. (2011)
Soyabean hulls	500, 2	850, 2	7.1 (8.65)	121 (208)	21 (137)	0.023 (0.061)	0.067 (0.067)	0.112 (0.163)	6.7 (9.5)	18 (16) Å	–	–	–	–	Girgis et al. (2011)
Lupine hulls	500, 2	850, 2	7.15 (8.9)	51 (216)	48 (105)	0.045 (0.048)	0.054 (0.103)	0.072 (0.187)	6.6 (10.9)	28 (17) Å	–	–	–	–	Girgis et al. (2011)
Sunflower hulls	500, 2	850, 2	7.35 (8.75)	118 (223)	7 (117)	0.008 (0.054)	0.093 (0.093)	0.134 (0.174)	9.7 (11.5)	23 (16) Å	–	–	–	–	Girgis et al. (2011)
Rice husk	700, 3	700, 0.75	9.9 (10.1)	236.7 (251.5)	–	–	–	0.05 (0.08)	39.2 (45.6)	5.29 (4.86)	50.6 (–)	1.29 (–)	0.65 (–)	7.67 (–)	Mayakaduwa et al. (2016)

In all tables, the values before and after activation are provided outside and inside of parenthesis, respectively. Å, Angstrom.
[a]Burn-off.

Thus, it can be concluded that the steam flow has no effect at lower temperatures, while the rate of steam flow yields an increase in gasification at higher temperatures. More details about the exact effect of temperature and duration are summarized in Table 4.

As an oxidizing agent, steam introduces oxygen-containing functional groups onto the surface of BC. In most cases, phenolic groups and carboxylic groups increase after steam activation, increasing BC hydrophilicity subsequently (Herath et al. 2016, Feng et al. 2017c). A reduction in pH after steam activation suggests the introduction of a more acidic group to the surface of BC. However, high-temperature steam activation (especially after a low-temperature pyrolysis) causes a severe loss of the three categories of surface functional groups: phenolic, carboxylic, and lactonic (Han et al. 2013, Shim et al. 2015, Mayakaduwa et al. 2016). Shim et al. (2015) suggested that the functional groups may have partially been degraded, as indicated by the decrease in the polarity index of BC (produced from miscanthus sacchariflorus) during the thermal activation using steam; however, they are not likely completely eliminated after this process. Fu et al. (2013) demonstrated that the intensities of OH (stretching vibration of hydroxyl at 3200–3500), C-O (stretching at 1043), and C=O (stretching vibration of quinoid structure at 1636) peaks of carbonized black liquor lignin decreased likely due to cracking of the functional groups. Generally, and as expected according to R1–R7, steam-activated BCs contain fewer quantities of carbon, hydrogen, and oxygen in their structure compared with original BCs. Exceptions are mainly those BCs synthesized at low temperatures (300–500°C) (Rajapaksha et al. 2015, Kim et al. 2016, Park et al. 2016). The ratios of C, H, and O after steam activation depend on the process temperature. It can be summarized that the quantity of oxygen functional groups increases with treatment time at lower temperatures, while an opposite trend has been observed at higher temperatures. This is attributed to the degradation of functional groups and the limited replacement of new functional groups at higher temperatures (Arriagada et al. 1997).

The sorption capacity of BCs activated under superheated steam usually increases due to an increase in surface area, micropore volume, and oxygen functional groups; hence, H_2O-ABC can efficiently remove contaminants from soil and water (Table 5). As an example, in terms of heavy metals, it was reported that the steam amendment of carbonaceous matters, regardless of pyrolysis conditions and biomass source, enhanced the immobilization of Cu(II), Ni(II), and Cd(II) in alkaline soil (Uchimiya et al. 2010). The improved sorption capacity of BC to Cu ions was also demonstrated by Shim et al. (2015). However, the success of steam-activated BC to immobilize Cu in soils or removing it from water depends on the conditions used. Longer activation durations or greater steam flow may reduce the Cu sorption capacity of BC. By analyzing four different activation rates (ranging from 15 to 60 min) along with different steam flow rates (ranging from 1 to 5 ml/min), Lima and Marshall (2005) demonstrated that the greatest Cu sorption was obtained when the BC was activated under a specific steam condition (3 ml/min, for 45 min). In order to obtain a higher adsorption capacity, some authors have used chemical activating agents in parallel with the steam flow. For instance, Ippolito et al. (2012) showed the potential of combined KOH- and steam-activated pecan shell BC in the adsorption of Cu ions from wastewaters at pH 6.

In recent years, great attention has also been dedicated to the behavior and life cycle of pharmaceutical compounds, most of which are, by nature, biologically active and hydrophilic, in order that the human body can take them up easily. Moreover, these compounds are persistent and are not degraded easily. Sulfamethazine and ranitidine hydrochloride (RH) are the two examples of pharmaceuticals compounds. Steam-activated BC has shown a significant improvement in adsorption of such compounds due to increased polarity and hydrophilicity. The sorption capacity of sulfamethazine on steam-activated BC showed a great improvement (55%) compared with the nonactivated BC (Rajapaksha et al. 2015), which may be attributed to the enhanced aromaticity and electronegativity of BC after activation. Steam-activated tea waste BC was also successfully used as an adsorbent of sulfamethazine from aqueous solution with the maximum capacity of 33.81 mg/g at pH 3, while the maximum capacities of activated BC under limited oxygen and N_2 were 30.06 mg/g and 7.12 mg/g, respectively (Rajapaksha et al. 2014). Mondal et al. (2016) reported the great sorption of RH (12 mg/g) from aqueous solution by using steam-activated BC. Apart from heavy metals and pharmaceutical compounds, the adsorption capacity of H_2O-ABC has been tested on pesticides too (Yu et al. 2009). It is concluded that steam activation of BC is capable of escalating its adsorption capacity by almost 60%. However, the final results depend on the operating conditions to a large extent. Generally, a steam flow rate between 3 and 5 ml/min with a temperature of between 700 and 800°C for 45–60 min has resulted in the highest adsorption capacity improvement.

2.1.2 CO_2 activation

As already stated, CO_2 can alternatively be used during either the pyrolysis of biomass or the activation of BC.

Table 5: Effects of steam modification on the adsorption capacity of biochar (numbers in parentheses refer to activated biochar).

Biochar source	Pyrolysis temperature (°C), time (h)	Steam temperature (°C), time (h)	Objective	Yield (mg/g)	pH	Reference
Burcucumber plants	300, –	300, 0.75	Sulfamethazine	15.6 (14.7)	5	Rajapaksha et al. (2015)
Burcucumber plants	700, –	700, 0.75	Sulfamethazine	18.8 (32.2)	5	Rajapaksha et al. (2015)
				20 (37)	3	
Tea waste	300, 2	700, –	Sulfamethazine	2.79 (1.88)	5	Rajapaksha et al. (2014)
Tea waste	700, 2	300, –	Sulfamethazine	30.06 (33.81)	3	Rajapaksha et al. (2014)
				26.8 (31)	5	
				26.5 (27.5)	7	
				16.7 (24.6)	9	
Broiler litter manure	700, –	800, 0.75	Cu sorption (S)	$4e^{-5}$ ($4.5e^{-5}$) M	–	Kołtowski et al. (2016), Uchimiya et al. (2010)
			Ni sorption (S)	$0.3e^{-4}$ ($0.5e^{-4}$) M		
			Cd sorption (S)	$1e^{-4}$ ($2.3e^{-4}$) M		
Broiler litter manure	350, –	800, 0.75	Cu sorption (S)	No sorp ($4.5e^{-5}$) M	–	Kołtowski et al. (2016), Uchimiya et al. (2010)
			Ni sorption (S)	$0.5e^{-4}$ ($1e^{-4}$) M		
			Cd sorption (S)	$3e^{-4}$ ($2.5e^{-4}$) M		
Broiler litter	700, –	800, 0.25–1.25 F_{Steam}: 1–5	Cu sorption	(1.4) mM/g	–	Lima and Marshall (2005)
Broiler cake	700, –	800, 0.25–1 F_{Steam}: 1–5	Cu sorption	(1.9) mM/g	–	Lima and Marshall (2005)
Giant Miscanthus	500, 1	600, –	Cu sorption	15.4 (8.87)	–	Shim et al. (2015)
Porphyra tenera	500, 1	700, 1	Cu sorption	(75.1)	–	Park et al. (2016)
Entermorpha compressa	500, 1	700, 1	Cu sorption	33 (137)	5.5	Kim et al. (2016), Rosales et al. (2017)
Mung bean husk	550, 1	650, –	Ranitidine hydrochloride sorption	(12)	–	Mondal et al. (2016)
Rice husk	700, 2	700, 5 ml/min, 0.75	Glyphosate sorption	(123.03)	4	Herath et al. (2016)
Activated carbon	–		Ammonia adsorption	(1.1)	–	Kastner et al. (2009)
Peanut hull char	472, –		Ammonia adsorption	(0.21)	–	Kastner et al. (2009)
Switchgrass	500, 1	800, 0.75	CU (II)	0.023 (0.112) mM/g	7	Han et al. (2013)
			Zn (II)	0.033 (0.138) mM/g	7	
			Phenol	1.15 (2.21) mM/g	–	
Hardwood	500, 1	800, 0.75	CU (II)	0.087 (0.4) mM/g	7	Han et al. (2013)
			Zn (II)	0.29 (0.077) mM/g	7	
			Phenol	1.35 (1.48) mM/g	–	
Softwood	500, 1	800, 0.75	CU (II)	0.053 (0.1) mM/g	7	Han et al. (2013)
			Zn (II)	0.011 (0.068) mM/g	7	
			Phenol	1.22 (1.57) mM/g	–	
Peanut hulls	500, 2	850, 2	MB	19.2 (33.1)	–	Girgis et al. (2011)
Cottonseed hulls	500, 2	850, 2	MB	10.6 (17.3)	–	Girgis et al. (2011)
Broad Bean hulls	500, 2	850, 2	MB	15.8 (20.6)	–	Girgis et al. (2011)
Soyabean hulls	500, 2	850, 2	MB	16.5 (12.0)	–	Girgis et al. (2011)
Lupine hulls	500, 2	850, 2	MB	10.5 (10.1)	–	Girgis et al. (2011)
Sunflower hulls	500, 2	850, 2	MB	14.4 (14.2)	–	Girgis et al. (2011)
Rice husk	700, 3	700, 0.75	Carbofuran	132.9 (160.8)	5	Mayakaduwa et al. (2016)

M, Molarity.

Elemental analysis showed that BC pyrolyzed under CO_2 flow contained more O and N than under N_2, while that produced under N_2 contained more C, H, and S (as per references collected in Table 6). Lower H/C ratio of BC pyrolyzed under CO_2 (PB-CO_2) means a higher degree of carbonization (highly condensed structures), and higher O/C ratios of PB-CO_2 indicate that it might be more hydrophilic than BC pyrolyzed under nitrogen (PB-N_2), as observed in others (Lee et al. 2017). It has also been reported that BC produced under CO_2 contained a much higher content of alkali metals (including Na, K, and Ca) than those pyrolyzed under N_2 atmosphere, especially at

Table 6: Effects of CO_2 modification on the physicochemical properties of biochar (numbers in parentheses refer to activated biochar).

Biochar source	Pyrolysis temperature (°C), time (h)	CO_2 temperature (°C), time (h)	Burn-off	Ash	S_{BET} (m^2/g)	S_{micro} (m^2/g)	V_{micro} (cm^3/g)	V_{meso} (cm^3/g)	V_p (cm^3/g)	R_p (nm)	C (%)	H (%)	N (%)	O (%)	Reference
Oak	500, –	800, 1	27	3.7 (7.1)	107 (786)	–	0.046 (0.328)	0.004 (0.0086)	0.050 (0.337)	–	80.9 (86.1)	2.9 (0.6)	0.5 (0.6)	12 (5.6)	Jung and Kim (2014)
		900, 1	67.1	3.7 (12.1)	107 (807)		0.046 (0.335)	0.004 (0.0099)	0.05 (0.01)		80.9 (85.1)	2.9 (0.4)	0.5 (1.1)	12 (1.3)	
Peat	CO_2-pyrolysis	650, –	–	73.5 (74.9)	85.43 (93.04)	–	–	–	–	–	25.5 (22.9)	0.65 (0.52)	0.57 (1.14)	4.13 (4.38	Lee et al. (2017)
Aspen wood	800, –	800, 0.3	–	–	440 (540)	–	0.17 (0.18)	0.02 (0.09)[a]	–	–	–	–	–	–	Veksha et al. (2016)
H_3PO_4, 500		800, 1.0			440 (690)		0.17 (0.16)	0.02 (0.22)[a]							
		800, 1.8			440 (750)		0.17 (0.22)	0.02 (0.21)[a]							
		800, 3.6			440 (910)		0.17 (0.30)	0.02 (0.19)[a]							
Rice husk	15% V H_2O, 700	–	–	–	–	–	–	–	–	–	86.3 (84.14)	–	0.51 (0.58)	12.5 (14.3)	Feng et al. (2017a)
	29% V CO_2, 700	–									86.3 (85.2)		0.51 (0.5)	12.5 (13.6)	
Willow tree	700, –	CO_2, 800, –	–	–	11.4 (512)	4.5 (380)	0.0016 (0.169)	–	0.006 (0.276)	1.08 (1.08)	–	–	–		Kołtowski et al.
		H_2O, 800, –			11.4 (840)	4.5 (509)	0.0016 (0.224)		0.006 (0.576)	1.08 (1.37)					(2017b)
		MW, 800, –			11.4 (443)	4.5 (259)	0.0016 (0.114)		0.006 (0.242)	1.08 (1.1)					
Oak	500, –	700, 1	31.8	–	92 (642)	–	– (0.27)	–	0.146 (0.41)	–	70.8 (NM)	3.16 (NM)	–	13.2 (NM)	Zhang et al. (2004)
		700, 2	41.8		92 (644)		– (0.24)		0.146 (0.40)						
		800, 1	43.0		92 (845)		– (0.32)		0.146 (0.60)						
		800, 2	51.4		92 (985)		– (0.38)		0.146 (0.64)						
Corn hulls	500, –	700, 1	32.3	–	48 (977)	–	– (0.33)	–	0.058 (0.89)	–	70.3 (NM)	6.97 (NM)	–	16.7 (NM)	Zhang et al. (2004)
		700, 2	37.0		48 (902)		– (0.33)		0.058 (0.82)						
		800, 1	44.4		48 (1010)		– (0.43)		0.058 (0.83)						
		800, 2	45.2		48 (975)		– (0.38)		0.058 (0.68)						
Corn stover	500, –	700, 1	41.5	–	38 (660)	–	– (0.38)	–	0.054 (0.48)	–	59.4 (NM)	3.06 (NM)	–	16.9 (NM)	Zhang et al. (2004)
		700, 2	41.7		38 (432)		– (0.18)		0.054 (0.33)						
		800, 1	42.6		38 (712)		– (0.28)		0.054 (0.54)						
		800, 2	50.2		38 (616)		– (0.23)		0.054 (0.42)						
Aspen wood	600, 0.5	780, 1.66	0 (76)	–	480 (886)	–	0.19 (0.29)	0.01 (0.16)		–	–	–	–	–	Veksha et al. (2015)
Oil palm shell	400–800, 25 min Under MW	600, 450 W	–	–	23 (151)	–	0.009 (0.077)	0.0057 (0.012)	0.015 (0.089)	–	–	–	–	–	Abioye and Ani (2015)
Willow tree	700, low O_2 < 2%	CO_2, 800, 1	–	7.72 (11.3)	11.4 (512)	4.5 (380)	0.002 (0.169)	–	0.002 (0.276)	–	69.9 (70.8)	2.08 (0.7)	1.13 (0.8)	19.1 (16.4)	Kołtowski et al.
		H_2O, 800, 1		7.72 (20.5)	11.4 (840.6)	4.5 (509)	0.002 (0.225)		0.002 (0.577)		69.9 (56.8)	2.08 (0.59)	1.13 (0.4)	19.1 (21.7)	(2017a)
		MW, 200, –		7.72 (15.8)	11.4 (443)	4.5 (258.6)	0.002 (0.114)		0.002 (0.242)		69.9 (73.9)	2.08 (0.95)	1.13 (0.7)	19.1 (8.7)	
Rice straw	700–900, 1, N_2	700, 1	–		280 (490)	–	–	–	–	21.3 Å	–	–	–	–	Yun et al. (2001)
		800, 1		34.2	550 (650)					22.5 Å	53.8 (–)	0.5 (–)	0.6 (–)	45.1 (–)	
		800, 3		–	680 (790) 530					23.9 Å	–	–	–	–	
		800, 6		73.3	(780)					26.2 Å	73.9 (–)	0.2 (–)	0.8 (–)	73.9 (–)	
		900, 1			430 (480)					26.9 Å	–	–	–	–	
Coconut shell	600, 2, N_2	750, 4	–		186 (613)	–	0.043 (0.307)	–	0.268 (0.44)	–	–	–	–	–	Guo et al. (2009)
		900, 4			186 (1391)		0.043 (0.73)		0.268 (0.84)						
		950, 4			186 (1323)		0.043 (0.671)		0.268 (0.88)						
Sewage sludge	–	750, –	17	66.1	13 (62)	–	–	–	0.01 (0.03)	–	24.4 (–)	1 (–)	2.7 (–)	14.9 (–)	Ros et al. (2006)
Olive stone	850, –	850, 1	–	–	349 (677)	–	0.168 (0.29)	–	0.188 (0.34)	–	–	–	–	–	El-Sheikh et al. (2004)
Pistachio-nut	300, 2	900, 0.5	–	1.1 (1.9)	– (361.8)	– (187.1)	– (0.086)	–	– (0.202)	–	–	–	–	–	Lua et al. (2004)
shells	600, 2			1.2 (2.4)	– (699.1)	– (452.0)	– (0.211)		– (0.408)						
	900, 2			2.0 (3.9)	– (748.8)	– (457.8)	– (0.213)		– (0.451)						
Pistachio-nut	500, 1	900, 0.5	–	–	– (637.5)	– (431.3)	– (0.201)	–	– (0.367)	–	–	–	–	–	Lua et al. (2004)
shells	500, 2			1.1 (2.1)	– (778.1)	– (476.9)	– (0.222)		– (0.466)						
	500, 3			–	– (688.3)	– (450.6)	– (0.219)		– (0.39)						

the higher temperatures (700°C) (Tian et al. 2017). Hence, CO_2-assisted pyrolysis process can potentially be used to control the properties of BC for various applications of adsorption and soil amendment.

The mechanism of char (C) activation with CO_2 involves the Boudouard reaction ($C + CO_2 \leftrightarrow 2CO$). In this process, CO_2 undergoes dissociative chemisorption on the carbon surface to form a surface oxide and carbon monoxide as shown in R12. The surface oxide, C(O), is subsequently desorbed from the surface, further developing the pore structure (R13). CO in the gaseous product can also be adsorbed on the carbon active site and retards the gasification (R14).

$$C_f + CO_2 \rightarrow C(O) + CO \quad (12)$$

$$C(O) \rightarrow CO \quad (13)$$

$$C_f + CO \rightarrow C(CO) \quad (14)$$

Thermodynamically, Boudouard reaction is endothermic, and due to its large positive enthalpy (~172 kJ/mol at 298 K), the equilibrium of Boudouard reaction does not favor CO production until temperatures >700°C. Thus, elevated temperatures promote the forward reaction, removing carbon atoms in activated carbon, which results in the increase in burn-off (Jung and Kim 2014). Moreover, similar to steam activation, an increase in the flow of carbon dioxide causes a higher concentration gradient, which compels the oxidant to enter the pores at a faster rate (i.e. bulk diffusion), enhancing the gasification yield. Generally, there are two similarities between steam and CO_2 activation. I) CO formed by Boudouard reaction may remain in the vicinity of the carbon surface to retard further reactions. II) The presence of oxygen in CO_2 increases the formation of O-containing functional groups on the BC surface (Feng et al. 2016). However, more O-containing functional groups are formed on the BC surface by H_2O than CO_2, and hence, H_2O-activated char is usually more active than CO_2-activated char (Feng et al. 2016). This may be attributed to the dimensions of water molecules, which is smaller than CO_2 and therefore facilitates the diffusion of steam into the porous network, inducing a faster reaction rate (Dalai and Azargohar 2007). In activation with CO_2, eliminations of O-H (phenolic at around 3620 cm^{-1}) and C=O (at 1700–1600 cm^{-1}) (Jung and Kim 2014) are normally observed, while a loss of carboxylic (COOH) and an increase in the content of phenolic functional group have been reported during activation with steam (Kołtowski et al. 2017a). This

Table 7: Effects of ozone modification on the physicochemical properties of biochar (numbers in parentheses refer to activated biochar).

Biochar source	Pyrolysis temperature (°C), time (h)	Ozone temperature (°C), time (h)	Burn-off	pH	S_{BET} (m^2/g)	S_{micro} (m^2/g)	V_{micro} (cm^3/g)	V_{meso} (cm^3/g)	V_p (cm^3/g)	R_p (nm)	C (%)	H (%)	N (%)	O (%)	Reference
Grape seed**	800, flash	250, 2	50%	–	47 (900)	–	–	0.03 (0.4)	0.007 (0.04)	1.37 (1.7)	–	–	–	–	Jimenez-Cordero et al. (2015)
		275, 2	75%		47 (1200)			0.03 (0.5)	0.007 (0.06)	1.37 (1.9)					
Peanut hull	500/0.67	Steam/Ozone 23, 0.5	–	5.9 (4.6)	1 (506)	–	–	–	–	–	–	–	–	–	Kastner et al. (2009)
Filtrasorb 400	Commercial	25, 0.16	–	8.8 (6)	1000 (1023)	53.7 (87) Ex	–	0.474 (0.472)	0.019 (0.031)	–	–	–	–	–	Valdés et al. (2002), Valdes et al. (2003)
	–	25, 0.33		8.8 (5.5)	1000 (943)	53.7 (74.8)		0.474 (0.437)	0.019 (0.027)						
		25, 2		8.8 (3.3)	1000 (632)	53.7 (64.4)		0.474 (0.297)	0.019 (0.023)						
Activated carbon	Unknown	NM-1	–	–	1200 (1102)	–	0.481 (0.435)	0.466 (0.423)	–	–	–	–	–	–	Park and Jin (2005)
		NM-2			1200 (1038)		0.481 (0.403)	0.466 (0.390)							
		NM-4			1200 (817)		0.481 (0.324)	0.466 (0.310)							
Carbon black	–	Ambient T	–	–	38.5 (36.7)	–	–	–	–	–	–	–	–	–	Chen et al. (2003)
Carbon black	–	Ambient T, air oxidized	–	–	38.5 (234)	–	–	–	–	–	–	–	–	–	Chen et al. (2003)
Activated carbon	–	– 0.5	–	–	783 (851)	677 (727)	0.367 (0.4)	0.32 (0.344)	–	14.6 (14.67)	86.5 (87.2)	1.69 (1.6)	0.22 (0.2)	10.9 (11.4)	Chiang et al. (2002a)

Cyclic activation (10 rounds) with ozone.
NM, Not mentioned; Ex, external surface area.

point has also been observed in reforming of model tar compounds using thermal cracking reactions. The more O-containing groups on the char surface activated by steam compared with CO_2-activated one, the more acidic centers are formed. The acidic centers can be combined with polyaromatic rings containing negatively charged electrons and activate the thermal cracking reaction (Feng et al. 2016). As another example, CO_2-activated BCs, especially those produced under higher pyrolysis temperature (800°C rather than 700°C), have demonstrated weaker results in adsorption of organic compounds compared to steam-activated ones (Toles et al. 2000). However, the effect of surface area should not be ignored. Consistently higher surface area for steam-activated BC compared with CO_2-activated samples (e.g. almond shell-based BC) has been observed in some published results when the same pyrolysis conditions, activation times, and temperatures had been applied (Toles et al. 2000).

Therefore, although not as significant as steam activation, CO_2 plays a particular role in promoting the surface area and improving the pore structure of BC in temperatures between 700 and 900°C. As an instance, Jung and Kim (2014) applied CO_2 activation under 800°C in three different conditions, including pyrolysis under N_2 followed by CO_2 activation without cooling in between, the same procedure with a cooling step in between, and both pyrolysis and activation under CO_2. The authors demonstrated that all three methods significantly increased the surface area from 249 to almost 720 m^2/g and porosity from 0.11 to ~0.33. Surprisingly, the increase in temperature from 800 to 900°C for 60 min (W/O cooling) remarkably increased these values to 1126 m^2/g and 0.49 cm^3/g. As another example, enhancing activation temperature to 900°C was favorable to the development of Brunauer–Emmett–Teller (BET) surface area (S_{BET}) and micropore volume of BC derived from coconut shells. A further increase in temperature widened the pores and increased the mesopores. In the same way, very long activation time (>4 h) would result in collapsing of pores, and a high flow rate of CO_2 (>400 cm^3/min) would lead carbon to burnout and was unfavorable to the formation of pores (Guo et al. 2009).

Unlike steam activation, which yields a wide distribution of micropores and mesopores, activation with carbon dioxide mainly develops micropores. Generally, having a wide pore size distribution is preferred as mesopores and macropores are responsible for the efficient removal of large molecules. Moreover, larger pore sizes act as "roadways" by which the target molecule can travel to its final adsorption site. But for adsorption of smaller molecules, micropores (high surface areas) are more important (Valderrama et al. 2008). Therefore, the development of a high quantity of micropores by burning of carbon matter in the BC and the simultaneous creation of new microporous structures in CO_2-activated BCs (Kołtowski et al. 2017b) make them a better absorbent for smaller molecules. Kołtowski et al. (2017b) compared the activation of BC using CO_2, steam, and microwave irradiation. They concluded that, although steam activation resulted in a higher surface area, the most effective adsorbents for reducing the concentration of 16 freely dissolved polyaromatic hydrocarbons (PAHs) were those activated under CO_2 rather than steam or microwave. This could be attributed to the higher concentration of micropores with respect to an SSA (74%) and the larger micropore volume with respect to the total pore volume (61%) in samples activated

Table 8: Effects of ozone modification on the adsorption capacity of biochar (numbers in parenthesis refer to activated biochar).

Biochar source (raw biochar)	Pyrolysis temperature (°C)	Ozone temperature (°C), time (h)	Objective	Adsorption (mg/g)	Capacity (mg/g)	Reference
Palm oil shell	500	23, 0.5	Ammonia adsorption	–	1.25	Kastner et al. (2009)
Peanut hull	500	23, 0.5	Ammonia adsorption	–	0.11	Kastner et al. (2009)
	500	23, 1			0.15	
Peanut hull	472/Steam	23, 0.5	Ammonia adsorption	–	0.17	Kastner et al. (2009)
Filtrasorb 400	–	25, 0.16	MB	–	98.8 (92.4)	Valdés et al. (2002)
	–	25, 0.33			98.8 (91.3)	
		25, 2			98.8 (77.3)	
Filtrasorb 400	Commercial	25, 0.5	2-mercaptobenzothiazole	250	170	Valdes et al. (2003)
	–					
Carbon black	–	Ambient T	Surfactant (Darex II)	30[a]	5.5[a]	Chen et al. (2003)
Carbon black	–	Ambient T	Surfactant (SDS)	25[a]	4[a]	Chen et al. (2003)
Carbon black	–	Ambient T	Surfactant (Tergitol)	32[a]	4[a]	Chen et al. (2003)

[a]Unit: 6 × ml surfactant solution/g-carbon.

under CO_2 atmosphere (Kołtowski et al. 2017b). As with gaseous-activation conditions, the nature of the BC plays a key role in activation under CO_2 atmosphere. According to the literature, CO_2 activation has demonstrated better results for those BCs containing higher quantities of C (lower H/C). Zhang et al. performed CO_2 activation on BCs produced from three different agricultural and forest residues. Among them, BCs produced from oak chips and corn hulls gave the highest C contents (70%) and maximum BET surface areas (ranging from 640 to 1010 m^2/g), while corn-stover-produced BC had lower C content (59%) and lower BET surface area values of 400–700 m^2/g (Zhang et al. 2004). CO_2 activation was ineffective for an efficient porosity development in sewage-sludge-based BC containing 31.4% of C (H/C = 15%) (Ros et al. 2006). Longer activation times with CO_2 at higher temperatures have also demonstrated a better effect on increasing the BET surface area and micropore and mesopore volumes of the BCs with lower H/C (Veksha et al. 2016). It has also been reported that gasification agents such as H_2O and CO_2 affect the aromatic rings of BC as well. During this process, the intermediate atoms (from the steam-char or CO_2-char reactions) penetrate into the char matrix, contributing to the transformation of small aromatic ring systems to large ring systems. Therefore, some small aromatic rings in char are removed or consumed, while some large rings become larger. According to Song et al. (2015), the gasification agent has showed a larger effect on the reforming of large aromatic ring systems compared with smaller and isolated aromatics. However, Feng et al. (2018) could catalytically increase the reforming of both large and small aromatic rings. As per their results, the effect of steam was larger than that of CO_2 on both single and multiple rings.

Toles et al. (2000) estimated the cost of carbon-dioxide-activated and steam-activated almond shell carbons for a manufacturing facility with an input of 14,000 kg of shells per day and a carbon yield of 16% for both processes. For such a process, the authors estimated an electricity usage of 7501 and 4075 (KWH/day) for carbon-dioxide- and steam-activation processes, respectively. Moreover, the cost differential between water and carbon dioxide gas is the other factor that makes steam activation considerably cheaper than carbon dioxide activation.

2.1.3 Ozone activation

Ultraviolet (UV) excitation of O_2 at 242 nm generates gaseous ozone, O_3, which involves the photodissociation of O_2 followed by collisions of an oxygen atom with an O_2 and a third body, either O_2 or N_2. O_3 decomposes to O_2 and oxygen atom either by collision with an oxygen atom or by photoirradiation in the wavelength range of 240–320 nm. The above stratospheric O_3 formation and destruction reactions collectively are called the Chapman mechanism (Seinfeld and Pandis 1998). In practice, ozone is produced by a UV-light or corona-discharge generator. Ozone is a strong oxidizing agent that plays a central role in the atmospheric chemistry and deployed water purification technologies. The stratospheric ozone oxidizes chorine species and nitrogen oxides, leading to the formation of polar ozone hole about 12 and 24 km altitude (Seinfeld and Pandis 1998). In the troposphere, photooxidation of organic compounds emitted from anthropogenic and biogenic processes (e.g. Atkinson and Arey 2003) by ground-level ozone creates smog that causes health and environmental impacts. Ozone's oxidizing strength has been widely used in water and wastewater treatment (e.g. Langlais et al. 1991, Von Sonntag and Von Gunten 2012). Bailey (1978, 1982) critically reviewed the historical development of ozone reactions with organic compounds and their mechanisms, in both gas and liquid phases. The kinetics and mechanisms of paraffin hydrocarbons and ozone were investigated by Schubert et al. (1956a,b). Oxidation of carbonaceous materials by Ozone has also been extensively used for activation of biochar (Tables 7 and 8).

Ozone attacks both the basal and edge carbons in the chars. Kamm et al. (1999) investigated the kinetics of ozone reaction with carbon on the basal plane of soot in the temperature range 238–330 K. Their study revealed four quasi-elementary reactions in three rate regimes (SS denotes reactive surface site):

	Rate parameter at 296 K		
$SS + O_3 \rightarrow SSO + O_2$	$\gamma_i = 3.3 \times 10^{-3}$	Fast surface coverage	(15)
$SSO + O_3 \rightarrow SS + 2O_2$	$\gamma_{2ab} = (1.0 \pm 0.6) \times 10^{-7}$	Slow scavenging of surface oxide by O_3	(16)
$SSO + O_3 \rightarrow SS' + O_2 + CO_2$		Slow carbon gasification by combined scavenging of surface oxide by O_3 and desorption of surface oxide	(17)

$SSO \rightarrow SS' + CO$	$\gamma_{2c} = (4.7 \pm 2.7) \times 10^{-5} (s^{-1})$	Slow carbon gasification by desorption of surface oxide	(18)
$SSO \rightarrow SS_p$	$k_3 = (2.3 \pm 0.6) \times 10^{-5} (s^{-1})$	Slow passivation	(19)
$O_3 \rightarrow$ products	$k_4 = (6.8 \pm 1.0) \times 10^{-5} (s^{-1})$	Wall loss	(20)

Lee et al. (2009) reported that ozone adsorption on the basal plane of the graphene is gentle and reversible. Their simulation based on ab initio density function theory and experimental work demonstrated that a physisorbed ozone molecule reacts with basal carbons and forms an epoxide and an oxygen molecule at 550 K. Cataldo (2007) investigated the reaction of ozone with milled grade graphite at ambient temperature and observed a two-stage process: a fast gasification stage followed by a slow surface functionalization. In the gasification stage, the first-order reaction rate of CO_2 production was identical to that of O_3 disappearance, implying O_3 attack of a simple specific site of graphite. FTIR analysis of the graphite after O_3 functionalization revealed the formation of surface oxides, including carboxyl, ketones, diketones, aldehyde, and cyclic carbonyl such as lactones and carbonates, mainly on the edge carbons of the graphite. Oxidation level and acidic oxygen functional groups increase with the O_3 exposure time (Valdés et al. 2002).

The combination of the two-stage activation, gasification and surface functionalization, has profound impacts on the adsorption capacity of activated carbon. Valdés et al. (2002) reported that the internal BET surface area, micropore volume, and methylene blue adsorption all decreased with increasing O_3 exposure of bituminous-origin activated carbon at 25°C, due to the fixation of oxygen functional groups on the internal surface that blocked the passage of methylene blue to the internal active sites. The low gasification rate of bituminous-origin activated carbon also contributed to the observed negative adsorption capacity. This study seems to imply that an optimal ozone treatment occurs when both gasification and functionalization reach a reasonably high level. Generally, unlike the other activation methods, applying ozone as an activating agent needs more control. Former studies have shown the ability of ozone on the development of porosity and modification of chemical composition in carbon materials under controlled condition (Jimenez-Cordero et al. 2015). Cordero et al. used a cyclic activation method to produce granular activated carbons with significant high surface area and porosity (mainly micropore) from grape seed. In each cycle, char was first oxidized by exposure to ozone and then was subjected to high temperature (850 and 950°C) in an inert atmosphere (N_2) to desorb oxygen groups formed. After seven to nine activation cycles, activated carbons with S_{BET} higher than 1200 $m^2\ g^{-1}$ and S_{DA} above 1500 $m^2\ g^{-1}$ were obtained (Jimenez-Cordero et al. 2015). However, in an uncontrolled condition, Park and Jin (2005) reported that the SSA and micropore volume of ACs were slightly destroyed as the ozone treatment time increased.

Ozone is effective in creating surface oxides on carbons, including BC. Mul et al. (1998) found that the surface oxides on fullerene after oxidation by air and ozone are similar. Among these oxides, ethers and quinones are relatively stable; acid anhydrides and lactones decompose at 525 K. Gómez-Serrano et al. (2002) reported the surface functional groups, kinetics, and Langmuir-Hinshelwood model of ozonation of char from cherry stone. Their study revealed the formation of extensive phenolic, hydroxyl, quinonic, carboxylic, and ether groups on BC during ozonation. Generally, the temperatures of both pyrolysis and ozonation have significant effects on the types and quantities of surface oxides. The formation of surface oxides is favored when the pyrolysis is conducted at 450 to 600°C and ozonation at about 100°C. Graphitization becomes important above 600°C during pyrolysis, which reduces the reactivity of BC. Ozone decomposes above 100°C, which also reduces its reactivity with BC.

Smith (2011) activated BCs with ozone to create acidic oxygen functional groups for enhancing the cation exchange capacity of soil. Exposure of BCs with high internal surface areas to ozone for 10 min led to ample amount of surface oxides and gasification of about 20–30% of BC mass. Acidic groups, such as carboxylic acid, form mainly on the aromatic carbons in BCs rather than on the aliphatic carbons, which typically occurs in BC oxidation by O_2. The surface acidic oxides increase the cation exchange capacity significantly but had little or no effect on phosphorus removal capacity. Generation of acidic functional groups (especially carboxylic and carbonyl groups followed by lactone groups) (Valdés et al. 2002) by ozone treatment on carbon surfaces has also been confirmed by other researchers (Figure 4) (Chiang et al. 2002a,b, Valdés et al. 2002, Kastner et al. 2009, Gümüş and Akbal 2017). The increase in phenolic groups has also been observed in

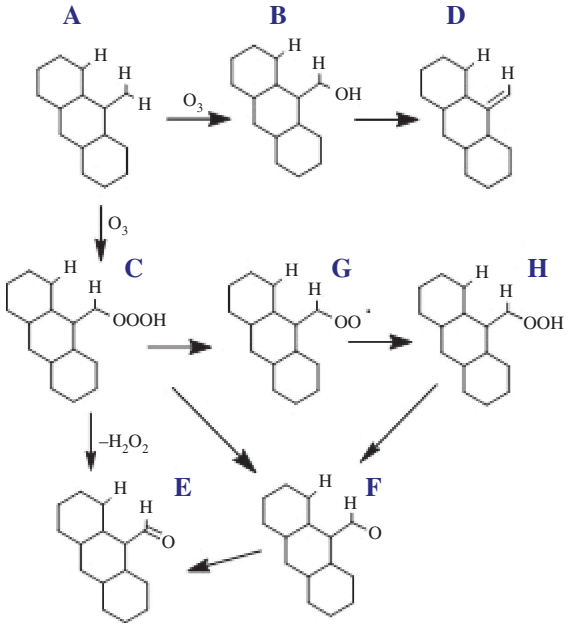

Figure 4: Proposed reaction pathways for O_3 reaction with activated carbon modified based on (Chiang et al. 2002b).

other studies (Chiang et al. 2002b). Acidic and polar functional groups on the carbon surface are responsible for the adsorption of polar compounds, e.g. ammonia adsorption (Park and Jin 2005). This observation has also been confirmed by Kastner et al. (2009). The authors demonstrated that short-term ozone treatment of BC at room temperature successfully increased acidic functional groups and, hence, the ammonia adsorption capacity of the palm oil shell char. The higher the ozone dose, the higher is the oxidation of the carbon and the lower is the point of zero charge (Valdés et al. 2002, Smith 2011). On the other hand, Chen et al. (2003) investigated the surfactant adsorption on the air-oxidized and ozone-treated carbon surface and found that adsorption capacity decreased with increasing surface oxidation. Surfactant adsorption takes place mainly on the nonpolar carbon surface, where it is driven by hydrophobic interactions. A similar observation was reported by Valdes et al. (2003) in case of 2-mercaptobenzothiazole (MBT). The authors reported that ozone treatment led to a significant reduction in the carbon's MBT adsorption capacity, due to the increase in polar hydrophilic groups. A detailed IR study of ozone adsorption on metal oxides dehydrated at different temperatures revealed at least four forms of ozone adsorption (Bulanin et al. 1995). These interactions are physical adsorption, the formation of weak hydrogen bonds with surface OH group, molecular adsorption via coordinative bonding to weak Lewis sites, and dissociative adsorption on interaction with strong Lewis sites, resulting in the formation of atomic oxygen atoms. The latter implies the possible catalytic role of ozone on carbon-containing metal oxides, such as CO oxidation.

Ozone as a selective oxidant has also emerged as an attractive oxidation agent in advanced oxidation process (AOP) for enhancing the oxidation rate in water and wastewater treatment. AOP involves either a combination of oxidants or oxidants with UV radiation (Glaze et al. 1987, Andreozzi et al. 1999). Oxygen-based AOPs include O_3/uv, O_3/H_2O_2, H_2O_2/uv, and O_3 at high pH. Glaze and Kang (1989) reported that the hydroxyl radical is reactive and nonselective and plays a pivotal role in the O_3/H_2O_2 system. Moreover, their experimental and mechanistic study validated that bicarbonate, carbonate, and natural organic matters are free radical scavengers and terminate the oxidation chain reactions. Bicarbonate and carbonate react with hydroxyl radical and forms water, CO_3^{-2}, and CO_3^{-1}, respectively (Weeks and Rabani 1966, Andreozzi et al. 1999). Activated carbon, in combination with ozone (O_3/AC), was introduced in AOP as an option to minimize the radical termination reactions. Kaptijn (1997), Zaror (1997), and Jans and Hoigné (1998) reported that activated carbon can accelerate ozone decomposition, resulting in the formation of hydroxyl radicals. The ratio between hydroxyl radical and ozone concentrations can increase up to 3–5 times. In a series of subsequent studies (Rivera-Utrilla et al. 2002, Rivera-Utrilla and Sánchez-Polo 2002, 2004, Sánchez-Polo and Rivera-Utrilla 2003, Sánchez-Polo et al. 2005), it has been demonstrated that bases on the carbon surface including metal centers, basal plane electrons, and other basic functional groups, such as pyrrole, are the main sites for the decomposition of O_3. The charged radical, O_2^-, is the major reaction intermediate. The activated carbon is consumed during the process, suggesting its role as an initiator or a promoter, rather than a catalyst, for the transformation. Valdés and Zaror (2006) reported the positive effects of activated carbon on the oxidation of benzothiazole in the aqueous phase during ozonation in the absence of radical scavenger. They also confirmed that the basic functional groups, such as the dissociated carboxylic acid anhydrides and carboxylic acids on the carbon surface, are responsible for the observed oxidation of ozone. Valdés et al. (2009) studied ozone decomposition promoted by natural zeolite and volcano sand. They demonstrated the roles of the basic sites of these minerals and that of a radical scavenger, acetic acid. The significant catalytic potential was observed when pistachio hull BC was introduced to the ozonation reactor for the decolorization and mineralization of RR198, a reactive azo dye (Moussavi and Khosravi 2012).

According to the results of different studies, ozone needs an activation energy of 44.4 ± 4.6 kJ mol^{-1} for the activation/gasification of BC in the temperature range 296–418 K (Stephens et al. 1989, Kamm et al. 1999). The endothermic activation of the carbonaceous structure needs an energy of 159–172 and 117 kJ mol^{-1} with the gasifying agents of CO_2 and steam, respectively. Accordingly, activation with ozone needs the least amount of energy (Toles et al. 2000, Aworn et al. 2008).

2.1.4 Air activation

Most processes to activate BC include heating the char (or carbon) in the presence of aggressive oxidizing reagents, either as a gas (e.g. steam, ozone, and CO_2) or liquid via wet impregnation (e.g. strong acids and ZnCl). Alternatively, a gaseous oxidizing agent, such as air, can be used (Table 9). Applying air (oxygen) as a gasifying agent is an economically attractive approach for physical activation, but challenging. Reactions of graphite with O_2 includes the formation of surface oxides on the edge, basal and off-plane carbons, followed by the formation of gaseous CO by desorption of surface oxide (Blyholder and Eyring 1959, Laurendeau 1978, Chen and Yang 1998). The *ab initio* molecular orbital study of Chen and Yang (1998) revealed the mechanisms of edge and near-edge carbon in graphite with O_2, H_2O, and CO_2 shown in Figure 5. For the $C + O_2$ reaction, the process starts with the dissociation of in-plane semiquinone oxygen with low activation energy (~58 kcal/mol) because epoxy oxygen weakens the C-CO bond (I). Meanwhile, the epoxy oxygen flips over to the edge to transform into in-plane carbonyl oxygen (II). In the next step, new epoxy oxygen is generated by further chemisorption of oxygen (III), and the carbonyl breaks off (by releasing CO) to regenerate the active edge carbon sites (IV). The process immediately is followed by the dissociative chemisorption of O_2 on active sites forming the semiquinone oxygen (I). The C-C bond in C-C=O (structure II) is not as strong as either one of the two C-C bonds in structure I. The breakage of carbonyl bond in structures of II and III includes only one C-C bond to release CO, while the breakage to free the semiquinone oxygen requires breaking two C-C bonds to free one CO, which is considered as the rate-limiting step.

For the $C + CO_2$ and $C + H_2O$ reactions, there is no remarkable quantity of the epoxy oxygen intermediate. Therefore, the activation energy of semiquinone oxygen (I) dissociation increases up to 85 kcal/mol, forming a dangling carbon bond (II). In the next step, chemisorption of oxygen to the dangling carbon generates carbonyl groups. Dissociation of these groups regenerates the bare edge sites, which lead to semiquinone oxygen by dissociative chemisorption of CO. As per the aforementioned discussion (for the $C + O_2$ reaction), the breakage of two C-C bonds to free the semiquinone CO is the rate-limiting step.

Air activation of carbonized charcoal is more complex than graphite/O_2 reaction and contains at least five major reaction steps as follows (Smith and Polley 1956, Laine et al. 1963, Bach 2007):

$2C_f + O_2(g) \rightarrow 2C(O)$	Oxygen chemisorption	(21)
$C(O) \rightarrow CO(g)$	Carbon gasification	(22)
$C_f + O_2(g) \rightarrow CO_2$	Carbon gasification by oxygen	(23)
$CO(g) + C(O) \rightarrow C_f + CO_2(g)$	Oxide gasification by carbon monoxide	(24)
$C_f + CO_2(g) \rightarrow 2CO(g)$	Carbon gasification by carbon dioxide	(25)

The mechanism starts with the chemisorption of oxygen onto the carbon to form surface oxides (R21), followed by desorption of CO and CO_2 (R22 and R23). In the first step, oxygen is bound to the surface in the form of various functional groups, which are similar to those known in organic chemistry. Since carbon-oxygen reactions are exothermic, chemisorption of oxygen rapidly happens even at low temperatures. However, desorption requires energy, and at temperatures below 380°C, only some of the surface oxides can desorb to form CO_2. In other words, lower temperatures favor the formation of stable surface oxides, making the second step challenging. Reactions with CO (R24) causes the concentration of surface oxides available to participate in R22 to decrease, inhibiting the of gasification (Walker et al. 1959). Thus, the relative amounts of active sites and stable surface oxides complicate studies of the kinetics of the carbon-oxygen reaction and predictions of the amount of oxygen chemisorbed. With respect to oxygen partial pressure, some researchers reported that the chemisorption and gasification reactions are close to first order. The apparent activation energies of oxygen chemisorption and gasification vary between 40 and 80 kJ/mol and 110 and 150 kJ/mol, respectively. Tam and Antal (1999) analyzed the gasification of macadamia nut shell and developed a model for the complex kinetics of carbon gasification by oxygen. According to their model, R21 is the formation of stable surface oxides, which occupy free active sites and reduce the sites for gasification (R22). R23 is the usual gasification of the active carbon sites to form CO_2. They also included an Eley-Rideal-type oxide gasification step (R24) based on

Table 9: Effects of air modification on the physicochemical properties of biochar (numbers in parenthesis refer to activated biochar).

Biochar source	Pyrolysis temperature (°C), time (h)	Air condition temperature (°C), time (h)	Burn-off	Ash	pH	S_{BET} (m^2/g)	V_{micro} (cm^3/g)	V_{meso} (cm^3/g)	V_p (cm^3/g)	R_p (nm)	C (%)	H (%)	N (%)	O (%)	Reference
Woods of hybrid	400, 0.5	250, 0.5	–	3.8	10.1 (9.8)	262 (277)[a]	0.10 (0.11)	–	0.28 (0.43)	–	76.2 (69.9)	4.5 (3.9)	0.45 (0.36)	13.4 (22)	Suliman et al. (2016)
Poplar	500, 0.5			4.8	10.5 (10)	404 (386)[a]	0.16 (0.15)		0.43 (0.54)		78.6 (74.7)	4.1 (3.6)	0.41 (0.43)	11.4 (16.4)	
	600, 0.5			6.0	10.4 (10)	500 (570)[a]	0.20 (0.23)		0.57 (0.75)		83.1 (81.4)	3.4 (3.4)	0.5 (0.41)	6.7 (8.8)	
Douglas fir	400, 0.5	250, 0.5	–	0.6	8.3 (8.0)	211 (227)[a]	0.08 (0.09)	–	0.20 (0.29)	–	74.5 (70.1)	5.1 (4.1)	0.29 (0.3)	19.2 (25)	Suliman et al. (2016)
	500, 0.5			0.9	8.8 (8.2)	318 (355)[a]	0.13 (0.14)		0.36 (0.47)		80 (76.3)	4.3 (3.6)	0.36 (0.33)	14.8 (18.9)	
	600, 0.5			0.9	8.8 (8.3)	424 (550)[a]	0.17 (0.22)		0.43 (0.81)		87.8 (85.1)	3.7 (3.4)	0.38 (0.32)	7.1 (10.3)	
Douglas fir bark	400, 0.5	250, 0.5	–	5.6	8 (6.9)	259 (257)[a]	0.10 (0.10)	–	0.31 (0.35)	–	69.8 (68.9)	4.5 (4.1)	0.65 (23.6)	18.6 (23.6)	Suliman et al. (2016)
	500, 0.5			7.4	9.9 (8.0)	361 (313)[a]	0.14 (0.13)		0.50 (0.91)		75 (69.8)	3.8 (3.5)	0.67 (18.6)	12.6 (18.6)	
	600, 0.5			7.7	10.2 (10)	417 (557)[a]	0.17 (0.22)		0.65 (0.87)		77.6 (78.1)	3.2 (3.3)	0.73 (10.2)	8.9 (10.2)	
Taiheiyo	NM	150, 1	–	–	–	–	0.062 (0.05)	–	–	–	77.8 (76.4)	6 (6.2)	–	–	Oda et al. (1981)
Bibai	NM	150, 1	–	–	–	–	0.065 (0.043)	–	–	–	81.1 (79.3)	6 (5.6)	–	–	Oda et al. (1981)
Akabira	NM	150, 1	–	–	–	–	0.054 (0.041)	–	–	–	83.4 (80.4)	6.2 (5.4)	–	–	Oda et al. (1981)
Miike	NM	150, 1	–	–	–	–	0.035 (0.02)	–	–	–	84.5 (85)	6.1 (5.8)	–	–	Oda et al. (1981)
Yubari	NM	150, 1	–	–	–	–	0.033 (0.031)	–	–	–	86.2 (87.7)	6.3 (5.7)	–	–	Oda et al. (1981)
Moura	NM	150, 1	–	–	–	–	0.053 (0.066)	–	–	–	87.6 (87.8)	5.3 (4.9)	–	–	Oda et al. (1981)
Nishikawachi	NM	150, 1	–	–	–	–	0.03 (0.038)	–	–	–	89.8 (90.4)	5.2 (4.8)	–	–	Oda et al. (1981)
Macadamia nut shell Chemi-Desorp	400	280, 6 5280, 14	–	1.04 (2.11)	–	510 (1 Cycle) 962 (3 Cycle) 1060 (4 Cycle)	0.32 cc/g 0.37 cc/g 0.32	–	0.36 (–) 0.58 (–) 0.8 (–)	–	94.6 (92.3)	0.97 (1.1)	0.47 (0.35)	2.9 (5.16)	Tam and Antal (1999)
Coconut shell Chemi-Desorp	400	280, 6 280, 14.5	–	2.8 (3.44)	–	474 (1 cycle) 833 (3 cycle) 1028 (4 cycle)	– – 0.32	–	– – 0.74 (–)	–	92.3 (91.7)	1.09 (1.07)	0.47 (0.19)	3.08 (4.37)	Tam and Antal (1999)
Waste rubber Chemi-Desorp	800, 0.17	O_2 21%, 500, 0.08 O_2 21%, 500, 0.5 O_2 10%, 500, 0.08 O_2 10%, 500, 0.5 O_2 10%, 500, 0.33 O_2 10%, 550, 0.33 O_2 10%, 600, 0.33	(5%) (80%) (5%) (28%) (15%) (22%) (25%)	–	–	142 (–) 237 (–) 160 (–) 282 (–) 252 (–) 272 (–) 170 (–)	0.018 (–) 0.045 (–) 0 (–) 0.069 (–) 0.06 (–) 0.062 (–) 0.024 (–)	0.039 (–) 0.050 (–) 0.011 (–) 0.015 (–) 0.012 (–) 0.062 (–) 0.024 (–)	–	–	–	–	–	–	Heras et al. (2004)
Waste rubber	800, 0.33	210 Chemisorption 750 Desorption		–	–	60 (240)	– (0.06)	0.02 (–)	–	60 (15)	–	–	–	–	Heras et al. (2009)
Ta90 Coconut based	–	200 Chemisorption 900 Desorption	22%	–	–	23 (56) Ex 23 (42) Ex	0.54 (0.6) 0.54 (0.48)	–	–	12 (19) Å (4 cycle) 12 (16) Å (7 cycle)		–	–	–	Py et al. (2003)
Ctpkn Pitch based	–	200 Chemisorption 900 Desorption	17% (4 cycle) 45% (7 cycle)	–	–	18 (38) Ex 18 (85) Ex	0.47 (0.62)	–	–	7.6 (15) Å (7 cycle)		–	–	–	Py et al. (2003)
CmS5A Coconut based	–	200 Chemisorption 900 Desorption	15% (7 Cycle)	–	–	18 (20) Ex	0.23 (0.25)	–	–	6.4 (6.7) Å (7 cycle)		–	–	–	Py et al. (2003)
Almond nutshell	700, 1, CO_2	300 Chemisorption	–	–	10 (10.3)	424 (497)	0.19 (0.32)	0.038 (0.073)	–	–	–	–	–	–	Wartelle and Marshall (2001)
Pecan	700, 1, CO_2	300 Chemisorption	–	–	9.5 (8.3)	466 (608)	0.21 (0.25)	0.051 (0.119)	–	–	–	–	–	–	Wartelle and Marshall (2001)
Pistachio nut	700, 1, CO_2	300 Chemisorption	–	–	9.6 (10)	544 (572)	0.24 (0.26)	0.042 (0.04)	–	–	–	–	–	–	Wartelle and Marshall (2001)
Hazelnut shell	700, 1, CO_2	300 Chemisorption	–	–	9.1 (8.3)	501 (745)	0.24 (0.3)	0.067 (0.256)	–	–	–	–	–	–	Wartelle and Marshall (2001)
Macadamia nut	700, 1, CO_2	300 Chemisorption	–	–	9.2 (5.6)	503 (791)	0.24 (0.28)	0.107 (0.28)	–	–	–	–	–	–	Wartelle and Marshall (2001)

Table 9 (continued)

Biochar source	Pyrolysis temperature (°C), time (h)	Air condition temperature (°C), time (h)	Burn-off	Ash	pH	S_{BET} (m^2/g)	V_{micro} (cm^3/g)	V_{meso} (cm^3/g)	V_p (cm^3/g)	R_p (nm)	C (%)	H (%)	N (%)	O (%)	Reference
Black walnut	700, 1, CO_2	300 Chemisorption	–	–	9.3 (8.4)	544 (749)	0.21 (0.293)	0.058 (0.208)	–	–	–	–	–	–	Wartelle and Marshall (2001)
English walnut	700, 1, CO_2	300 Chemisorption	–	–	9.6 (9.5)	579 (733)	0.22 (0.32)	0.048 (0.195)	–	–	–	–	–	–	Wartelle and Marshall (2001)

CTPKN, a laboratory-made carbon molecular sieve obtained by a slight KOH activation; TA90, coconut activated carbon manufactured by Pica (France); CMS5A, Biochar made of coconut manufactured by Takeda Chemical Industries (Japan).
Å, Angstrom; Ex, external surface area.
[a]Carbon dioxide (CO_2) adsorption isotherm analysis for S_{BET} A n investigation of the porosity of carbons prepared by constant rate activation in air.

the results reported by Zhuang et al. (1996), who observed the formation of $C^{16}O^{18}O$ by oxygen during carbon gasification when the flow of $^{18}O_2$ was switched to $^{16}O_2$ at low temperatures. They also found the values of 91, 126, and 125 kJ mol^{-1} for oxygen chemisorption, carbon gasification, and oxide gasification, respectively (Tam and Antal 1999). Hence, the second step of the oxygen activation should be followed by a high-temperature treatment in a nitrogen atmosphere, removing oxygen-containing groups. In desorption, the carbon-oxygen complexes are decomposed into CO and CO_2 and fresh unsaturated carbon sites are formed at the edge of the carbon matrix (Py et al. 2003).

In order to control the high reactivity of oxygen and overcome the difficulties associated with it, cyclic oxygen chemisorption/desorption was used by Py et al. (2003). The first cycle of this method consists of the chemisorption of oxygen at moderate temperatures in an air or oxygen-containing mixture and the second cycle consists of the desorption of the chemisorbed oxygen at a high temperature in an inert atmosphere. This cycle could be repeated to reach the desired BC properties. So, the desorbed oxygen leaves the surface in the form of CO and CO_2, which not only creates the new active sites but also widens the pores size. Chemisorption and desorption in the presence of oxygen are competitive phenomena, and hence, activation by cyclic oxygen chemisorption-desorption is sensitive to the temperature and the duration of each step to a high extent. At low temperatures, chemisorption is the dominant process, while desorption prevails at high temperatures. The temperature of the second cycle (desorption) significantly affects the amount of carbon that is evolved as CO or CO_2 and type of the oxygen-carbon decomposed, giving rise to pore development (Heras et al. 2009). Py et al. (2003) used this approach for activating three coconut- and pitch-based activated carbon in 10 repeating cycles and reported that each cycle is responsible for a regular increase of 1–2 Å pore size widening depending on the material origin. Heras et al. (2009) have also used this approach for activating the char obtained from pyrolysis of waste tires and could obtain the BET surface area of 140 m^2/g at burn-off values lower than 17% at chemisorption and desorption temperatures of 210 and 550°C, respectively. A further increase in desorption temperature up to 750°C led to the surface area of 240 m^2/g at a burn-off of 22%. The authors also reported that in the first activation cycles, the porosity developed mostly by the generation of narrow mesopores, and microporosity was developed from the cycles of 4–9 and then it was reduced till the 12th cycle (Heras et al. 2009).

Air as an oxidizing agent can be easily integrated into the BC pyrolysis cooling step. Hence, pyrolysis

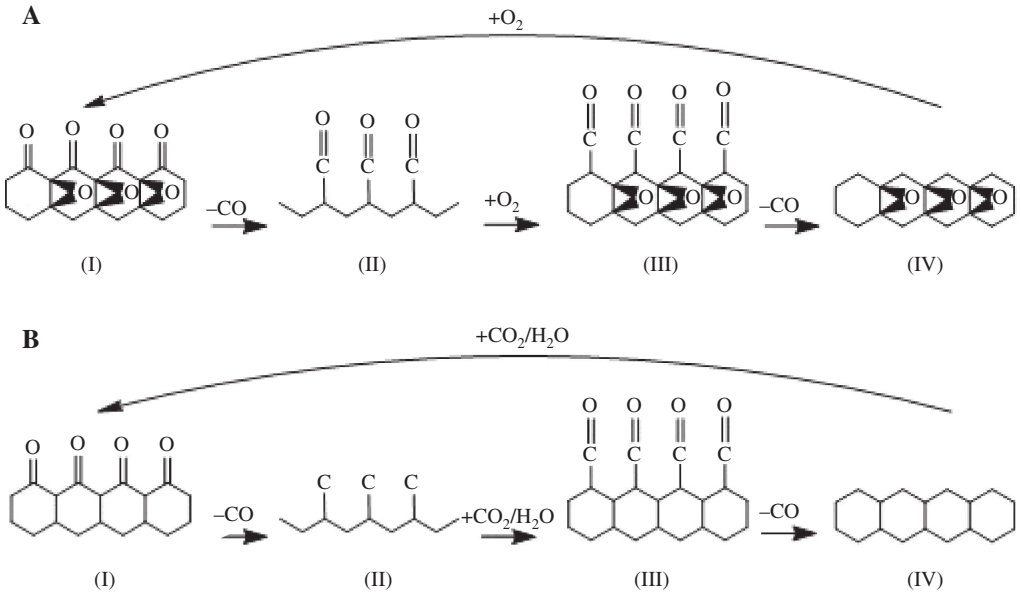

Figure 5: Reaction pathways for (A) graphite gasification by O_2 (activation energy: 58 kcal/mol), (B) graphite gasification by CO_2 and H_2O (activation energy: 85 kcal/mol), from ab initial orbital study, including three oxygen intermediates semiquinone, carbonyl and off-plane epoxyl; modified based on Chen and Yang (1998).

temperature plays an important role in the final structure and the susceptibility of carbonaceous materials to air oxidation. Working on three different feedstocks, Suliman et al. (2016) reported that the quantity of C, H, and N decreased in all oxidized BC compared to the unoxidized ones. These changes were more significant for those synthesized at lower temperatures (<500°C), which were more susceptible to oxidation due to the removal of labile C and volatile organic compounds compared with higher temperature ones. As per Table 10, the bulk oxygen mass fraction in BC increases with air oxidation due to the formation of oxygenated functional groups. The values are again more pronounced for BCs produced at a low temperature, which have a higher mass fraction of volatile and less stabilized aromatic carbon (Suliman et al. 2016). These observations have been confirmed by the other researchers too. Oda et al. analyzed seven different sources of BC and reported that although oxidation of all of the coals employed resulted in hydrogen-poor and oxygen-rich products, oxidation of samples with a higher content of carbon lasted more than 1 h to show the reduction of C content. The reason is that BCs synthesized at higher temperatures have a denser and robust graphitic structure. These observations were confirmed with the content of functional groups in BC after oxidation. FTIR analysis of BC after oxidation demonstrates an increase in carbonyl and carboxyl group due to which negative surface charge in most air activated BCs increased too. In some cases, carbonyl increase is more significant (e.g. in almond-based BC) (Toles et al. 2000), while in some others, carboxyl (e.g. Douglas fir Bark BCs) (Suliman et al. 2016), and in some cases, both of the groups increased

Table 10: Effects of air modification on the adsorption capacity of biochar (numbers in parentheses refer to activated biochar).

Biochar source	Pyrolysis cond. temperature (°C), time (h)	Air temperature (°C)	Objective	Adsorption capacity	Reference
Almond nutshell	700, 1, CO_2	300 Chemisorption	Removal of Cu^{2+}	607.8 (620.3)	Wartelle and Marshall (2001)
Pecan	700, 1, CO_2	300 Chemisorption	Removal of Cu^{2+}	689.8 (664.3)	Wartelle and Marshall (2001)
Pistachio nut	700, 1, CO_2	300 Chemisorption	Removal of Cu^{2+}	687.4 (690.4)	Wartelle and Marshall (2001)
Hazelnut shell	700, 1, CO_2	300 Chemisorption	Removal of Cu^{2+}	637 (608.7)	Wartelle and Marshall (2001)
Macadamia nut	700, 1, CO_2	300 Chemisorption	Removal of Cu^{2+}	543.1 (589.0)	Wartelle and Marshall (2001)
Black walnut	700, 1, CO_2	300 Chemisorption	Removal of Cu^{2+}	618.2 (627.6)	Wartelle and Marshall (2001)
English walnut	700, 1, CO_2	300 Chemisorption	Removal of Cu^{2+}	697.5 (667.2)	Wartelle and Marshall (2001)

(e.g. Douglas fir wood BCs and poplar wood BCs) (Suliman et al. 2016). Although the quantity of acidic functional groups increases in all BCs oxidized by air, the trend of oxidation decreases with pyrolysis temperature. Similar results were found by Dong et al. (2013), who reported high-temperature BCs contained a lower quantity of oxygen functional groups. In other words, the susceptibility of BCs to oxidation by air has a reverse relation with pyrolysis temperature as more stable poly-aromatic structures are formed at high temperature. In terms of physical structure, oxygenation using air does not change the microporous structure and surface area of BC produced at lower temperatures significantly. Surface area has slightly increased in some cases pyrolyzed at high temperatures. The decrease in microporous volume can be explained by the partial blockage of micropores by oxygen-containing functional groups, and the slight increase in area may attribute to the oxidation and removal of some of the carbonaceous walls (Suliman et al. 2016). Oda et al. also reported that the micropore volume decreased with slight oxidation (1 h) but increased considerably with extensive oxidation (5–10 h). Similar results were reported by Tam and Antal (1999), who worked on oxidizing the macadamia nut and coconut shells in different durations. As per their results, BET surface area significantly increased with activation cycles and the duration from 240 to 840 min. However, the micropore volume slightly increased from 32 to 37 cc/g. It should be noted that a further increase in oxidization duration considerably increased the meso and macropore volume while it slightly reduced the micropore volume (Tam and Antal 1999).

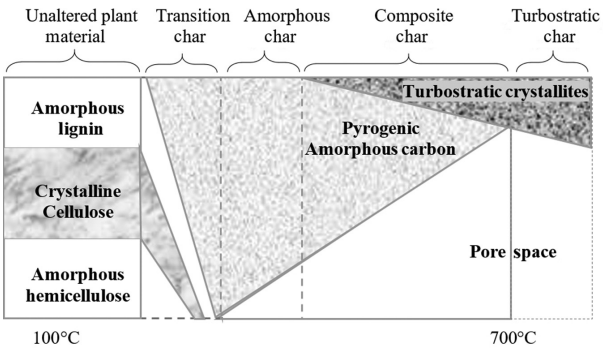

Figure 6: Phase conversion of biochar under different temperatures, modified based on Lehmann and Joseph (2015).

2.2 Thermal activation

2.2.1 Conventional thermal activation

Thermal decomposition of biomass in an oxygen-depleted atmosphere leads to a series of phenomena, including decomposition, transformation, and rearrangement in biomass molecular structure (Figure 6). At low temperatures (100–200°C), biomass is mainly dehydrated and remains almost unaltered. As temperature increases, connections between organic molecules (including cellulose, lignin, and hemicellulose biopolymers, which are the main organic structures in biomass) are decomposed, and subsequently, isolated aromatic rings (transition BC) begin to form. By a further increase in temperature, all recognizable biopolymers are completely degraded and substituted with isolated aromatic molecules with two to three rings (amorphous BC). These small and somewhat defective sheets of aromatic rings stack up at higher temperatures and form small three-dimensional structures, consisting of three to five stacked C sheets with a lateral extension of 2–5 nm and a vertical height of 12 nm (turbostratic crystallites). However, the exact dimensions depend on feedstock type and its mineral content, as well as treatment temperature. In a wide range of temperatures, a significant quantity of both amorphous material and turbostratic crystallites presents in BC structure (composite BC). As soon as all amorphous organic C is either converted into aromatic rings or volatilized, a BC is recognized as "carbonized" or "turbostratic." BCs do not usually get to this region as they either require heating temperatures beyond 700°C or prolonged residence during pyrolysis. Hence, most BCs have a highly disordered and heterogeneous carbon structure (belonging to either amorphous or composite categories), and hence, the thermal treatment process has considerable influences on their structures and gasification behavior (Keiluweit et al. 2010, Claoston et al. 2014).

In a conventional thermal modification, BC is heated to a high temperature (600–1500°C) for a desired duration (1–2 h) (Table 11 and Figure 7). Thermal treatment removes the hydrogen and heteroatoms such as oxygen via the release of gases, resulting in a reduction of BC yield. Therefore, a more condensed/ordered carbonaceous structure is generated. The heterogeneity of the carbon structure is reduced through two simultaneous processes: I) loss of that part of the amorphous structure during gas release and II) transformation of the amorphous and disordered structures into larger aromatic ring system (Kleber et al. 2015). Dehydrogenation and aromatization reactions assist the formation of larger polynuclear aromatic hydrocarbons at higher activation temperatures and eventually increase the carbonization yield (Dodevski et al. 2017). The effect of thermal treatment is more significant at initial steps, and it gradually decreases with further release of heteroatoms. Under these conditions,

Table 11: Effects of conventional thermal modification on the physicochemical properties of biochar (numbers in parentheses refer to activated biochar).

Biochar source	Pyrolysis temperature (°C), time (h)	Agent	Ash	Agent temperature (°C), time (h)	Objective	Yield (mg/g)	pH	S_{BET} (m^2/g)	S_{micro} (m^2/g)	V_{micro} (cm^3/g)	V_{meso} (cm^3/g)	V_p (cm^3/g)	R_p (nm)	C (%)	H (%)	O (%)	N (%)	Reference
Aspen wood	600, 0.5	–	–	CO_2, 780, 1.7	MO, W	0 (93.46%)		480 (886)	–	–	0.19 (0.29)	0.01 (0.16)	–	–	–	–	–	Veksha et al. (2015)
Oak	500, –	–	3.7 (7.1)	CO_2, 800, 1	–	–	8.3 (8.8)	107 (786)	–	0.05 (0.04)	0.046 (0.328)	0.004 (0.008)	–	81 (86)	2.9 (0.6)	12 (5.6)	0.5 (0.6)	Jung and Kim (2014)
			3.7 (12.1)	CO_2, 900, 1			8.3 (9.7)	107 (807)		0.05 (0.35)	0.046 (0.335)	0.004 (0.01)		81 (85)	2.9 (0.4)	12 (1.3)	0.5 (1.1)	
Pistachio nutshells	450, –	–	–	CO_2, 800, –	Physical comparison	–	–	– (543)	–	– (0.22)	– (0.208)	–	–	–	–	–	–	Işıtan et al. (2016)
				CO_2, 900, –				– (680)		– (0.29)	– (0.262)							
Pistachio nutshells	550, –	–	–	CO_2, 800, –	–	–	–	– (554)	–	– (0.23)	– (0.217)	–	–	–	–	–	–	Işıtan et al. (2016)
				CO_2, 900, –				– (650)		– (0.27)	– (0.257)							
Pistachio nutshells	650, –	–	–	CO_2, 800, –	–	–	–	– (606)	–	– (0.25)	– (0.233)	–	–	–	–	–	–	Işıtan et al. (2016)
				CO_2, 900, –				– (810)		– (0.34)	– (0.313)							
Palm kernel shells	–	–	–	CO_2, 900, 1	Iodine adsorption	–	–	34 (600)	–	0.022 (0.28)	0.015 (0.25)	0.007 (0.031)	–	–	–	–	–	Choi et al. (2015)
				CO_2, 900, 2				34 (695)		0.022 (0.34)	0.015 (0.29)	0.007 (0.044)						
				CO_2, 900, 3				34 (807)		0.022 (0.38)	0.015 (0.34)	0.007 (0.044)						
Forestry waste	400, –	–	3.6	CO_2, 400, 2	Analysis of temperature effect	–	–	52 (73)	4.8 (8)	0.036 (0.039)	0.0017 (0.0016)	–	2.75 (2.14)	–	–	–	–	Grima-Olmedo et al. (2016)
			3.5	CO_2, 400, 4				37.5 (135)	4.08 (17.8)	0.034 (0.069)	0.0013 (0.0038)		3.71 (2.05)					
Forestry waste	600, –	–	4.7	CO_2, 600, 2	–	–	–	370.5 (377)	296 (304)	0.19 (0.19)	0.138 (0.142)	–	1.6 (1.55)	–	–	–	–	Grima-Olmedo et al. (2016)
			5.0	CO_2, 600, 4				367 (390)	299 (337)	0.199 (0.199)	0.139 (0.16)		1.57 (1.54)					
Forestry waste	800, –	–	10.6	CO_2, 800, 2	–	–	–	435 (905)	366.7 (544)	0.23 (0.55)	0.173 (0.25)	–	1.58 (1.79)	–	–	–	–	Grima-Olmedo et al. (2016)
			25.4	CO_2, 800, 4				436 (1034)	371.1 (570)	0.23 (0.61)	0.174 (0.26)		1.57 (1.78)					
Pistachio nut shell	350, 2	–	–	CO_2, 900, 2	–	–	–	– (611)	–	– (0.393)	– (0.18)	– (0.213)	– (2.57)	–	–	–	10	Lua and Yang (2004)
	500, 2							– (896)		– (0.532)	– (0.237)	– (0.295)	– (2.38)					
	800, 2							– (724)		– (0.454)	– (0.17)	– (0.284)	– (2.51)					
Oak	–	–	(31.8)	CO_2, 700, 1	–	–	–	– (642)	–	– (0.4113)	– (0.2704)	–	–	70.84 (–)	3.165 (–)	13.225 (–)	–	Zhang et al. (2004)
			(43)	CO_2, 800, 1				– (845)		– (0.6011)	– (0.3212)							
Corn hulls	–	–	(32.3)	CO_2, 700, 1	–	–	–	– (977)	–	– (0.8923)	– (0.3352)	–	–	70.33 (–)	3.226 (–)	16.733 (–)	–	Zhang et al. (2004)
			(44.4)	CO_2, 800, 1				– (1010)		– (0.8341)	– (0.4348)							
Corn stover	–	–	(41.5)	CO_2, 700, 1	–	–	–	– (660)	–	– (0.4879)	– (0.2817)	–	–	59.36 (–)	3.06 (–)	16.936 (–)	–	Zhang et al. (2004)
			(42.6)	CO_2, 800, 1				– (712)		– (0.5494)	– (0.2849)							
Willow tree	700, –	–	–	CO2, 900, 1	PAH removal,	85.12	–	11.4 (512)	4.5 (380)	0.006 (0.276)	0.0016 (0.169)	–	1.08 (1.08)	–	–	–	–	Kołtowski et al. (2017b)
Willow tree	700, –	–	–	MW, 200, 0.5	PAH removal,	81.00	–	11.4 (443)	4.5 (259)	0.006 (0.242)	0.0016 (0.1138)	–	1.08 (1.10)	–	–	–	–	Kołtowski et al. (2017b)
Willow tree	700, –	–	–	Steam, 800, 1	PAH removal,	74.93	–	11.4 (841)	4.5 (509)	0.006 (0.576)	0.0016 (0.2245)	–	1.08 (1.37)	–	–	–	–	Kołtowski et al. (2017b)
Wheat straw	650, –	–	–	Steam, 800, 1.3	PAH removal,	67%↑	9.9 (8.8)	26.3 (246)	10.8 (140)	0.0256 (0.16)	0.0046 (0.0622)	–	1.95 (1.02)	–	–	–	–	Kołtowski et al. (2016)
Coconut	650, –	–	–	Steam, 800, 1.3	PAH removal,	83.4%↑	8.0 (7.2)	3 (626.8)	2.3 (472)	0.001 (0.336)	0.0087 (0.0219)	–	0.6 (0.85)	–	–	–	–	Kołtowski et al. (2016)
Willow	650, –	–	–	Steam, 800, 1.3	PAH removal,	51.0%↑	9.1 (8.2)	11.4 (841)	4.5 (509)	0.006 (0.576)	0.0016 (0.2245)	–	1.08 (1.09)	–	–	–	–	Kołtowski et al. (2016)
Wheat straw		–	–	Steam, 900, 1	Cd immob., S	14.2 (8.9)	7.6 (7.8)	137 (961)	–	–	–	–	–	–	–	–	–	Wu et al. (2016)
Wheat straw		–	–	Steam, 900, 1	Cu immob., S	45.7 (12.58)	–	–	–	–	–	–	–	–	–	–	–	Wu et al. (2016)
Miscanthus sacchariflorus	500, –	–	3.81 (3.92)	Steam, 800,–	Cu sorption	15.4 (13.8)	–	181 (322)	–	–	–	–	–	80.9 (82.1)	2.8 (2.67)	12.2 (11)	0.29 (0.31)	Shim et al. (2015)
Pine nut shell	–	–	–	Steam, 750, 1.3	Iodine adsorption	At least 17%↑	–	800 (–)	–	–	–	–	–	–	–	–	–	Chen et al. (2016)
				Steam, 850, 1.3				1020 (–)										
				Steam, 950, 1.3				750 (–)										

Table 11 (continued)

Biochar source	Pyrolysis temperature (°C), time (h)	Agent	Ash	Agent temperature (°C), time (h)	Objective	Yield (mg/g)	pH	S_{BET} (m^2/g)	S_{micro} (m^2/g)	V_{micro} (cm^3/g)	V_{meso} (cm^3/g)	V_p (cm^3/g)	R_p (nm)	C (%)	H (%)	O (%)	N (%)	Reference
Pine nut shell	–	–	–	Steam, 850, 0.7 Steam, 850, 1.3 Steam, 850, 2	Iodine adsorption	At least 17%↑	–	750 (–) 1020 (–) 850	–	–	–	–	–	–	–	–	–	Chen et al. (2016)
Sugar cane bagasse	460, – 	–	14 (22) 14 (16.1) 14 (12.2)	Steam, 700, 1 Steam, 800, 1 Steam, 900, 1	MB	16%↑		259 (441) 259 (570) 259 (561)	194 (399) 194 (345) 194 (289)	0.136 (0.189) 0.136 (0.356) 0.136 (0.526)	0.088 (0.181) 0.088 (0.157) 0.088 (0.131)	–	21 (33) 21 (25.5) 21 (20.4)	62.5 (73.6) 62.5 (77.9) 62.5 (78.2)	1.7 (0.6) 1.7 (0.6) 1.7 (0.6)	–	0.9 (0.7) 0.9 (0.9) 0.9 (0.6)	Carrier et al. (2012)
Oak	200, 1 400, 1 600, 1	–	800	Steam/$CO_2$200 Steam/$CO_2$400 Steam/$CO_2$600	Good Comparison	–	4.6 (9.6) 6.9 (9.6) 9.6 (9.6)	–	–	–	–	–	–	48.8 (30.6) 42.7 (30.3) 45.5 (37.1)	–	–	0.2 (0.5) 0.3 (0.5) 0.4 (0.4)	Zhang et al. (2015)
Poplar wood	550	NaOH	3.7 (4.55)	750, 2	Organic compounds	83.7%↑	–	–	–	–	–	–	–	80.3 (85)	2.8 (1.55)	12.8 (8.8)	0.34 (0.1)	de Caprariis et al. (2017)
Debarked loblolly pine chips	300, – 500, – 700, –	NaOH	–	300, – 500, – 700, –	PAH removal	29.91↑	–	1.41 (1250) 239 (346) 321 (57)	–	–	0 (0.289) 0.076 (0.128) 0.129 (0.013)	0.009 (0.78) 0.075 (0.16) 0.045 (0.04)	–	23.6 (79.7) 79.4 (86.5) 87.1 (83.8)	–	–	–	Park et al. (2013)
Torrefied loblolly pine chips	300, 0.25	NaOH	–	800, 2	Cd	167.3	–	1150.7	–	↑	–	–	–	–	–	–	–	Park et al. (2017)
Safflower seeds	500, 1	KOH	–	800, 1	Iodine adsorption	–	–	14.14 (1277)	– (1133)	– (0.663)	– (0.49)	–	– (2.08)	62.45 (72.1	1.85 (2.7)	31.6 (22.5)	4.07 (2.8)	Angın et al. (2013b)
Unknown provenance	600, fast	KOH	–	475, 2 675, 2 875, 2	Comparison of electrical conductivity	–	–	– (894) – (1807) – (2247)	–	–	– (0.35) – (0.73) – (0.08)	– (0.06) – (0.09) – (1.41)	– (1.95) – (1.90) – (2.76)	–	–	–	–	Dehkhoda et al. (2016)
Pistachio nut shell		KOH	–	–	–	–	–	700.5	–	–				–	–	–	–	Foo and Hameed (2011b)
Bamboo chips	700, 2	KOH	–	700, 2	[BMIM][Cl]	(0.513)$^{mmol/g}$	–	355 (1195)	–	0.195 (0.585)	0.127 (0.436)	0.069 (0.149)	0.6 (0.548)	–	–	–	–	Yu et al. (2016)
Hazelnut shells, M3	500, 1	KOH	W C	900, 1	–		–	2319	–	– (0.936)	KOH	– (0.042)		– (40.96)		– (56.78)		Kwiatkowski and Broniek (2017)
DDGS	600, 45 min	KOH	–	KOH, 950, 3 KOH, 1050, 3	Analysis of temperature effect	1.78f↑ F/g	–	2959 (2684)	–	– (1.52) – (2.72)	– (0.99) – (0.5)	– (0.39) – (2.19)		– (892) – (90.8)		– (10.01) – (9.067)	(1.790)	Jin et al. (2014)
Bamboo	550, –	–	W C	800, air, 2	Furfural	109 (253)	–	42.8 (494)	35 (427)	0.022 (0.24)	0.016 (0.198)	–	2.04 (1.94)	63.5 (70.7)	2.9 (1.1)	33 (27.6)	0.55 (0.58)	Li et al. (2014)
Corn straw	500, 1.5	KOH	–	800, 0.5	Hg^{2+}	0.91 (1.19)	–	32.85 (466)	–	0.0148 (0.08)	–	0.018 (0.093)	5.01 (4.4)	42.3 (67.2)	1.16 (0.8)	1.2 (6.8)	0.82 (0.53)	Tan et al. (2016)
Corn straw	500, 1.5	KOH	–	–	Hg^{2+}	0.91 (0.98)	–	32.85 (59)	–	0.0148 (0.02)	–	0.018 (0.026)	5.01 (7.6)	42.3 (43.08)	1.16 (1.14)	1.2 (15.4)	0.82 (0.86)	Tan et al. (2016)
Corn straw	500, 1.5	KOH		800, 0.5	Atrazine	2.5 (74.23)	–		–	–	–	–	–	–	–	–	–	Tan et al. (2016)
Corn straw	500, 1.5	KOH	–	–	Atrazine	2.5 (2.82)	–		–	–	–	–	–	–	–	–	–	Tan et al. (2016)
Corn straw	500, 1.5	Na_2S	–	–	Atrazine	2.5 (2.74)	–		–	–	–	–	–	–	–	–	–	Tan et al. (2016)
Corn straw	500, 1.5	Na_2S	–	–	Hg^{2+}	0.91 (1.24)	–	32.85 (53)	–	0.0148 (0.02)		0.018 (0.024)	5.01 (5.84)	42.3 (42.92)	1.16 (1)	1.2 (15.09)	0.82 (0.49)	Tan et al. (2016)
Hazelnut shells	500, 1	CO_2	WO/C	800, 0.5	–	–	–	921	–	– (0.443)		– (0.098)	–	– (27.45)		– (59.81)	–	Kwiatkowski and Broniek (2017)

Table 11 (continued)

Biochar source	Pyrolysis temperature (°C), time (h)	Agent	Ash	Agent temperature (°C), time (h)	Objective	Yield (mg/g)	pH	S_{BET} (m^2/g)	S_{micro} (m^2/g)	V_{micro} (cm^3/g)	V_{meso} (cm^3/g)	V_p (cm^3/g)	R_p (nm)	C (%)	H (%)	O (%)	N (%)	Reference
Hazelnut shells	500, 1	H_2O	WO/C	900, 0.5	–	–	–	922	–	– (0.553)		– (0.105)	–	– (26.64)		– (60.05)	–	Kwiatkowski and Broniek (2017)
Golden shower	800, 4	K_2CO_3	–	800, air, 4	MG 5	32.6 (233.6)	5.25 (7.25)	1413 (812)	1302 (684)	0.66 (0.38)	0.55 (0.26)	0.11 (0.12)	1.86 (1.87)	71 (76.3)	0.59 (0.19)	27.8 (22.8)	0.6 (0.65)	Tran et al. (2017a,b)
Hazelnut shells	500, 1	K_2CO_3	W C	900, 1	–	–	–	887	–	– (0.403)	–	– (0.013)	–	– (37.61)		– (58.93)	–	Kwiatkowski and Broniek (2017)
Hazelnut shells, M3	450, 1	H_3PO_4	–	–	–	–	–	1492	–	– (1.055)	–	– (0.166)	–	– (39.43)		– (57.67)	–	Kwiatkowski and Broniek (2017)
Hazelnut shells	500, 1	$ZnCl_2$	–	–	–	–	–	1731 m^2/g	–	– (1.043)	–	– (0.110)	–	– (39.95)		– (56.2)	–	Kwiatkowski and Broniek (2017)
Safflower seed	500, –	$ZnCl_2$	–	600, 1	MB	– (16.2)	–	14.1 (249)	(188)	– (0.151)	– (0.08)	– (0.07)	– (2.42)	62.4 (70.44)	1.8 (2.8)	31.6 (23.3)	4.1 (3.5)	Angın et al. (2013a)
				700, 1		– (62.1)		14.1 (491)	(424)	– (0.249)	– (0.17)	– (0.08)	– (2.02)	62.4 (71.7)	1.8 (2.66)	31.6 (22.5)	4.1 (3.1)	
				800, 1		– (107.5)		14.1 (772)	(701)	– (0.357)	– (0.28)	– (0.08)	– (1.85)	62.4 (73.8)	1.8 (2.39)	31.6 (20.8)	4.1 (2.97)	
				900, 1		– (128.2)		14.1 (801)	(707)	– (0.393)	– (0.28)	– (0.11)	– (1.96)	62.4 (76.3)	1.8 (2.26)	31.6 (18.9)	4.1 (2.48)	
Almond Shell, M3	103 days	$ZnCl_2$	(67)	750–850, 2	Phenol, MB	– (70.4) – (1.33)	–	– (736)	–	–	–	–	–	– (79.2)	– (0.64)	–	–	Aygün et al. (2003)
Apricot Stone, M3	103 days	$ZnCl_2$	(70)	750–850, 2	Phenol MB	– (100) – (3.53)	–	– (783)	–	–	–	–	–	– (76)	– (0.49)	–	–	Aygün et al. (2003)
Hazelnut Shells, M3	103 days	$ZnCl_2$	(63)	750–850, 2	Phenol MB	– (145) – (8.82)	–	– (793)	–	–	–	–	–	– (72)	– (1.8)	–	–	Aygün et al. (2003)
Walnut Shell, M3	103 days	$ZnCl_2$	(70)	750–850, 2	Phenol MB	– (126) – (4.11)	–	– (774)	–	–	–	–	–	– (75.3)	– (0.71)	–	–	Aygün et al. (2003)

RBBR, Remazol Brilliant Blue R; PAH, polycyclic aromatic hydrocarbon; d, dehydration process; W C, with cooling, Cu immob.; S, copper immobilization in soil.

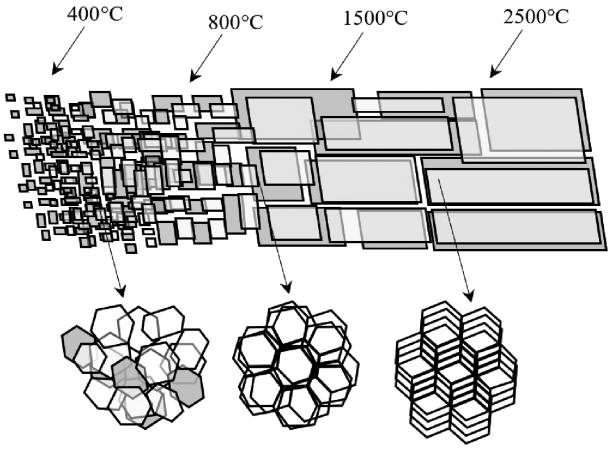

Figure 7: The effect of high temperature thermal treatment (HTT) on biochar structure development: (A) increased proportion of highly disordered aromatic rings in amorphous mass, (B) growing and turbostratically arranging sheets of conjugated aromatic carbon, and (C) structure becomes graphitic with order in the third dimension modified based on Emmerich et al. (1987).

the inorganic species in BC undergo relatively lower conversion to a gaseous phase.

Thermal treatment in the absence of an electron donor or acceptor (inert atmosphere) is accompanied by chemical changes. In thermal treatment, carbonization is a complex process including simultaneous dehydrogenation, isomerization, and hydrogen transfer. This process results in the formation and condensation of C rings and their growth into larger sheets and stacks. When C atoms are transformed into rings with C=C double bonds, the overlap of P-orbitals can probably happen and π-electrons can become delocalized, creating aromatic molecules (Figure 8). Hence, aromaticity increases while the opposite trend is observed for polarity. Higher temperatures cause higher aromaticity (indicated by aromaticity index) and lower polarity (indicated by polarity index (O + N)/C) (Table 12) (Park et al. 2017).

As it is expected, with the progress of thermal annealing, carbon content increases while the oxygen and hydrogen contents decrease due to the loss of H- and O-containing functional groups by dehydration and decarboxylation reactions. A decrease in the oxygen and hydrogen contents is coupled with the release of H_2, CO, CO_2, and CH_4. The evolution of hydrocarbons (e.g. C_2H_4 and C_2H_6), is normally observed at low temperatures, undergoing a slight reduction in high temperatures (Yip et al. 2011). CO and H_2 concentrations increase with temperature, while a reduction in CO_2 concentration is observed. The variation in CO_2 and CO concentrations is justified by the reaction between CO_2 and carbon that produces CO; in other words, a portion of CO_2 is converted to CO at higher temperatures:

$$C(s)+CO_2(g) \leftrightarrow 2CO(g) \qquad \Delta H_{298K} = 173\ kJ/mol \qquad (26)$$

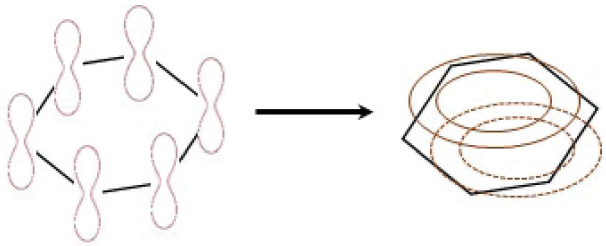

Figure 8: Overlap of P-orbitals and creation of aromatic molecules.

Yip et al. (2011) analyzed BC thermal annealing at temperatures of 750 and 900°C. The authors reported that the gaseous products were predominantly H_2 and, to a much less extent, CO, plus trace amounts of CO_2 and CH_4 at both modifying temperatures. Thermal treatment can be accomplished either in an inert atmosphere (nitrogen, argon) or in the presence of hydrogen or oxidants such as CO_2, steam, air, and/or a strong base (e.g. KOH). As per Table 12, the increment of C content, but in lower intensity, could also be observed for BCs activated under CO_2 or steam atmospheres, which is due to the oxidation followed by desorption of surface oxide as CO from the BC. Reduction of C and O content was also reported wherein the CO desorption is more severe, such as activation under the mixture of steam, CO_2 (Zhang et al. 2015) or under limited oxygen. Zarifyanz et al. (1967) demonstrated that oxygen reacts with graphite at temperatures below −40°C to form surface oxides, which can be readily removed as CO_2 or CO at temperatures above 200°C.

Thermal posttreatment modifies not only the carbonaceous matrix of BC but also the concentration or even the nature of surface functional groups. Generally, carboxylic and lactone groups begin to decompose at about 250°C, and the phenol and quinone groups almost completely decompose between 500 and 900°C. At 900°C, the hydroxyl group decreases drastically and the other oxygen-containing surface functional groups are completely eliminated (Kinoshita 1988, Chiang et al. 2002a). Hence, thermal treatment under an inert atmosphere at a specific temperature could be used to selectively reduce the concentration of surface oxygen groups, while heating in an oxidizing gas or liquid phase might increase such groups. Moreover, heat treatment of BC in an inert atmosphere could increase carbon hydrophobicity by removing hydrophilic groups, particularly acidic surface functionalities (Shin et al. 1997).

Table 12: Effects of microwave irradiation on the physicochemical properties of biochar (numbers in parentheses refer to activated biochar).

Biochar source	Pyrolysis temperature (°C) or MW power (W), time (h)	MW power (W) or temperature (°C), time (min)	Agent time (h)	Adsorbate (mg/g)	Yield (mg/g)	S_{BET} (m^2/g)	S_{micro} (m^2/g)	V_{micro} (cm^3/g)	V_{meso} (cm^3/g)	V_p (cm^3/g)	R_p (nm)	C (%)	H (%)	O (%)	N (%)	Reference
Oat hull	600°C, 3	100°C, 30	Sulfuric acid	–	–	49.3 (30.6)	–	0.008 (0.055)	–	–	–	81.6 (70.6)	2.0 (1.98)	–	1.14 (1.3)	González et al. (2017)
		140°C, 30				49.3 (5.43)		0.008 (0.008)				81.6 (66.3)	2.0 (1.99)		1.14 (0.83)	
Willow	700°C, slow	800°C, 78	CO_2	–	–	11.4 (512.0)	4.5 (380)	0.006 (0.276)	0.002 (0.17)	–	–	69.94 (70.82)	2.08 (0.70)	19.13 (16.37)	1.13 (0.82)	Kołtowski et al. (2017a)
		200°C, 30	H_2O			11.4 (840.6)	4.5 (509)	0.006 (0.577)	0.002 (0.225)			69.94 (56.86)	2.08 (0.59)	19.13 (21.68)	1.13 (0.37)	
		300 W, 45 bar, 10	MW			11.4 (443.2)	4.5 (259)	0.006 (0.242)	0.002 (0.114)			69.94 (73.92)	2.08 (0.95)	19.13 (8.72)	1.13 (0.66)	
Dairy manure	600°C, 4	–	Ni-loaded	–	–	37.4 (36.1)	–	–	0.017 (0.012)	0.018 (0.17)	–	77.6 (75.2)	2.3 (2.17)	8.1 (8.05)		Wang et al. (2017)
		1000 W, 30	Ni-loaded			37.4 (29.8)			0.017 (0.013)	0.018 (0.015)		77.6 (55.3)	2.3 (1.1)	8.1 (65.2)		
Sewage sludge	600°C, 4	–	Ni-loaded	–	–	47 (45.2)	–	–	0.012 (0.011)	0.014 (0.013)	–	65.1 (63.2)	4.42 (4.51)	16.6 (16.5)		Wang et al. (2017)
		1000 W, 30	Ni-loaded			47 (31.5)			0.012 (0.009)	0.014 (0.013)		65.1 (43.1)	4.42 (3.31)	16.6 (39.3)		
Prosopis juliflora	MW-assisted	–	H_2O_2, 24	MB	–	–	–	–	–	–	–	76.44 (70.56)	0.69 (0.28)	20.91 (27.89)	1.96 (1.27)	Nair and Vinu (2016)
		600 W, –	H_2O_2, 24		91.0	(357)	(82.6) Ex	– (0.13)			– (35.4)	76.44 (77.80)	0.69 (0.58)	20.91 (20.65)	1.96 (0.97)	
		300 W, –	H_2O_2, 24		–	(277.5)	(127.2) Ex	– (0.07)			– (94.4)	76.44 (75.13)	0.69 (0.21)	20.91 (22.99)	1.96 (1.67)	
Prosopis juliflora	560 W, 6–0.25	–	H_2O_2, 24	RBBR	–				–	–	–	–	–	–	–	Nair and Vinu (2016)
	500–600°C	600 W, –	H_2O_2, 24		83.3											
		300 W, –	H_2O_2, 24		–											
Peanut hull, M3	500 W, 0.17		H_3PO_4, 24	RBBR	149.3	952.6 (–)		0.8807 (–)	0.2777 (–)	–	–	–	–	–	–	Zhong et al. (2012)
Rice husk	700°C, –	600 W, 7	In KOH	MB	362.6	164 (752)	52 (406) Ex	0.1 (0.64)	0.06 (0.26)	0.04 (0.38)	24.4 (34.1)	–	–	–	–	Foo and Hameed (2011c)
Rice husk	700°C, –	600 W, 7	In K_2CO_3	MB	441.52	164 (1165)	52 (558) Ex	0.1 (0.78)	0.06 (0.33)	0.04 (0.45)	24.4 (26.89)	–	–	–	–	Foo and Hameed (2011c)
Cotton stalk	560 W, 0.15	Best	In $ZnCl_2$	MB	170	794.84 (–)		0.63 (–)	0.083 (–)	–	–	–	–	–	–	Deng et al. (2009)
Orange peel	700°C, –	600 W, 6	K_2CO_3	MB	379.63	6.9 (1104.45)	3.6 (684) Ex	0.615 (0.615)	0.008 (0.247)	0.008 (0.368)	24.8 (22.3)	57.16 (72.66)	1.42 (0.76)	38.37 (24.83)	2.83 (1.54)	Foo and Hameed (2012a)
Jatropha hull	600°C, 1	3000 W, –	–	–	–	480 (1350)	–	0.42 (1.07)	0.4366 (–)	–	3.5 (3.1)	–	–	–	–	Xin-hui et al. (2011b)
Bamboo, M3	350 W, 0.33	–	H_3PO_4	–	–	1432	–	0.696 (–)	0.503 (–)	–	–	84.7 (–)	–	14.0 (–)	–	Liu et al. (2010)
	600°C, 0.5					1215		0.56 (–)	0.448 (–)			83.6 (–)		14.6 (–)		
	600°C, 1					1416		0.673 (–)	0.511 (–)							
Pistachio shell	–	600 W, 7	KOH	MB	296.57	115.5 (700.5)	–	0.069 (0.375)		–	23.4 (21.4) Å		–	–	–	Foo and Hameed (2011b)
Cotton stalk	–	680 W, 10	KOH	MB	294.12	729.3	529.5 (–)	0.38 (–)	0.26 (–)	–	2.08 (–)		–	–	–	Deng et al. (2010)
			K_2CO_3		285.7	621.5	384.7 (–)	0.38 (–)	0.11 (–)		2.43 (–)					
Jatropha hull	–	900°C, 22, Conv.	Steam	–	–	480 (748)	–	0.42 (0.53)		–	3.5 (2.85)		–	–	–	Xin-hui et al. (2011a)
		900°C, 40, Conv.	CO_2			480 (1207)		0.42 (0.86)			3.5 (2.86)					
		900°C, 19, MW	Steam			480 (1350)		0.42 (1.07)			3.5 (3.10)					
		900°C, 30, MW	CO_2			480 (1284)		0.42 (0.87)			3.5 (2.71)					
Pulp mill sludge	400°C, 2	1200 W, 5	KOH:C (1:1)	–	–	– (700)	–	– (0.20)	– (0.36)	– (0.56)	–		–	–	–	Namazi et al. (2016)
		1200 W, 5	KOH:C (3:1)			– (300)		– (0.25)	– (0.16)	– (0.41)						
		1200 W, 5	NaOH:C (1:1)			– (400)		– (0.07)	– (0.11)	– (0.18)						
		1200 W, 5	NaOH:C (3:1)			– (1200)		– (0.056)	– (0.42)	– (0.98)						
		800°C, 120	KOH:C (1:1)			– (500)		– (0.13)	– (0.35)	– (0.48)						
		800°C, 120	KOH:C (3:1)			– (2100)		– (0.46)	– (0.54)	– (1.00)						

Ex, External surface area; MB, methylene blue; RBBR, Remazol Brilliant Blue R; Ye, Conv.: conventional heating; Å, Angstrom.

Exposure to hydrogen gas can effectively stabilize the carbon surface by deactivating some active sites (i.e. by formatting stable C-H bonds and/or gasification of unstable and reactive carbon atoms) and thus producing a more stable and basic carbon surface (Menéndez et al. 1995, Radovic et al. 1997). Accordingly, carbons thermally treated under H_2 atmosphere are expected to have much lower reactivity toward chemical agents and oxygen compared to those treated in an inert atmosphere, indicating that H_2 treatment effectively stabilizes the surfaces of various carbons. As an instance, Dastgheib and Karanfil (2004) found that thermally activated coal-based AC and a commercial AC fiber at 900°C under hydrogen flow had lower amounts of oxygen uptake than the vacuum-treated carbons (Dastgheib and Karanfil 2004).

The effect of oxidants has been discussed in the previous parts of this review, and hence, a brief comparison is presented here to clarify the role of thermal treatment, with a particular focus on the temperature and duration of the process. The mechanism of char (C) activation with CO_2 involves the endothermic Boudouard reaction ($C + CO_2 \leftrightarrow 2CO$), which was explained in Section 2.1.2. The rate of the carbon-CO_2 reaction is temperature dependent and is slow at temperatures below 800°C (Işıtan et al. 2016). Although at high temperatures, micropores are converted to mesopores due to the faster C-CO_2 reaction, it has been reported that both those porosities were identified with an increase in activation temperature from 750 to 850°C (Dodevski et al. 2016). However, a very long activation time, along with a high temperature under CO_2, would destroy the pore skeleton, thereby reducing S_{BET} and the micropore volume of BC (Choi et al. 2015). Similarly, steam activation should also be accompanied by thermal treatment. Hence, in this process, super-heated steam is applied, which enlarges the diameters of smaller pores created during pyrolysis and forms new pores (Kołtowski et al. 2017b). Similar to CO_2 activation, the increase in temperature up to 850°C induces a more severe reaction between carbon and steam that, in turn, raises the number of the activated carbon atoms, generating abundant microporous and some mesopore structures, but with moderate yield. However, since H_2O molecule is smaller than CO_2, the former easily and deeply diffuses to all pores in the network, which increases the reaction rate and the final product. Hence, thermal activation under superheated steam is more effective compared with CO_2 atmosphere (Kołtowski et al. 2017b). In order to raise the effectiveness of CO_2 activation, a prolonged process is recommended. Most authors have applied the thermal treatment of 80 min in the presence of steam, while longer activation periods up to 2 h have been used for CO_2 treatment. At either temperatures above 850°C or activation time beyond 80 min (for steam) and 120 min (for CO_2), the micropores are constantly transformed into mesopores or even macropores. The collapse and loss in numbers of the formed pores result in low adsorption capacity and SSA of the activated carbon.

Compared with steam and CO_2, thermal activation using air is more sensitive to temperature. Hence, most of the research works have focused on physical activation using CO_2 or steam, whereas little attention has been dedicated to oxygen as an alternative approach (Heras et al. 2009). The challenge is that oxygen exhibits a very high reactivity with chars, and the process is very difficult to control. High-temperature air activation may be associated with high burn-off and a poor development of porosity with high percentages of macropores (Heras et al. 2009). On the other hand, activation in low-temperature air (<400°C) favors the formation of stable surface oxides. At higher temperatures (<650°C), only some of the surface oxides can desorb from the surface, and hence, the analysis of relative amounts of stable surface oxides and active sites is more complex in this range of temperature (400–650°C) (Tam and Antal 1999). In order to get benefit from low-temperature activation with air, but also overcoming the problems associated with a high-temperature process, Tam and Antal (1999) used an alternative strategy involving a controlled low-temperature air oxidation by stepwise heating from 180 to 390°C temperatures, followed by thermal treatment at high temperature in an inert gas. By doing so, the authors could produce activated carbons with surface areas greater than 1000 m^2/g. Li et al. (2014) used another strategy by applying a high-temperature thermal treatment followed by cooling and air injection at room temperature. This process caused the formation of new functional groups onto the BC surface. These groups were identified as basic pyrone-type groups resulting from the residual carbonyl group and the ether-type groups formed during pyrolysis.

The synergistic contribution of combined thermal treatment and chemical modification is another determinant factor that will be discussed in a sequel to this study. Aside from the effects of activating agents, three points should be considered in thermal treatment. I) Most authors have reported that final activation temperature had a greater effect on microporosity than final activation time did (Angın et al. 2013a, Jung and Kim 2014). II) Porosity, surface area, and the other physicochemical properties are improved if the BC is cooled down between pyrolysis and the subsequent thermal treatment, compared with processes without cooling (Tam and Antal 1999, Jung and Kim 2014, Kwiatkowski and Broniek 2017). III) Pyrolysis

at temperatures beyond 400°C, prior to thermal activation, has minimal effects on the properties of the resultant activated chars, but the impacts of pyrolysis temperatures lower than 400°C become serious (Işıtan et al. 2016).

The interactions among pore size distribution, surface area, and surface functional groups govern the adsorption capacity of activated BC. After thermal treatment, both the positive and negative impacts of these variables on adsorption capacities have been observed. Here, we discuss the effects of thermal treatment on the adsorption of heavy metals, methylene orange, and PAHs. It should be noted that acid-base reactions and surface charges often govern these interactions in the cases discussed below. Thermal treatment of BC in steam atmosphere showed a negative effect on both Cu and Cd immobilization. The reason is the loss of carboxylic acid (-COOH), carbonyl (C=O), and phenol (-OH) groups at high temperature. These groups could form stable complexes with heavy metals (e.g. $(SCO)_2Cu^{2+}$, $(SCO)_2Cu(OH)^-$ at $pH < 7$), and thus, reduction of their quantity has a negative effect on the specific adsorption of the metals (Shim et al. 2015, Wu et al. 2016). In order to overcome this challenge and utilize the highly condensed aromatic structure and greater micropore volume of thermally treated BC, Park et al. (2017) added humic acid (HA) to the adsorption solution and found that negatively charged surfaces for HA-coated BC enhanced the Cd(II) uptake at low pH. In this case, π-electron delocalization of BC acted as a Lewis base to donate unshared pairs of electrons to metal ions as a Lewis acid (Park et al. 2017). In terms of Hg(II), a remarkable increase in surface area (from 32 to 466 m^2/g) in spite of the reduction in acidic functional groups helped the adsorption process. Hence, thermal treatment, along with KOH modification, resulted in a moderate improvement in the removal of Hg(II) and a significant improvement in the removal of atrazine, compared to pristine BC (Tan et al. 2016).

Thermal activation of BC donates extra adsorption ability to BC too. Veksha et al. (2015) have found that thermally activated BC could remove methylene orange up to 99.48% under microwave irradiation, while unactivated BC could not adsorb it under the same condition. No evidence was found for the formation of hydroxyl radicals or "hot" spots on the BC surface that would cause degradation of methyl orange. In other words, the methyl orange was adsorbed by activated carbon rather than degraded. Similar effects have been reported for adsorption of hydrophobic pollutants such as polycyclic aromatic hydrocarbons. In those cases, BCs synthesized at higher temperatures, which have higher aromaticity than those synthesized at lower temperatures, have been shown to be better sorbents due to higher hydrophobicity and π-π interactions (Park et al. 2013). Hence, thermal treatment of the latter resulted in a great improvement in PAH adsorption compared with high-temperature synthesized BC (Kołtowski et al. 2017b). These results have been confirmed by the other researchers. As an instance, Jung et al. (2013) concluded that thermal activation increased the adsorption capacity toward endocrine disrupting compounds/pharmaceutical active compounds compared to commercialized powdered activated carbon.

2.2.2 Microwave activation

Microwaves are electromagnetic waves with frequencies between 300 MHz (100 cm) and 300 GHz (0.1 cm) and wavelength ranging from 1 m to 1 mm (Huang et al. 2016). Irradiation of microwaves offers quick and uniform internal and volumetric heating through three mechanisms, including ionic conduction, dipole polarization, and the combination of those two, which is called interfacial polarization (Wang et al. 2017). Unlike conventional heating, where heat is transferred from the surface of the material to its interior through convection and conduction phenomena, the entire volume of the material is heated with limited temperature gradient under microwave irradiation via dielectric heating. Heat is then transferred from the core of the material toward its surface. Microwave heating generates tiny microplasma spots throughout the reaction mixture, enhancing the local temperature even at low bulk temperatures. Therefore, the rates of chemical reactions are selectively accelerated while energy consumption is minimized. Although microwave is very beneficial, especially in advanced applications such as BC activation, it cannot be easily employed in large scales (Chu et al. 2017), limiting its industrial application.

Recently, microwave-assisted synthesis and activation of BC have gained much attention. It should be noted that microwave-assisted pyrolysis (MAP) is different from microwave-assisted activation. In the former, microwave energy is used for thermal treatment of biomass to produce BC, while in the latter, microwave energy associated with various chemical reagents is used to selectively treat and modify functional groups in BC that is a key step in chemical activation. In both of these concepts, microwave energy accelerates the process at a lower activation temperature with a shorter duration, which considerably reduces the energy consumption. It was reported that microwave heating can be achieved at pyrolysis temperatures around 200°C (Mašek et al. 2013). Under microwave

irradiation, the polar atoms or molecules of biomass absorb energy, oscillate, and collide with their neighbors. These collisions eventually generate thermal energy that promotes the production of volatiles and the development of a porous structure inside the biomass. An increase in the release of gases like H_2, CO, CO_2, CH_4, C_2H_4, and C_2H_6 under microwave irradiation compared to conventional heating assists the formation of pores in the char.

However, due to localized high temperatures, CO_2 concentration in the gases produced under microwave irradiation is significantly lower compared with those produced with conventional heating. Consistent with this and aforementioned hypothesis, Menéndez et al. (2007) reported that the CO/CO_2 ratio is much higher for microwave pyrolysis than that under conventional pyrolysis in an electrical furnace at a relatively low temperature of 500°C. Moreover, localized high temperatures also assist the H_2 and CO production reactions:

$$CH_4 + CO_2 \leftrightarrow 2CO + 2H_2 \qquad \Delta H_{298\,K} = 260.5\ \text{kJ/mol} \tag{27}$$

$$CH_4 \leftrightarrow C + 2H_2 \qquad \Delta H_{298\,K} = 75.6\ \text{kJ/mol} \tag{28}$$

Hence, the concentrations of H_2 and CO in the gases produced by microwave were much higher than that of their counterparts obtained by conventional heating (Menéndez et al. 2007). Aside from temperatures, the yield of pyrolysis under microwave irradiation is greatly influenced by feedstock materials (Chu et al. 2017). In other words, microwave absorber (Lin and Chen 2015) plays a significant role in the pyrolysis yield. Microwave adsorption abilities are not similar for all materials, and biomass is among the materials with low absorption ability. Thus, the desired pyrolysis temperature cannot be obtained by just irradiating a pure biomass with direct microwave irradiation. Hence, microwave absorbers (e.g. metallic oxides or charcoal) can be impregnated into biomass structure, be heated by microwave radiation, and then indirectly transfer the heat energy to the neighbors by conduction, causing them to decompose. However, in such a condition, the catalytic effects of the microwave absorber, the mechanism of the process, and biomass pyrolysis char cannot be easily specified (Menéndez et al. 2004, Wang et al. 2009). More details about MAP in the production of BC with different pore structures and surface areas can be found in Ahmed (2016) and Nair and Vinu (2016). A comprehensive literature review in this area was also presented by Li et al. (2016).

Aside from pyrolysis, there are three major characteristics of microwave-assisted activation compared with the conventional thermal activation. I) Temperature is controlled by both activating agent ratio and the microwave power. II) Activation temperature during the process is not constant, due to the reactions involving carbon loss from BC and consumption of the activating agent. III) Activation rate is normally higher when heating with microwaves (Namazi et al. 2016). Hence, microwave power and duration should be carefully designed and controlled to develop an efficient process for the activation of BC. Higher activation power should be associated with shorter duration and vice versa. As per Table 12, depending on the biomass source, the best results with the activation power of 200 and 350 W are obtained in 30 and 25 min, respectively, while as the microwave power increased up to 600, 800, and 1200 W, the process can be accomplished in shorter durations of 6–7, 4–5, and 2–3 min, respectively. However, it should be noted that microwave activation could only be achieved in a very short period of time compared to furnace activation. An increase in either power intensity or activation duration beyond the optimal value results in a reduction of micropore and mesopore volumes and, hence, SSA, micropore, mesopore, and total pore volumes (Namazi et al. 2016). Optimal microwave power is usually adopted when the average SSA and pore diameter/area/volume are at their maximal, but microwave power does not cause any overgasification with its detrimental impact. Generally, increasing the microwave power until its optimal value enhances the number of microscale explosions, joining the micropores together, and ultimately results in the formation of narrow and deep mesopores. Beyond optimal power, overgasification might occur due to the higher density of microplasma spots, resulting in the destruction of the pore structures and carbon burn (Foo and Hameed 2011a, 2012b, Nair and Vinu 2016, Chu et al. 2017). In other words, more micropore and mesopores are created at optimal conditions (power, duration, and temperature), while an increase in those parameters beyond their optimal values destroys the porosity of the BC structure. However, the addition of chemical reagents changes the balance of the activation reaction. Compounds such as KOH, NaOH, K_2CO_3, and H_2O_2 under microwave irradiation are expected to be the main wave absorbers. These compounds assist the process to promptly reach the activation temperature (in the range of 500–800°C) (Namazi et al. 2016). Therefore, chemical supply should be sufficient to accelerate the activation reaction and develop the surface area as carbon is consumed. The addition of chemical activation with alkali metal hydroxides resulted in the generation of a highly porous and dense carbon AC with a high surface area (Lam et al. 2017). Namazi et al. (2016) investigated the effect of KOH and NaOH during

chemical activation of a BC sample using microwaves. The authors found that NaOH-activated carbon produced with microwaves in a short duration (5 min) had similar properties and yield with those activated by the conventional furnace in 1.5 h. In other words, KOH and NaOH as microwave absorbers increased the rate of activation by 15 times compared with the furnace activation. The SSA and micropore and mesopore volumes all were significantly higher in NaOH-activated BC, while activation yield was greater in the system containing KOH. The authors concluded that the smaller size of NaOH ions could facilitate the temperature rise during microwave activation, and hence, the rate of the NaOH activation reaction is higher than that with KOH in microwaves (Namazi et al. 2016).

In terms of the potential benefits of microwaves compared to conventional heating methods, most authors have reported that microwave-assisted production or activation is a more efficient process due to its rapid rise and uniform distribution of temperature in carbon substrates. For example, Chu et al. (2017) compared the properties of peanut shell BCs produced by using MW and muffle furnace. At an equal temperature, MW BCs possessed larger surface areas due to the higher population of micropores and exhibited higher adsorption of bisphenol A and carbamazepine than those produced in the conventional furnace.

Although carbonization and condensation in both conventional and microwave heating result in decreased O and H and increased C contents with increased temperature, the quantity of elemental composition change is less dramatic in MW BCs. Therefore, the atomic ratios of H/C and (O + N)/C and the subsequent polarity and the abundance of functional groups are usually higher for MW-treated BCs (Chu et al. 2017). Additionally, if the solution is air bubbled, microwave activation can capture more O element from the air and transfer it on BC surface, resulting in oxidation of the surface groups (Park and Sujandi 2008, Yin et al. 2009). Hence, MW oxidation is an effective method for activation of BC to adsorb heavy metals. As an example, Wang et al. (2017) used microwave oxidation in order to convert the heavy metal-loaded BC into supercapacitor and to promote its electrochemical property. The results showed an increase in capacitance of the MW-treated Ni-loaded BC supercapacitor, mainly because of the conversion of Ni into NiO and NiOOH. H_2O_2 is another oxidizing agent that can induce the generation of hydroxyl radical during the microwave treatment (Huff and Lee 2016). BC treated by H_2O_2-assisted microwave exhibited superior performance compared to untreated char in the adsorption of dyes (60% improvement) (Nair and Vinu 2016). Other functional groups can also be easily introduced to the structure of BC under microwave irradiation. As an example, in order to produce an efficient catalyst for transesterification reaction (biodiesel production), González introduced sulfonic groups in BC using a microwave reactor, which resulted in a 90% increment in transesterification yield (González et al. 2017).

2.3 Ultrasound activation

Acoustic cavitation consists of at least three distinct, successive stages: nucleation, bubble growth, and implosive collapse (Ince et al. 2001). During the collapse stage, the energy released is so extreme that trapped gases undergo molecular fragmentation, which is the underlying phenomenon in homogeneous sonochemistry. This collapse is accompanied by the emission of light, or sonoluminescence (SL; Suslick and Flannigan 2008). Spectroscopic analysis of SL reveals that temperature and pressure can reach 5000 K and 1000 bar, respectively, in clouds of cavitating bubbles and even more extreme conditions in isolated single bubble cavitation. The implosive collapse of bubbles generates a shock wave that propagates out into the liquid medium. The thin shell of liquid surrounding the collapsing bubbles and the liquid droplets injected into the bubbles can reach 1900 and 5200 K, respectively. Moreover, bubble collapse near a solid surface disrupts the spherical shape of the bubble and induces the formation of microjets that can impact the surface in addition to the shock wave. The results of this physical process include mixing, erosion, and particle collisions. The combined primary sonochemical reactions in the gas phase, the secondary sonochemical reactions in the liquid phase, and the physical impact of bubble collapse have generated many novel technological concepts in the last three decades (see, e.g. Chatel and Colmenares 2017), such as the manufacturing the nanostructured materials (Hinman and Suslick 2017). In the case where water is sonicated, water splitting during the bubble-collapse stage leads to the formation of oxygen, hydroxyl, and peroxyl radicals (Kohno et al. 2011), which are attractive for oxidizing organic waste in water and for the oxidative desulfurization of fuels (Pethrick 1991). Strongly reducing protons also form during water splitting. Thus, oxidation, hydrogenation, and hydroxylation can take place simultaneously in sonicated aqueous solutions.

Sonication has been widely adopted to enhance mixing and reduce mass transfer limitations in liquid/solid interactions. Ultrasound is also capable of leaching fine minerals such as K, Na, S, Cl, P, Mg, Ca, Fe, and Al from porous carbonaceous materials (Ahmad et al. 2004). As a result of

leaching of minerals and swelling of BC by a solvent such as water, the internal surface area of the carbon increases. The internal surface area is a major factor governing the adsorption capacity and latitude to chemically functionalize the interface surface of BC for subsequent adsorption. Three to five stacked graphitic and graphitic oxide sheets with a vertical height of 1–2 nm and a lateral extension of 2–5 nm form the backbone of the BC structure (Kleber et al. 2015). Graphite can be oxidized to graphite oxide, producing intercalated hydroxyl and epoxide groups and a disrupted sp^2-bonded carbon network. Stankovich et al. (2006) demonstrated that graphite oxide in phenyl isocyanate can be completely exfoliated by ultrasound (150 W) for 1 h, producing single-layer graphene oxide (GO). Exfoliated GO platelets are expected to offer higher contact surface area than graphitic oxide clusters.

The water splitting, leaching of minerals, and exfoliation stated above provide bases for a novel approach for activating BC (Chen et al. 2014, Mulabagal et al. 2017). It was demonstrated that exfoliation of graphitic oxide clusters, reductive CO_2 fixation, hydrogenation, and leaching of minerals take place simultaneously in a single-stage BC/CO_2/H_2O system under ultrasound irradiation at 65°C and 1 atm. The ultrasonic treatment simultaneously induces desired physical and chemical changes on BC, including not only graphite oxide exfoliation, water splitting, and leaching of minerals but also carboxylation, hydrogenation, and swelling. The treated BCs mainly have a higher internal surface area, heating value, and reaction rates. The energy throughput for this activation is much lower than the traditional methods. As a comparison, thermal treatment alone without acoustic irradiation induces a similar increase in internal surface area, but a loss in hydrogen and no notable change in carbon content.

Specifically, the BET surface area of BC samples were found to increase from 12.9 to 151.4 m^2/g after acoustic treatment in water/CO_2 (Chen et al. 2014). It was observed that CO_2 plays an important role in enhancing the internal surface area. This activation approach is simple and requires only reagents that are readily available everywhere, as shown in Figure 9. Considering the remarkably lower temperature adopted in the proposed treatment, the energy and cost of the new activation procedure are likely to be competitive in comparison with current carbon activation methods. Our calculation revealed that the energy consumptions in traditional thermal and acoustics activation are 18,600 and 1135 kcal/kg of activated BC produced, respectively (Chen et al. 2014). Due to this notably low energy consumption, the cost of activated carbon production is reduced to $1.56 per pound. The current listed price of activated carbon from coconut shell on the Internet varies from the US$2.83 to US$4.8 per pound (Delta Adsorbent 2018). The acoustic activation concept is still in its very early stages of development. The observed synergisms of sorghum BC of Chen et al. (2014) likely depend on biomass origin, the thermal history of BC, and treatment conditions. Moreover, surface functionality and pollutant adsorption capacity have not been systematically investigated. Nevertheless, our recent studies revealed that ultrasound treatment of BC in a CO_2/H_2O system enhances the adsorption capacity of spilled oil in contaminated water. We also found that ultrasound-assisted functionalization of BC enhances the CO_2 capture capacity up to 9 times greater than that of raw BC. As a summary, recent studies of ultrasound activation of BC have demonstrated that it is a fruitful research topic that can lead to many exciting new technologies. Ultrasound-assisted surface modification of BC seems to be an emerging research topic to explore.

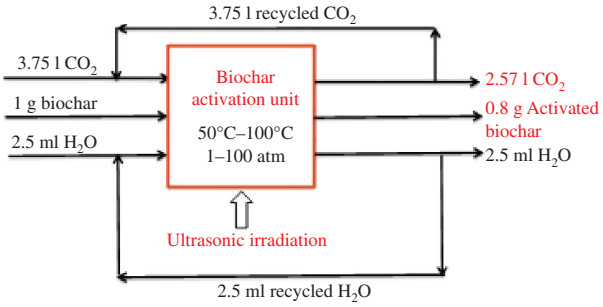

Figure 9: The proposed biochar activation by ultrasound. Raw biochar is produced from inert-gas pyrolysis of biomass in bio-oil production or lignin after pretreatment in a biological conversion of biomass. The proposed activation is conducted at 65°C, a temperature that is well below traditional char activation temperatures, 600–900°C. The activated biochar has a significantly higher internal surface area and will be tested for adsorption of pollutants in water and waste water (Chen et al. 2014, Mulabagal et al. 2017).

2.4 Plasma activation

Plasma is the fourth state of matter, which, unlike the other three (gas, liquid, and solid), does not naturally exist and is produced by electric discharge. Electric current and voltage affect the neutral and charged particles in the plasma, which, in turn, affect the temperature and ionization density of the plasma. Plasma systems are typically classified on the basis of their plasma generation method, and/or thermodynamic equilibrium state of the plasma. In the former, direct current, alternate current, radiofrequency (RF), and microwave make the main plasma generators, and the latter category is divided

into equilibrium plasma (high temperature or fusion plasma), quasi-equilibrium plasma (thermal plasma or low-temperature plasma), and nonequilibrium plasma (nonthermal plasma [NTP] or cold plasma) (Karim et al. 2017). Depending upon the application, thermal plasma reactors operate with power levels ranging from few hundred watts to tens of megawatts (Karim et al. 2017). The thermal plasma process is a promising method for pyrolysis and gasification. Compared with conventional heating in traditional furnaces or reactors, the presence of a highly active plasma environment with different activated ions, electrons, atoms, and molecule in plasma reactors leads to a higher energy density, faster reaction rate, and lower formation of heavy tarry compounds. Quick start-up and shut down of the plasma reactors due to their rapid heating and cooling rate are the other benefits of such reactors over conventional furnaces (Karim et al. 2017). NTP has also gained much attention in BC activation and modification. The high electron energy emitted by the plasma can easily break the surface chemical bonds in a short duration (a few minutes to 30 min; Gupta et al. 2015, Niu et al. 2017) and chemically transform the surface to the desired textural properties with the least undesired changes. Unlike traditional activation methods in which chemical washing and prolonged drying are of the necessary steps, no chemical compound is added to plasma system and no toxic pollutant is generated as well; hence, plasma treatment is considered as an eco-friendly method (Niu et al. 2017). Depending on the desired functional groups to be created, the addition of gas species is a key step in NTP modification. In order to increase the quantity of oxygen-containing functional groups on the surface, BC is usually exposed to the ionized oxygen for at least 0.1–5 min (maximum 60 min) within a temperature range of about 15–30°C (Lee 2013, pp. 39–40). According to Gudmundsson et al. (2000), four charged species can be formed in oxygen plasma: i) electrons; ii) O_2^+ created by electron impact ionization of the O_2 molecule and the metastable oxygen molecule $O_2(a^1\Delta_g)$; iii) O^+ created by electron impact ionization of excited oxygen atoms $O(^1D)$, oxygen atoms $O(^3P)$, and O_2 pair creation; and iv) O^- created mainly by dissociative attachment. These species contribute to a set of chain reactions, which have been summarized by Gudmundsson et al. (2000), as also provided in Table 13. In these equations, $O(^3P)$ and $O(^1D)$ are very reactive atomic oxygens that tend to quickly bond with nearby molecules. The O atom in an excited singlet state is named $O(^1D)$, which is rapidly stabilized to $O(^3P)$ by collision with O_2 (R27) or a third party (M, e.g. N_2 if there is in the system [R28]). O atom in the ground-level triplet state with two unpaired electrons is named $O(^3P)$, which is rapidly combined with O_2 to form ozone ($O(^3P) + O_2 + M \rightarrow O_3 + M$) (Biedenkapp et al. 1970, Gudmundsson et al. 2000, Kogelschatz 2003). These active species might react with carbon surface and generate oxygen-containing functional groups, especially carbonyl groups. Zhou et al. (2012) observed that plasma modification of activated carbon fibers using a mixture of N_2 and O_2 results in a significant increase in C=O (at 287.0 ev) (55.6%), a remarkable decrease in C-O (at 285.5 ev, C-OH, C-O-C) (46% reduction), and slight increases in COOH quantity. In the presence of steam, water ion clusters ($O_2^+ \cdot H_2O$) are generated, which are further dissociated to ·OH (R28 and R29). Afterward, O_3 (which is produced from the reaction between $O(^3P)$ and O_2) might be consumed to produce ·OH (R30 and R31), participating in the generation of more oxygen-containing functional groups (OCFGs). Moreover, the presence of H_2O in the gas mixture facilitates the direct decomposition of H_2O into ·OH via R32, and the ·OH generated is involved in producing the OCFGs onto carbon surface (Bai et al. 2012, Niu et al. 2017). However, in dried oxygen-containing gas or air, reactive oxygen species (O_2^+) may be quenched due to its short lifetime.

$$O_2^+ + H_2O + M \rightarrow O_2^+ \cdot H_2O + M \quad (29)$$

$$O_2^+ \cdot H_2O + H_2O \rightarrow O_2 + H_3O^+ + \cdot OH \quad (30)$$

$$H_2O + O_3 \rightarrow H_2O_2 + O_2 \quad (31)$$

$$H_2O_2 \rightarrow {}^{\cdot}OH + {}^{\cdot}OH \quad (32)$$

$$e + H_2O \rightarrow e + {}^{\cdot}OH + H \quad (33)$$

Niu et al. (2017) introduced different concentrations of moisture in a plasma containing N_2 and O_2. The authors reported an increase in the C=O functional group up to 3-fold of that in raw BC (28.44% in modified BC versus 9.45% in raw BC), which, in turn, enhanced the adsorption capacity of the modified BC for elemental mercury (Hg^0) up to 3.2 and 4.7 times compared with two commercial activated carbons. The authors observed a slight decrease in the surface area and pore volume of modified BCs due to the damage to pore structure. Although exposure to the ionized oxygen is normally used in plasma treatment of BC, other gases have also been used. In order to enhance energy storage in supercapacitors, Fan et al. (2016) activated BC by using a methane (10%)/argon mixture. The results showed a significant improvement in specific capacitance of BC (from 135.6 to

Table 13: The reaction set for oxygen plasma.

Reaction	Rate coefficient ($m^3\ s^{-1}$)	Reference
$e+O_2 \rightarrow O_2^+ + 2e$	$k_1 = 9\times10^{-16} T_e^2 \exp(-12.6/T_e)$	Lee et al. (1993)
$e+O_2^+ \rightarrow O+O$	$k_2 = 5.2\times10^{-15}/T_e$	Kossyi et al. (1992)
$e+O_2 \rightarrow O(^3P)+O^-$	$k_3 = 8.8\times10^{-17} \exp(-4.4/T_e)$	Lieberman and Lichtenberg (2005)
$e+O(^3P) \rightarrow O^+ + 2e$	$k_4 = 9\times10^{-15} T_e^{0.7} \exp(-13.6/T_e)$	Lieberman and Lichtenberg (2005)
$O^- + O_2^+ \rightarrow O(^3P)+O_2$	$k_5 = 1.5\times10^{-13} (300/T_g)^{1/2}$	Lee et al. (1993)
$O^- + O_2^+ \rightarrow O(^3P)+O(^3P)$	$k_6 = 2.5\times10^{-13}(300/T_g)^{1/2}$	Lee et al. (1993)
$e+O^- \rightarrow O(^3P)+2e$	$k_7 = 2\times10^{-13} \exp(-5.5/T_e)$	Lieberman and Lichtenberg (2005)
$e+O_2 \rightarrow O(^3P)+(^3P)+e$	$k_8 = 4.2\times10^{-15} \exp(-5.6/T_e)$	Lee et al. (1993)
$O+O^- \rightarrow O_2+e$	$k_9 = 3.0\times10^{-16}(300/T_e)^{1/2}$	Lieberman and Lichtenberg (2005)
$e+O_2 \rightarrow O^- + O^+ + e$	$k_{10} = 7.1\times10^{-17} T_e^{0.5} \exp(-17/T_e)$	Lieberman and Lichtenberg (2005)
$e+O_2 \rightarrow O^- + O^+ + 2e$	$k_{11} = 5.3\times10^{-16} T_e^{0.9} \exp(-20/T_e)$	Lieberman and Lichtenberg (2005)
$O^+ + O_2 \rightarrow O(^3P)+O_2^+$	$k_{12} = 2\times10^{-17}(300/T_g)^{1/2}$	Eliasson et al. (1986)
$e+O_2 \rightarrow O(^3P)+O(^1D)+2e$	$k_{13} = 5\times10^{-14} \exp(-8.4/T_e)$	Lee et al. (1993)
$e+O(^3P) \rightarrow O(^1D)+e$	$k_{14} = 4.5\times10^{-15} \exp(-2.29/T_e)$	Lee et al. (1993)
$O(^1D)+O_2 \rightarrow O(^3P)+O_2$	$k_{15} = 4.11\times10^{-17}$	Lee et al. (1993)
$O(^1D)+O \rightarrow 2O(^3P)$	$k_{16} = 8.1\times10^{-18}$	Lee et al. (1993)
$e+O(^1D) \rightarrow O^+ + 2e$	$k_{17} = 9\times10^{-15} T_e^{0.7} \exp(-11.6/T_e)$	Lee et al. (1993)
$e+O_2 \rightarrow O_2(a^1\Delta_g)+e$	$k_{18} = 1.7\times10^{-15} \exp(-3.1/T_e)$	Lieberman and Lichtenberg (2005)
$e+O_2(a^1\Delta_g) \rightarrow O_2(a^1\Delta_g)+2e$	$k_{19} = 9.0\times10^{-16} T_e^2 \exp(-11.6/T_e)$	Lieberman and Lichtenberg (2005)
$e+O_2(a^1\Delta_g) \rightarrow O^- + O$	$k_{20} = 2.28\times10^{-16} \exp(-2.29/T_e)$	Burrow (1973)
$e+O_2(a^1\Delta_g) \rightarrow O_2+e$	$k_{21} = 5.6\times10^{-15} T_e^2 \exp(-2.2/T_e)$	Lieberman and Lichtenberg (2005)
$e+O_2(a^1\Delta_g) \rightarrow 2O+e$	$k_{22} = 4.2\times10^{-15} T_e^2 \exp(-4.6/T_e)$	Lieberman and Lichtenberg (2005)

T_g, Gas "temperature" (K); T_e, electron "temperature" (eV).

149 F g^{-1} for oxygen and 149.4 F g^{-1} for methane) and its impedance (from 0.65 to 2.37 Ω for oxygen and 1.22 Ω for methane). Decomposition of methane follows the bellow mechanism (where e* is the energetic electron) (Futamura and Annadurai 2005):

$$CH_4 + e^* \rightarrow {}^{\cdot}CH_3 + {}^{\cdot}H + e \quad (34)$$

$$CH_4 + {}^{\cdot}H \rightarrow {}^{\cdot}CH_3 + H_2 \quad (35)$$

Recently, Wang et al. 2018 used chlorine (Cl) NTP to increase Cl active sites on six BCs of different origins to promote elemental mercury removal. BC from tobacco straw showed a 36-fold increase in mercury adsorption capacity after treatment with Cl_2 plasma. An XPS study revealed that the main reason for this remarkable improvement in BCs relied on the increased number of C-Cl groups on the surface of the BCs, which functioned as active sites and promoted the conversion of Hg^0 to HgCl and $HgCl_2$. The plasma induces higher porosity, but surface area is not the major variable governing the enhancement in adsorption capacity. The plasma treatment also caused transformation of S and O functionalities of BCs.

BC activation by plasma is a relatively new field, and only a few researchers have compared it with other modification methods. In their patent, Fan et al. (2016) analyzed the activation of BC by oxygen plasma and compared it with chemical activation by using NaOH followed by a thermal treatment. The authors reported that 5 min of plasma activation at 50 W RF significantly increased

the oxygen content of BC (from 9.86 to 15.69%), while O content enhanced to the value of 12.86% in chemical activation by NaOH. Gupta et al. (2015) reported that oxygen plasma activated yellow pine BC yielded much higher specific capacitance (e.g. 171.4 F g^{-1}) than chemically activated BC (99.5 F g^{-1}) and untreated BC (60.4 F g^{-1}). The authors also demonstrated that, unlike chemical activation, which created uniformly sized micropores, oxygen plasma efficiently created porous structures that combined micropores, mesopores, and macropores (Gupta et al. 2015).

The surface chemical bonds of carbonaceous compound can easily be broken by the highly active free radicals generated in plasma medium. Therefore, plasma treatment usually takes a short time. In most of the aforementioned examples, BCs have mainly been exposed to plasma for a minimum duration of 0.1–5 min to a maximum of 60 min (Lee 2013, pp. 39–40). Moreover, both high temperature (around 100°C; Gupta et al. 2015) and low temperature (e.g. room temperature; Lee 2013, pp. 39–40) can be used to introduce oxygen functional groups onto BC and increase BC O:C ratios. Besides, RF source (e.g. 13.56 MHz at an RF power of about 10–100 W) is used to ionize the oxygen. Therefore, a very low amount of energy is consumed in this procedure. However, the C and O content and their ratio depend on the competition of oxygen-containing functional groups. For example, C-C (284 eV) and C=O (287 eV) significantly increased, while an opposite trend was observed for C-O (285.5 eV). Hence, the resultant surface element (O/C) decreased in modified BC in the work of Zhou et al. (2012), while a slight increase in (O/C) was observed in the work of Niu et al. (2017) due to the significant increase in C=O (531.1 eV) and some other oxygen-containing peaks at 532.3 eV. Therefore, although plasma treatment can be considered as a promising technique for BC modification or activation, it is not a simple process of introducing oxygen-containing functional groups into a sample surface, but a complicated process of tradeoff and refreshing.

2.5 Electro/electrochemical modification

An electric field can also modify the physicochemical properties of BC. Enhancement of BC surface area and impregnation of chemicals on the surface are simultaneously achieved in electro or electrochemical modification, which was first suggested by Jung et al. (2015a). The authors successfully modified the physical (porosity) and chemical (functionality) properties of BC by applying a current of 93.96 mA/cm^2 in a system of aluminum-based electrode with the presence of H_2SO_4 and NaOH solutions within 5 min, followed by pyrolysis at 450°C for 2 h. Generally, in the electrochemical process, hypochlorous acid and hypochlorite ions ($HOCl/OCl^-$) are generated in the presence of NaCl solution. These two strong oxidants can significantly improve the porosity and morphology of BC. Simultaneously, if an aluminum electrode is used in the process, aluminum ions are generated at the anode side. These ions, which predominantly exist in the solution below pH 4.0, can be employed as a precursor for the formation of the nanosized crystalline structures containing aluminum (AlOOH, beohemite), which is an environmentally friendly material for applications in natural water, onto the BC surface (Jung et al. 2015a). Based on the aforementioned discussion, Jung and Ahn (2016) developed a combined electrochemical modification (CEM) method, using a graphite electrode-based electric field and $MgCl_2$ as the electrolyte, in their subsequent work. The authors immersed the dried marine macroalgae in the $MgCl_2$ solution prior to pyrolysis to prepare porosity-enhanced BC containing periclase (MgO) nanocomposites, under the voltage of 20 V for 10 min. The dual advantages of electrochemical modification of CEM-modified BC by using the aluminum and graphite electrode-based setup were further demonstrated by a significant increase (up to 4 (Jung et al. 2015a) to 7 (Jung and Ahn 2016) times) in BC adsorption capacities toward phosphate, compared to raw BC. $MgCl_2$ as an electrolyte creates strong oxidants (i.e. HOCl and OCl^-) in the aluminum-electrode-based system that further improves the porosity and texture properties of BC, and disperses of Mg-nanocomposites (e.g. MgO, spinel $MgAl_2O_4$, AlOOH, and Al_2O_3) on the surface resulted in higher phosphate adsorption (Jung et al. 2015b). It should be noted that electric techniques have great potentiality in BC modification or activation. Therefore, further researches in this field are required, which can be an open topic for future work.

3 Conclusion

With the rapid increase in the application of BCs, the necessity of improving its physicochemical properties in an environmentally friendly manner at a reasonable cost, but with the most desired outcome, has become increasingly important. Therefore, studies on classic physical or chemical modification methods have significantly increased. Meanwhile, various promising strategies are also being developed. This review lays great emphasis on the physical modification and activation of BC that are categorized into traditional gas modifications (using steam,

CO_2, ozone, and air), thermal modifications (conventional and microwave), and the most recent techniques including ultrasound modification, plasma modification, and electrochemical modification. Moreover, the synergistic and antagonistic interaction between pyrolysis and modification conditions was presented with significant attention to their effects on micro/macro surface area (S_{micro} and S_{BET}), micro/macro pore volume (V_{micro} and V_{macro}), total pore volume (V_p), pore size (R_p), ash content, pH, aromaticity (H/C), and polarity (O + N)/C of BC. In addition, the effect of each activation method on the distribution of the various functional groups and their impacts on BC applications were discussed. This review also highlighted the effect of each modification method on its related BC application, along with the recent advances that are undergoing more research studies and are therefore open topics for future works.

Acknowledgments: The authors are grateful for the financial support by the National Science Foundation (NSF EPSCoR RII grant no. OIA-1632899). Various other support from the University of Mississippi is also gratefully acknowledged.

References

Abioye AM, Ani FN. The characteristics of oil palm shell biochar and activated carbon produced via microwave heating. Appl Mech Mater 2015; 695: 12–15.

Ahmad I, Khan MA, Shakirullah M, Ishaq M. Effect of leaching time on the removal of lithophile elements of operational concern from coal samples. J Chem Soc Pak 2004; 26: 107–110.

Ahmed MJ. Application of agricultural based activated carbons by microwave and conventional activations for basic dye adsorption: review. J Environ Chem Eng 2016; 4: 89–99.

Ahmed MB, Zhou JL, Ngo HH, Guo W, Chen M. Progress in the preparation and application of modified biochar for improved contaminant removal from water and wastewater. Bioresource Technol 2016; 214: 836–851.

Andreozzi R, Caprio V, Insola A, Marotta R. Advanced oxidation processes (AOP) for water purification and recovery. Catalysis Today 1999; 53: 51–59.

Angın D, Altintig E, Köse TE. Influence of process parameters on the surface and chemical properties of activated carbon obtained from biochar by chemical activation. Bioresource Technol 2013a; 148: 542–549.

Angın D, Köse TE, Selengil U. Production and characterization of activated carbon prepared from safflower seed cake biochar and its ability to absorb reactive dyestuff. Appl Surf Sci 2013b; 280: 705–710.

Arriagada R, García R. Molina-Sabio M, Rodriguez-Reinoso F. Effect of steam activation on the porosity and chemical nature of activated carbons from Eucalyptus globulus and peach stones. Microporous Mater 1997; 8: 123–130.

Atkinson R, Arey J. Gas-phase tropospheric chemistry of biogenic volatile organic compounds: a review. Atmospheric Environ 2003; 37: 197–219.

Aworn A, Thiravetyan P, Nakbanpote W. Preparation and characteristics of agricultural waste activated carbon by physical activation having micro- and mesopores. J Analytical Appl Pyrolysis 2008; 82: 279–285.

Aygün A, Yenisoy-Karakaş S, Duman I. Production of granular activated carbon from fruit stones and nutshells and evaluation of their physical, chemical and adsorption properties. Microporous Mesoporous Mater 2003; 66: 189–195.

Bach MT. Impact of surface chemistry on adsorption: tailoring of activated carbon. Florida: University of Florida, 2007.

Bach Q-V, Chen W-H, Chu Y-S, Skreiberg Ø. Predictions of biochar yield and elemental composition during torrefaction of forest residues. Bioresour Technol 2016; 215: 239–246.

Bai M, Zhang Z, Bai M. Simultaneous desulfurization and denitrification of flue gas by ·OH radicals produced from O^{2+} and water vapor in a duct. Environ Sci Technol 2012; 46: 10161–10168.

Bailey PS. Ozonation in organic chemistry volume 1: olefinic compounds. New York: Academic Press, 1978.

Bailey PS. Ozonation in organic chemistry volume 2: nonolefinic compounds. New York: Academic Press, 1982.

Bamdad H, Hawboldt K, MacQuarrie S. A review on common adsorbents for acid gases removal: focus on biochar. Renew Sust Energ Rev 2017; 81: 1705–1720.

Biedenkapp D, Hartshorn LG, Bair EJ. The O(1D) + H2O reaction. Chem Phys Lett 1970; 5: 379–381.

Biniak S, Pakuła M, Szymański GS, Świątkowski A. Effect of activated carbon surface oxygen- and/or nitrogen-containing groups on adsorption of copper(II) ions from aqueous solution. Langmuir 1999; 15: 6117–6122.

Blyholder G, Eyring H. Kinetics of graphite oxidation II. J Phys Chem 1959; 63: 1004–1008.

Boehm HP. Chemical identification of surface groups. Adv Catal 1966; 16: 179–274.

Boehm HP. Surface oxides on carbon and their analysis: a critical assessment. Carbon 2002; 40: 145–149.

Bulanin KM, Lavalley JC, Tsyganenko AA. IR spectra of adsorbed ozone. Colloids Surf A Physicochem Eng Asp 1995; 101: 153–158.

Burrow PD. Dissociative attachment from the O2(a1Δg) state. J Chem Phys 1973; 59: 4922–4931.

Calo JM, Hall PJ. Applications of energetic distributions of oxygen surface complexes to carbon and char reactivity and characterization. In: Lahaye J, Ehrburger P, editors. Fundamental issues in control of carbon gasification reactivity. Springer Netherlands, Dordrecht, 1991: 329–368.

Carrier M, Hardie AG, Uras Ü, Görgens J, Knoetze J. Production of char from vacuum pyrolysis of South-African sugar cane bagasse and its characterization as activated carbon and biochar. J Anal Appl Pyrolysis 2012; 96: 24–32.

Cataldo F. Ozone reaction with carbon nanostructures. 2: the reaction of ozone with milled graphite and different carbon black grades. J Nanosci Nanotechnol 2007; 7: 1446–1454.

Cha JS, Park SH, Jung S-C, Ryu C, Jeon J-K, Shin M-C, Park Y-K. Production and utilization of biochar: a review. J Ind Eng Chem 2016; 40: 1–15.

Chatel G, Colmenares JC. Sonochemistry: from basic principles to innovative applications. Top Curr Chem 2017; 375: 8.

Chen N, Yang RT. Ab Initio molecular orbital study of the unified mechanism and pathways for gas-carbon reactions. J Phys Chem A 1998; 102: 6348–6356.
Chen X, Farber M, Gao Y, Kulaots I, Suuberg EM, Hurt RH. Mechanisms of surfactant adsorption on non-polar, air-oxidized and ozone-treated carbon surfaces. Carbon 2003; 41: 1489–1500.
Chen W-Y, Shi G, Wan S. Characterization of early-stage coal oxidation by temperature-programmed desorption. Energy Fuels 2008; 22: 3724–3735.
Chen W-Y, Mattern DL, Okinedo E, Senter JC, Mattei AA, Redwine CW. Photochemical and acoustic interactions of biochar with CO_2 and H_2O: applications in power generation and CO_2 capture. AIChE J 2014; 60: 1054–1065.
Chen W-H, Peng J, Bi XT. A state-of-the-art review of biomass torrefaction, densification and applications. Renew Sust Energ Rev 2015; 44: 847–866.
Chen D, Chen X, Sun J, Zheng Z, Fu K. Pyrolysis polygeneration of pine nut shell: quality of pyrolysis products and study on the preparation of activated carbon from biochar. Bioresour Technol 2016; 216: 629–636.
Chen W-H, Hsu H-J, Kumar G, Budzianowski WM, Ong HC. Predictions of biochar production and torrefaction performance from sugarcane bagasse using interpolation and regression analysis. Bioresour Technol 2017; 246: 12–19.
Chiang H-L, Chiang PC, Huang CP. Ozonation of activated carbon and its effects on the adsorption of VOCs exemplified by methylethylketone and benzene. Chemosphere 2002a; 47: 267–275.
Chiang H-L, Huang CP, Chiang PC. The surface characteristics of activated carbon as affected by ozone and alkaline treatment. Chemosphere 2002b; 47: 257–265.
Choi G-G, Oh S-J, Lee S-J, Kim J-S. Production of bio-based phenolic resin and activated carbon from bio-oil and biochar derived from fast pyrolysis of palm kernel shells. Bioresour Technol 2015; 178: 99–107.
Chu G, Zhao J, Chen F, Dong X, Zhou D, Liang N, Wu M, Pan B, Steinberg CEW. Physi-chemical and sorption properties of biochars prepared from peanut shell using thermal pyrolysis and microwave irradiation. Environ Pollut 2017; 227: 372–379.
Claoston N, Samsuri AW, Husni MHA, Amran MSM. Effects of pyrolysis temperature on the physicochemical properties of empty fruit bunch and rice husk biochars. Waste Manag Res 2014; 32: 331–339.
Cookson J. Adsorption mechanism: the chemistry of organic adsorption on activated carbon. In: Cheremisinoff PN, Ellerbuseh F, editors. Carbon adsorption handbook. New York: Ann Arbor Science, 1978: 241–280.
Corapcioglu MO, Huang CP. The surface acidity and characterization of some commercial activated carbons. Carbon 1987; 25: 569–578.
Dalai AK, Azargohar R. Production of activated carbon from biochar using chemical and physical activation: mechanism and modeling, materials, chemicals, and energy from forest biomass. Am Chem Soc 2007; 463–476.
Daniel JJ. Introduction to atmospheric chemistry, Chapter 10. Princeton, New Jersey: Princeton University Press, 1999.
Dastgheib SA, Karanfil T. Adsorption of oxygen by heat-treated granular and fibrous activated carbons. J Colloid Interface Sci 2004; 274: 1–8.
de Caprariis B, De Filippis P, Hernandez AD, Petrucci E, Petrullo A, Scarsella M, Turchi M. Pyrolysis wastewater treatment by adsorption on biochars produced by poplar biomass. J Environ Manage 2017; 197: 231–238.
Dehkhoda AM, Gyenge E, Ellis N. A novel method to tailor the porous structure of KOH-activated biochar and its application in capacitive deionization and energy storage. Biomass Bioenerg 2016; 87: 107–121.
Delta Adsorbent. Activated carbon granular coconut shell based 4×8 mesh. Delta Enterprises Inc. 2018. https://www.deltaadsorbents.com/activated-carbon-coconut-shell-granular.
Demiral H, Demiral İ, Karabacakoğlu B, Tümsek F. Production of activated carbon from olive bagasse by physical activation. Chem Eng Res Des 2011; 89: 206–213.
Deng H, Yang L, Tao G, Dai J. Preparation and characterization of activated carbon from cotton stalk by microwave assisted chemical activation – application in methylene blue adsorption from aqueous solution. J Hazard Mater 2009; 166: 1514–1521.
Deng H, Li G, Yang H, Tang J, Tang J. Preparation of activated carbons from cotton stalk by microwave assisted KOH and K2CO3 activation. Chem Eng J 2010; 163: 373–381.
Derry GN. Chapter 5-Surface segregation in binary metal alloys A2. Nalwa, Hari Singh, Handbook of surfaces and interfaces of materials. Burlington: Academic Press, 2001: 329–382.
Dodevski V, Stojmenović M, Vujković M, Krstić J, Krstić S, Bajuk-Bogdanović D, Kuzmanović B, Kaluđerović B, Mentus S. Complex insight into the charge storage behavior of active carbons obtained by carbonization of the plane tree seed. Electrochim Acta 2016; 222: 156–171.
Dodevski V, Janković B, Stojmenović M, Krstić S, Popović J, Pagnacco MC, Popović M, Pašalić S. Plane tree seed biomass used for preparation of activated carbons (AC) derived from pyrolysis. Modeling the activation process. Colloids Surf A Physicochem Eng Asp 2017; 522: 83–96.
Dong X, Ma LQ, Zhu Y, Li Y, Gu B. Mechanistic investigation of mercury sorption by brazilian pepper biochars of different pyrolytic temperatures based on x-ray photoelectron spectroscopy and flow calorimetry. Environ Sci Technol 2013; 47: 12156–12164.
El-Sheikh AH, Newman AP, Al-Daffaee HK, Phull S, Cresswell N. Characterization of activated carbon prepared from a single cultivar of Jordanian Olive stones by chemical and physicochemical techniques. J Anal Appl Pyrolysis 2004; 71: 151–164.
Eliasson B, Kogelschatz U, Boveri ABBAB, Segelhof BBF. Basic data for modelling of electrical discharges in gases: oxygen. ABB Asea Brown Boveri, Baden, 1986.
Emmerich WE, Frasier GW, Fink DH. Relation between soil properties and effectiveness of low-cost water-harvesting treatments. Sci Soc Am J 1987; 51: 213–219.
Fan M, Marshall W, Daugaard D, Brown RC. Steam activation of chars produced from oat hulls and corn stover. Bioresour Technol 2004; 93: 103–107.
Fan QH, Dubey MK, Gu ZR. Method for plasma activation of biochar material. Google Patents, 2016.
Fang Q, Chen B, Lin Y, Guan Y. Aromatic and hydrophobic surfaces of wood-derived biochar enhance perchlorate adsorption via hydrogen bonding to oxygen-containing organic groups. Environ Sci Technol 2014; 48: 279–288.

Feng D, Zhao Y, Zhang Y, Sun S, Meng S, Guo Y, Huang Y. Effects of K and Ca on reforming of model tar compounds with pyrolysis biochars under H2O or CO2. Chem Eng J 2016; 306: 422–432.

Feng D, Zhao Y, Zhang Y, Gao J, Sun S. Changes of biochar physiochemical structures during tar H_2O and CO_2 heterogeneous reforming with biochar. Fuel Process Technol 2017a; 165: 72–79.

Feng D, Zhao Y, Zhang Y, Zhang Z, Che H, Sun S. Experimental comparison of biochar species on in-situ biomass tar H2O reforming over biochar. Int J Hydrogen Energy 2017b; 42: 24035–24046.

Feng D, Zhao Y, Zhang Y, Zhang Z, Zhang L, Gao J, Sun S. Synergetic effects of biochar structure and AAEM species on reactivity of H2O-activated biochar from cyclone air gasification. Int J Hydrogen Energy 2017c; 42: 16045–16053.

Feng D, Zhang Y, Zhao Y, Sun S, Gao J. Improvement and maintenance of biochar catalytic activity for in-situ biomass tar reforming during pyrolysis and H2O/CO2 gasification. Fuel Process Technol 2018; 172: 106–114.

Ferreira SD, Lazzarotto IP, Junges J, Manera C, Godinho M, Osório E. Steam gasification of biochar derived from elephant grass pyrolysis in a screw reactor. Energy Convers Manag 2017; 153: 163–174.

Foo KY, Hameed BH. Microwave-assisted preparation of oil palm fiber activated carbon for methylene blue adsorption. Chem Eng J 2011a; 166: 792–795.

Foo KY, Hameed BH. Preparation and characterization of activated carbon from pistachio nut shells via microwave-induced chemical activation. Biomass Bioenergy 2011b; 35: 3257–3261.

Foo KY, Hameed BH. Utilization of rice husks as a feedstock for preparation of activated carbon by microwave induced KOH and K2CO3 activation. Bioresour Technol 2011c; 102: 9814–9817.

Foo KY, Hameed BH. Preparation, characterization and evaluation of adsorptive properties of orange peel based activated carbon via microwave induced K2CO3 activation. Bioresour Technol 2012a; 104: 679–686.

Foo KY, Hameed BH. Textural porosity, surface chemistry and adsorptive properties of durian shell derived activated carbon prepared by microwave assisted NaOH activation. Chem Eng J 2012b; 187: 53–62.

Franklin RE. Crystallite growth in graphitizing and non-graphitizing carbons. Proc R Soc Lond A Math Phys Sci 1951; 209: 196–218.

Fu K, Yue Q, Gao B, Sun Y, Zhu L. Preparation, characterization and application of lignin-based activated carbon from black liquor lignin by steam activation. Chem Eng J 2013; 228: 1074–1082.

Futamura S, Annadurai G. Plasma reforming of aliphatic hydrocarbons with CO2. IEEE Trans Ind Appl 2005; 41: 1515–1521.

Girgis BS, Soliman AM, Fathy NA. Development of micro-mesoporous carbons from several seed hulls under varying conditions of activation. Micropor Mesopor Mater 2011; 142: 518–525.

Glaze WH, Kang JW. Advanced oxidation processes. Description of a kinetic model for the oxidation of hazardous materials in aqueous media with ozone and hydrogen peroxide in a semibatch reactor. Ind Eng Chem Res 1989; 28: 1573–1580.

Glaze WH, Kang JW, Chapin DH. The chemistry of water treatment processes involving ozone, hydrogen peroxide and ultraviolet radiation, ozone. Sci Eng 1987; 9: 335–352.

Gogoi D, Bordoloi N, Goswami R, Narzari R, Saikia R, Sut D, Gogoi L, Kataki R. Effect of torrefaction on yield and quality of pyrolytic products of arecanut husk: an agro-processing wastes. Bioresour Technol 2017; 242: 36–44.

Gómez-Serrano V, Álvarez PM, Jaramillo J, Beltrán FJ. Formation of oxygen complexes by ozonation of carbonaceous materials prepared from cherry stones. Carbon 2002; 40: 513–522.

González ME, Cea M, Reyes D, Romero-Hermoso L, Hidalgo P, Meier S, Benito N, Navia R. Functionalization of biochar derived from lignocellulosic biomass using microwave technology for catalytic application in biodiesel production. Energy Convers Manag 2017; 137: 165–173.

Grima-Olmedo C, Ramírez-Gómez Á, Gómez-Limón D, Clemente-Jul C. Activated carbon from flash pyrolysis of eucalyptus residue. Heliyon 2016; 2: e00155.

Gudmundsson JT, Marakhtanov AM, Patel KK, Gopinath VP, Lieberman MA. On the plasma parameters of a planar inductive oxygen discharge. J Phys D Appl Phys 2000; 33: 1323–1331.

Gümüş D, Akbal F. A comparative study of ozonation, iron coated zeolite catalyzed ozonation and granular activated carbon catalyzed ozonation of humic acid. Chemosphere 2017; 174: 218–231.

Guo S, Peng J, Li W, Yang K, Zhang L, Zhang S, Xia H. Effects of CO2 activation on porous structures of coconut shell-based activated carbons. Appl Surf Sci 2009; 255: 8443–8449.

Gupta RK, Dubey M, Kharel P, Gu Z, Fan QH. Biochar activated by oxygen plasma for supercapacitors. J Power Sources 2015; 274: 1300–1305.

Hammes K, Schmidt MWI. Changes of biochar in soil. In: Lehmann J, Joseph S, editors. Biochar for environmental management, science and technology. United Kingdom: EarthScan, 2009.

Han Y, Boateng AA, Qi PX, Lima IM, Chang J. Heavy metal and phenol adsorptive properties of biochars from pyrolyzed switchgrass and woody biomass in correlation with surface properties. J Environ Manage 2013; 118: 196–204.

Han L, Qian L, Yan J, Chen M. Effects of the biochar aromaticity and molecular structures of the chlorinated organic compounds on the adsorption characteristics. Environ Sci Pollut Res 2017; 24: 5554–5565.

Heras F, Castrodá S, Alonso-Morales N, Gilarranz MA, González V, Rodríguez JJ. Activation with oxygen of the char obtained by waste tyres rubber pyrolysis. Madrid: Universidad Autónoma de Madrid, 2004.

Heras F, Alonso N, Gilarranz MÁ, Rodriguez JJ. Activation of waste tire char upon cyclic oxygen chemisorption-desorption. Ind Eng Chem Res 2009; 48: 4664–4670.

Herath I, Kumarathilaka P, Al-Wabel MI, Abduljabbar A, Ahmad M, Usman ARA, Vithanage M. Mechanistic modeling of glyphosate interaction with rice husk derived engineered biochar. Micropor Mesopor Mater 2016; 225: 280–288.

Hermann G, HÜttinger KJ. Mechanism of water vapour gasification of carbon – a new model. Carbon 1986; 24: 705–713.

Hinman JJ, Suslick KS. Nanostructured materials synthesis using ultrasound. Top Curr Chem 2017; 375: 12.

Huang Y-F, Chiueh P-T, Kuan W-H, Lo S-L. Microwave pyrolysis of lignocellulosic biomass: heating performance and reaction kinetics. Energy 2016; 100: 137–144.

Huff MD, Lee JW. Biochar-surface oxygenation with hydrogen peroxide. J Environ Manage 2016; 165: 17–21.

Hulicova-Jurcakova D, Seredych M, Lu GQ, Bandosz TJ. Combined effect of nitrogen- and oxygen-containing functional groups of microporous activated carbon on its electrochemical performance in supercapacitors. Adv Funct Mater 2009; 19: 438–447.

Ince NH, Tezcanli G, Belen RK, Apikyan İG. Ultrasound as a catalyzer of aqueous reaction systems: the state of the art and environmental applications. Appl Catal B Environ 2001; 29: 167–176.

Ippolito JA, Strawn DG, Scheckel KG, Novak JM, Ahmedna M, Niandou MA. Macroscopic and molecular investigations of copper sorption by a steam-activated biochar. J Environ Qual 2012; 41: 1150–1156.

Işıtan S, Ceylan S, Topcu Y, Hintz C, Tefft J, Chellappa T, Guo J, Goldfarb JL. Product quality optimization in an integrated biorefinery: conversion of pistachio nutshell biomass to biofuels and activated biochars via pyrolysis. Energy Convers Manag 2016; 127: 576–588.

Jans U, Hoigné J. Activated carbon and carbon black catalyzed transformation of aqueous ozone into OH-radicals. Ozone Sci Eng 1998; 20: 67–90.

Jimenez-Cordero D, Heras F, Alonso-Morales N, Gilarranz MA, Rodriguez JJ. Ozone as oxidation agent in cyclic activation of biochar. Fuel Process Technol 2015; 139: 42–48.

Jin H, Wang X, Gu Z, Anderson G, Muthukumarappan K. Distillers dried grains with soluble (DDGS) bio-char based activated carbon for supercapacitors with organic electrolyte tetraethylammonium tetrafluoroborate. J Environ Chem Eng 2014; 2: 1404–1409.

Jung K-W, Ahn K-H. Fabrication of porosity-enhanced MgO/biochar for removal of phosphate from aqueous solution: application of a novel combined electrochemical modification method. Bioresour Technol 2016; 200: 1029–1032.

Jung S-H, Kim J-S. Production of biochars by intermediate pyrolysis and activated carbons from oak by three activation methods using CO2. J Anal Appl Pyrolysis 2014; 107: 116–122.

Jung C, Park J, Lim KH, Park S, Heo J, Her N, Oh J, Yun S, Yoon Y. Adsorption of selected endocrine disrupting compounds and pharmaceuticals on activated biochars. J Hazard Mater 2013; 263: 702–710.

Jung K-W, Hwang M-J, Jeong T-U, Ahn K-H. A novel approach for preparation of modified-biochar derived from marine macroalgae: dual purpose electro-modification for improvement of surface area and metal impregnation. Bioresour Technol 2015a; 191: 342–345.

Jung K-W, Jeong T-U, Hwang M-J, Kim K, Ahn K-H. Phosphate adsorption ability of biochar/Mg–Al assembled nanocomposites prepared by aluminum-electrode based electro-assisted modification method with MgCl2 as electrolyte. Bioresour Technol 2015b; 198: 603–610.

Kamm S, Möhler O, Naumann KH, Saathoff H, Schurath U. The heterogeneous reaction of ozone with soot aerosol. Atmos Environ 1999; 33: 4651–4661.

Kaptijn JP. The Ecoclear® Process. Results from full-scale installations. Ozone Sci Eng 1997; 19: 297–305.

Karim AA, Kumar M, Singh SK, Panda CR, Mishra BK. Potassium enriched biochar production by thermal plasma processing of banana peduncle for soil application. J Anal Appl Pyrolysis 2017; 123: 165–172.

Kastner JR, Miller J, Das KC, Pyrolysis conditions and ozone oxidation effects on ammonia adsorption in biomass generated chars. J Hazard Mater 2009; 164: 1420–1427.

Keiluweit M, Nico PS, Johnson MG, Kleber M. Dynamic molecular structure of plant biomass-derived black carbon (biochar). Environ Sci Technol 2010; 44: 1247–1253.

Kim B-S, Lee HW, Park SH, Baek K. Removal of Cu2+ by biochars derived from green macroalgae. Environ Sci Pollu Res Int 2016; 23: 985–994.

Kinoshita K. Carbon: electrochemical and physicochemical properties. New York: Wiley, 1988.

Kleber M, Hockaday W, Nico PS. Characteristics of biochar: macro-molecular properties, Chapter 6. In: Lehmann J, Joseph S, editors. Biochar for environmental management: science and technology and implementation. New York: Routledge, 2015.

Klüpfel L, Keiluweit M, Kleber M, Sander M. Redox properties of plant biomass-derived black carbon (biochar). Environ Sci Technol 2014; 48: 5601–5611.

Kogelschatz U. Dielectric-barrier discharges: their history, discharge physics, and industrial applications. Plasma Chem Plasma Process 2003; 23: 1–46.

Kohno M, Mokudai T, Ozawa T, Niwano Y. Free radical formation from sonolysis of water in the presence of different gases. J Clin Biochem Nutr 2011; 49: 96–101.

Kołtowski M, Hilber I, Bucheli TD, Oleszczuk P. Effect of steam activated biochar application to industrially contaminated soils on bioavailability of polycyclic aromatic hydrocarbons and ecotoxicity of soils. Sci Total Environ 2016; 566: 1023–1031.

Kołtowski M, Charmas B, Skubiszewska-Zięba J, Oleszczuk P. Effect of biochar activation by different methods on toxicity of soil contaminated by industrial activity. Ecotoxicol Environ Saf 2017a; 136: 119–125.

Kołtowski M, Hilber I, Bucheli TD, Charmas B, Skubiszewska-Zięba J, Oleszczuk P. Activated biochars reduce the exposure of polycyclic aromatic hydrocarbons in industrially contaminated soils. Chem Eng J 2017b; 310, Part 1: 33–40.

Komiyama T, Kobayashi A, Yahagi M. The chemical characteristics of ashes from cattle, swine and poultry manure. J Mater Cycles Waste Manage 2013; 15: 106–110.

Kossyi IA, Kostinsky AY, Matveyev AA, Silakov VP. Kinetic scheme of the non-equilibrium discharge in nitrogen-oxygen mixtures. Plasma Sources Sci Technol 1992; 1: 207–220.

Kwiatkowski M, Broniek E. An analysis of the porous structure of activated carbons obtained from hazelnut shells by various physical and chemical methods of activation. Colloids Surf A Physicochem Eng Asp 2017; 529: 443–453.

Laine NR, Vastola FJ, Walker PL. The importance of active surface area in the carbon-oxygen reaction. J Phys Chem 1963; 67: 2030–2034.

Lam SS, Liew RK, Wong YM, Peter Yek NY, Ma NL, Lee CL, Chase HA. Microwave-assisted pyrolysis with chemical activation, an innovative method to convert orange peel into activated carbon with improved properties as dye adsorbent. J Clean Prod 2017; 162: 1376–1387.

Langlais B, Reckhow DA, Brink DR. Ozone in water treatment: application and engineering. Boca Roton, Florida: CRC Press, 1991.

Laurendeau NM. Heterogeneous kinetics of coal char gasification and combustion. Prog Energy Combust Sci 1978; 4: 221–270.

Lee JW. Advanced biofuels and bioproducts. Springer New York Heidelberg Dordrecht London, London, 2013: 1101.

Lee C, Graves DB, Lieberman MA, Hess DW. Global model of plasma chemistry in a high density oxygen discharge. J. Electrochem. Soc. 1993; 141: 1546–1555.
Lee G, Lee B, Kim J, Cho K. Ozone Adsorption on graphene: ab initio study and experimental validation. J Phys Chem C 2009; 113: 14225–14229.
Lee J, Yang X, Song H, Ok YS, Kwon EE. Effects of carbon dioxide on pyrolysis of peat. Energy 2017; 120: 929–936.
Lehmann J, Joseph S. Biochar for environmental management: science, technology and implementation. New York: Routledge, 2015: 976.
Li Y, Shao J, Wang X, Deng Y, Yang H, Chen H. Characterization of modified biochars derived from bamboo pyrolysis and their utilization for target component (furfural) adsorption. Energy Fuels 2014; 28: 5119–5127.
Li J, Dai J, Liu G, Zhang H, Gao Z, Fu J, He Y, Huang Y. Biochar from microwave pyrolysis of biomass: a review. Biomass Bioenergy 2016; 94: 228–244.
Li H, Dong X, da Silva EB, de Oliveira LM, Chen Y, Ma LQ. Mechanisms of metal sorption by biochars: biochar characteristics and modifications. Chemosphere 2017; 178: 466–478.
Lieberman MA, Lichtenberg AJ. Molecular collisions, principles of plasma discharges and materials processing. Hoboken, New Jersey: John Wiley & Sons, Inc., 2005: 235–283.
Lima IM, Marshall WE. Granular activated carbons from broiler manure: physical, chemical and adsorptive properties. Bioresour Technol 2005; 96: 699–706.
Lin B-J, Chen W-H. Sugarcane bagasse pyrolysis in a carbon dioxide atmosphere with conventional and microwave-assisted heating. Front Energy Res 2015; 3: 1–9.
Liu Q-S, Zheng T, Wang P, Guo L. Preparation and characterization of activated carbon from bamboo by microwave-induced phosphoric acid activation. Ind Crops Prod 2010; 31: 233–238.
Lua AC, Yang T. Effects of vacuum pyrolysis conditions on the characteristics of activated carbons derived from pistachio-nut shells. J Colloid Interface Sci 2004; 276: 364–372.
Lua AC, Yang T, Guo J. Effects of pyrolysis conditions on the properties of activated carbons prepared from pistachio-nut shells. J Anal Appl Pyrolysis 2004; 72: 279–287.
Lussier MG, Zhang Z, Miller DJ. Characterizing rate inhibition in steam/hydrogen gasification via analysis of adsorbed hydrogen. Carbon 1998; 36: 1361–1369.
Lützenkirchen J, Preočanin T, Kovačević D, Tomišić V, Lövgren L, Kallay N. Potentiometric titrations as a tool for surface charge determination. Croat Chem Acta 2012; 85: 391–417.
Mark HB, Mattson JS. Activated carbon: surface chemistry and adsorption from solution. In: Dekker M, editor. New York, 1971.
Marsh H, Reinoso FR. Activated carbon. Netherland: Elsevier, 2006.
Marsh H, Heintz EA, Rodríguez-Reinoso F. Introduction to carbon technologies. Universidad de Alicante, Servicio de Publicaciones, 1997.
Martín-Gullón I, Asensio M, Font R, Marcilla A. Steam-activated carbons from a bituminous coal in a continuous multistage fluidized bed pilot plant. Carbon 1996; 34: 1515–1520.
Mašek O, Budarin V, Gronnow M, Crombie K, Brownsort P, Fitzpatrick E, Hurst P. Microwave and slow pyrolysis biochar – comparison of physical and functional properties. J Anal Appl Pyrolysis 2013; 100: 41–48.
Mayakaduwa SS, Herath I, Ok YS, Mohan D, Vithanage M. Insights into aqueous carbofuran removal by modified and non-modified rice husk biochars. Environ Sci Pollu Res 2016; 24: 22755–22763.
Menéndez JA, Illán-Gómez MJ, y León CAL, Radovic LR. On the difference between the isoelectric point and the point of zero charge of carbons. Carbon 1995; 33: 1655–1657.
Menéndez JA, Domínguez A, Inguanzo M, Pis JJ. Microwave pyrolysis of sewage sludge: analysis of the gas fraction. J Anal Appl Pyrolysis 2004; 71: 657–667.
Menéndez JA, Domínguez A, Fernández Y, Pis JJ. Evidence of self-gasification during the microwave-induced pyrolysis of coffee hulls. Energy Fuels 2007; 21: 373–378.
Mohan D, Pittman CU, Steele PH. Pyrolysis of wood/biomass for bio-oil: a critical review. Energy Fuels 2006; 20: 848–889.
Mondal S, Aikat K, Halder G. Ranitidine hydrochloride sorption onto superheated steam activated biochar derived from mung bean husk in fixed bed column. J Environ Chem Eng 2016; 4: 488–497.
Moussavi G, Khosravi R. Preparation and characterization of a biochar from pistachio hull biomass and its catalytic potential for ozonation of water recalcitrant contaminants. Bioresour Technol 2012; 119: 66–71.
Mul G, Neeft JPA, Kapteijn F, Moulijn JA. The formation of carbon surface oxygen complexes by oxygen and ozone. The effect of transition metal oxides. Carbon 1998; 36: 1269–1276.
Mulabagal V, Baah DA, Egiebor NO, Chen WY. Biochar from biomass: a strategy for carbon dioxide sequestration, soil amendment, power generation, and CO2 utilization. In Handbook of Climate change mitigation and adaptation, 2nd edition, Vol. III. In: Chen WY, Suzuki T, Lackner M, editors. Switzerland: Springer International Publishing, 2017.
Nair V, Vinu R. Peroxide-assisted microwave activation of pyrolysis char for adsorption of dyes from wastewater. Bioresour Technol 2016; 216: 511–519.
Namazi AB, Allen DG, Jia CQ. Benefits of microwave heating method in production of activated carbon. Can J Chem Eng 2016; 94: 1262–1268.
Niu Q, Luo J, Xia Y, Sun S, Chen Q. Surface modification of bio-char by dielectric barrier discharge plasma for Hg0 removal. Fuel Process Technol 2017; 156: 310–316.
Oda H, Takeuchi M, Yokokawa C. Effect of air-oxidation on the pore-structure of coals and cokes or chars obtained from oxidized coals. Fuel 1981; 60: 390–396.
Park S-J, Jin S-Y. Effect of ozone treatment on ammonia removal of activated carbons. J Colloid Inter Sci 2005; 286: 417–419.
Park S-E, Sujandi, Green approaches via nanocatalysis with nanoporous materials: functionalization of mesoporous materials for single site catalysis. Curr Appl Phys 2008; 8: 664–668.
Park J, Hung I, Gan Z, Rojas OJ, Lim KH, Park S. Activated carbon from biochar: influence of its physicochemical properties on the sorption characteristics of phenanthrene. Bioresour Technol 2013; 149: 383–389.
Park SH, Cho HJ, Ryu C, Park Y-K. Removal of copper(II) in aqueous solution using pyrolytic biochars derived from red macroalga Porphyra tenera. J Ind Eng Chem 2016; 36: 314–319.
Park CM, Han J, Chu KH, Al-Hamadani YAJ, Her N, Heo J, Yoon Y. Influence of solution pH, ionic strength, and humic acid on cadmium adsorption onto activated biochar: experiment and modeling. J Ind Eng Chem 2017; 48: 186–193.

Pethrick RA. Chemistry with ultrasound. Critical reports on applied chemistry, vol. 28. Edited by T. J. Mason, published for SCI by Elsevier Science Publishers, London, 1990. pp. vii + 195, price £46.00. ISBN 1-85166-422-X. Polymer International 1991; 24: 62–62.

Py X, Guillot A, Cagnon B. Activated carbon porosity tailoring by cyclic sorption/decomposition of molecular oxygen. Carbon 2003; 41: 1533–1543.

Qambrani NA, Rahman MM, Won S, Shim S, Ra C. Biochar properties and eco-friendly applications for climate change mitigation, waste management, and wastewater treatment: a review. Renew Sust Energ Rev 2017; 79: 255–273.

Qian K, Kumar A, Zhang H, Bellmer D, Huhnke R. Recent advances in utilization of biochar. Renew Sust Energ Rev 2015; 42: 1055–1064.

Qiu M, Sun K, Jin J, Gao B, Yan Y, Han L, Wu F, Xing B. Properties of the plant- and manure-derived biochars and their sorption of dibutyl phthalate and phenanthrene. Sci Rep 2014; 4: 5295.

Radovic LR, Silva IF, Ume JI, Menéndez JA, Leon CALY, Scaroni AW. An experimental and theoretical study of the adsorption of aromatics possessing electron-withdrawing and electron-donating functional groups by chemically modified activated carbons. Carbon 1997; 35: 1339–1348.

Rafiq MK, Bachmann RT, Rafiq MT, Shang Z, Joseph S, Long R. Influence of pyrolysis temperature on physico-chemical properties of corn stover (Zea mays L.) biochar and feasibility for carbon capture and energy balance. PLoS One 2016; 11: e0156894.

Rajapaksha AU, Vithanage M, Zhang M, Ahmad M, Mohan D, Chang SX, Ok YS. Pyrolysis condition affected sulfamethazine sorption by tea waste biochars. Bioresour Technol 2014; 166: 303–308.

Rajapaksha AU, Vithanage M, Ahmad M, Seo D-C, Cho J-S, Lee S-E, Lee SS, Ok YS. Enhanced sulfamethazine removal by steam-activated invasive plant-derived biochar. J Hazard Mater 2015; 290: 43–50.

Rajapaksha AU, Chen SS, Tsang DCW, Zhang M, Vithanage M, Mandal S, Gao B, Bolan NS, Ok YS. Engineered/designer biochar for contaminant removal/immobilization from soil and water: potential and implication of biochar modification. Chemosphere 2016; 148: 276–291.

Redmond JP, Walker PL. Hydrogen sorption on graphite at elevated temperatures. J Phys Chem 1960; 64: 1093–1099.

Rivera-Utrilla J, Sánchez-Polo M. Ozonation of 1,3,6-naphthalenetrisulphonic acid catalysed by activated carbon in aqueous phase. Appl Catal B Environ 2002; 39: 319–329.

Rivera-Utrilla J, Sánchez-Polo M. Ozonation of naphthalenesulphonic acid in the aqueous phase in the presence of basic activated carbons. Langmuir 2004; 20: 9217–9222.

Rivera-Utrilla J, Sánchez-Polo M. Mondaca M, Zaror C. Effect of ozone and ozone/activated carbon treatments on genotoxic activity of naphthalenesulfonic acids. J Chem Technol Biotechnol 2002; 77: 883–890.

Rodríguez-Reinoso F, Molina-Sabio M, González MT. The use of steam and CO2 as activating agents in the preparation of activated carbons. Carbon 1995; 33: 15–23.

Ros A, Lillo-Ródenas MA, Fuente E, Montes-Morán MA, Martín MJ, Linares-Solano A. High surface area materials prepared from sewage sludge-based precursors. Chemosphere 2006; 65: 132–140.

Rosales E, Meijide J, Pazos M, Sanromán MA. Challenges and recent advances in biochar as low-cost biosorbent: from batch assays to continuous-flow systems. Bioresour Technol 2017; 246: 176–192.

Sánchez-Polo M, Rivera-Utrilla J. Effect of the ozone-carbon reaction on the catalytic activity of activated carbon during the degradation of 1,3,6-naphthalenetrisulphonic acid with ozone. Carbon 2003; 41: 303–307.

Sánchez-Polo M, von Gunten U, Rivera-Utrilla J. Efficiency of activated carbon to transform ozone into OH radicals: influence of operational parameters. Water Res 2005; 39: 3189–3198.

Santos RM, Santos AO, Sussuchi EM, Nascimento JS, Lima ÁS, Freitas LS. Pyrolysis of mangaba seed: production and characterization of bio-oil. Bioresour Technol 2015; 196: 43–48.

Saquing JM, Yu Y-H, Chiu PC. Wood-derived black carbon (biochar) as a microbial electron donor and acceptor. Environ Sci Technol Lett 2016; 3: 62–66.

Sattar A, Leeke GA, Hornung A, Wood J. Steam gasification of rapeseed, wood, sewage sludge and miscanthus biochars for the production of a hydrogen-rich syngas. Biomass Bioenergy 2014; 69: 276–286.

Schubert CC, Schubert SJ, Pease RN. The oxidation of lower paraffin hydrocarbons. I. Room temperature reaction of methane, propane, n-butane and isobutane with ozonized oxygen. J Am Chem Soc 1956a; 78: 2044–2048.

Schubert CC, Schubert SJ, Pease RN. The oxidation of lower paraffin hydrocarbons. II. Observations on the role of ozone in the slow combustion of isobutane. J Am Chem Soc 1956b; 78: 5553–5556.

Seinfeld JH, Pandis S. Atmospheric chemistry and physics, from air pollution to climate change, New York: Wiley-Interscience, 1998.

Shim T, Yoo J, Ryu C, Park Y-K, Jung J. Effect of steam activation of biochar produced from a giant Miscanthus on copper sorption and toxicity. Bioresour Technol 2015; 197: 85–90.

Shin S, Jang J, Yoon SH, Mochida I. A study on the effect of heat treatment on functional groups of pitch based activated carbon fiber using FTIR. Carbon 1997; 35: 1739–1743.

Smith M. Evolution of acidic functional groups on biochars by ozone oxidation to improve performance as a soil amendment. Biological and agricultural engineering. Washington State University, 2011.

Smith WR, Polley MH. The oxidation of graphitized carbon black. J Phys Chem 1956; 60: 689–691.

Song Y, Wang Y, Hu X, Xiang J, Hu S, Mourant D, Li T, Wu L, Li C-Z. Effects of volatile-char interactions on in-situ destruction of nascent tar during the pyrolysis and gasification of biomass. Part II. Roles of steam. Fuel 2015; 143: 555–562.

Spokas KA, Cantrell KB, Novak JM, Archer DW, Ippolito JA, Collins HP, Boateng AA, Lima IM, Lamb MC, McAloon AJ, Lentz RD, Nichols KA. Biochar: a synthesis of its agronomic impact beyond carbon sequestration. J Environ Qual 2012; 41: 973–989.

Stankovich S, Dikin DA, Dommett GHB, Kohlhaas KM, Zimney EJ, Stach EA, Piner RD, Nguyen ST, Ruoff RS. Graphene-based composite materials. Nature 2006; 442: 282–286.

Stephens SL, Birks JW, Calvert JG. Ozone as a sink for atmospheric carbon aerosols today and following nuclear war. Aerosol Sci Technol 1989; 10: 326–331.

Suliman W, Harsh JB, Abu-Lail NI, Fortuna A-M, Dallmeyer I, Garcia-Perez M. Modification of biochar surface by air oxidation: role of pyrolysis temperature. Biomass Bioenergy 2016; 85: 1–11.

Suslick KS, Flannigan DJ. Inside a collapsing bubble: sonoluminescence and the conditions during cavitation. Annu Rev Phys Chem 2008; 59: 659–683.

Tam MS, Antal MJ. Preparation of activated carbons from macadamia nut shell and coconut shell by air activation. Ind Eng Chem Res 1999; 38: 4268–4276.

Tan G, Sun W, Xu Y, Wang H, Xu N. Sorption of mercury (II) and atrazine by biochar, modified biochars and biochar based activated carbon in aqueous solution. Bioresour Technol 2016; 211: 727–735.

Tan Z, Lin CSK, Ji X, Rainey TJ. Returning biochar to fields: a review. Appl Soil Ecol 2017; 116: 1–11.

Tian S, Tan Z, Kasiulienė A, Ai P. Transformation mechanism of nutrient elements in the process of biochar preparation for returning biochar to soil. Chinese J Chem Eng 2017; 25: 477–486.

Toles CA, Marshall WE, Wartelle LH, McAloon A. Steam- or carbon dioxide-activated carbons from almond shells: physical, chemical and adsorptive properties and estimated cost of production. Bioresour Technol 2000; 75: 197–203.

Tran HN, Chao H-P, You S-J. Activated carbons from golden shower upon different chemical activation methods: synthesis and characterizations. Adsorpt Sci Technol 2017a: 0263617416684837.

Tran HN, You S-J, Chao H-P. Fast and efficient adsorption of methylene green 5 on activated carbon prepared from new chemical activation method. J Environ Manage 2017b; 188: 322–336.

Tumuluru JS, Wright CT, Hess JR, Kenney KL. A review of biomass densification systems to develop uniform feedstock commodities for bioenergy application. Biofuels Bioprod Bior 2011; 5: 683–707.

Uchimiya M, Lima IM, Klasson KT, Wartelle LH. Contaminant immobilization and nutrient release by biochar soil amendment: roles of natural organic matter. Chemosphere 2010; 80: 935–940.

Valderrama C, Gamisans X, de las Heras X, Farrán A, Cortina JL. Sorption kinetics of polycyclic aromatic hydrocarbons removal using granular activated carbon: intraparticle diffusion coefficients. J Hazard Mater 2008; 157: 386–396.

Valdés H, Zaror CA. Heterogeneous and homogeneous catalytic ozonation of benzothiazole promoted by activated carbon: kinetic approach. Chemosphere 2006; 65: 1131–1136.

Valdés H, Sánchez-Polo M, Rivera-Utrilla J, Zaror CA. Effect of ozone treatment on surface properties of activated carbon. Langmuir 2002; 18: 2111–2116.

Valdes H, Sanchez-Polo M, Zaror CA. Effect of ozonation on the activated carbon surface chemical properties and on 2-mercaptobenzothiazole adsorption. Lat Am Appl Res 2003; 18: 2111–2116.

Valdés H, Farfán VJ, Manoli JA, Zaror CA. Catalytic ozone aqueous decomposition promoted by natural zeolite and volcanic sand. J Hazard Mater 2009; 165: 915–922.

Veksha A, Pandya P, Hill JM. The removal of methyl orange from aqueous solution by biochar and activated carbon under microwave irradiation and in the presence of hydrogen peroxide. J Environ Chem Eng 2015; 3: 1452–1458.

Veksha A, Bhuiyan TI, Hill JM. Activation of Aspen wood with carbon dioxide and phosphoric acid for removal of total organic carbon from oil sands produced water: increasing the yield with bio-oil recycling. Materials 2016; 9: 20.

Von Sonntag C, Von Gunten U. Chemistry of ozone in water and wastewater treatment. London, UK: IWA Publishing, 2012.

Wahi R, Zuhaidi NFQ, Yusof Y, Jamel J, Kanakaraju D, Ngaini Z. Chemically treated microwave-derived biochar: an overview. Biomass and Bioenergy 2017; 107: 411–421.

Walker PL, Rusinko F, Austin LG. Gas reactions of carbon. In: Eley DD, Selwood PW, Weisz PB, editors. Pennsylvania: Academic Press, 1959: 133–221.

Wang X-H, Chen H-P, Ding X-J, Yang H-P, Zhang S-H, Shen Y-Q. Properties of gas and char from microwave pyrolysis of pine sawdust. BioResources 2009; 4: 946–959.

Wang Y, Zhang Y, Pei L, Ying D, Xu X, Zhao L, Jia J, Cao X. Converting Ni-loaded biochars into supercapacitors: implication on the reuse of exhausted carbonaceous sorbents. Sci Rep 2017; 7: 415–423.

Wang T, Liu J, Zhang Y, Zhang H, Chen W-Y, Norris P, Pan W-P. Use of a non-thermal plasma technique to increase the number of chlorine active sites on biochar for improved mercury removal. Chem Eng J 2018; 331: 536–544.

Wartelle LH, Marshall WE. Nutshells as granular activated carbons: physical, chemical and adsorptive properties. J Chem Technol Biotechnol 2001; 76: 451–455.

Weeks JL, Rabani J. The pulse radiolysis of deaerated aqueous carbonate solutions. I. Transient optical spectrum and mechanism. II. pK for OH radicals. J Phys Chem 1966; 70: 2100–2106.

Wu B, Cheng G, Jiao K, Shi W, Wang C, Xu H. Mycoextraction by Clitocybe maxima combined with metal immobilization by biochar and activated carbon in an aged soil. Sci Total Environ 2016; 562: 732–739.

Xin-hui D, Srinivasakannan C, Jin-hui P, Li-bo Z, Zheng-yong Z. Comparison of activated carbon prepared from Jatropha hull by conventional heating and microwave heating. Biomass Bioenergy 2011a; 35: 3920–3926.

Xin-hui D, Srinivasakannan C, Jin-hui P, Li-bo Z, Zheng-yong Z. Preparation of activated carbon from Jatropha hull with microwave heating: optimization using response surface methodology. Fuel Process Technol 2011b; 92: 394–400.

Xu R-k, Zhao A-z, Yuan J-h, Jiang J. pH buffering capacity of acid soils from tropical and subtropical regions of China as influenced by incorporation of crop straw biochars. J Soils Sediments 2012; 12: 494–502.

Yin S, Shen PK, Song S, Jiang SP. Functionalization of carbon nanotubes by an effective intermittent microwave heating-assisted HF/H2O2 treatment for electrocatalyst support of fuel cells. Electrochim Acta 2009; 54: 6954–6958.

Yip K, Xu M, Li C-Z, Jiang SP, Wu H. Biochar as a fuel: 3. Mechanistic Understanding on biochar thermal annealing at mild temperatures and its effect on biochar reactivity. Energy Fuels 2011; 25: 406–414.

You S, Ok YS, Chen SS, Tsang DCW, Kwon EE, Lee J, Wang C-H. A critical review on sustainable biochar system through gasification: energy and environmental applications. Bioresour Technol 2017; 246: 242–253.

Yu X-Y, Ying G-G, Kookana RS. Reduced plant uptake of pesticides with biochar additions to soil. Chemosphere 2009; 76: 665–671.

Yu F, Zhou Y, Gao B, Qiao H, Li Y, Wang E, Pang L, Bao C. Effective removal of ionic liquid using modified biochar and its biological effects. J Taiwan Inst Chem Eng 2016; 67: 318–324.

Yuan J-H, Xu R-K, Zhang H. The forms of alkalis in the biochar produced from crop residues at different temperatures. Bioresour Technol 2011; 102: 3488–3497.

Yun CH, Park YH, Park CR. Effects of pre-carbonization on porosity development of activated carbons from rice straw. Carbon 2001; 39: 559–567.

Zarifyanz YA, Kisekv VF, Lezhnev NN, Nikitina OV. Interaction of graphite fresh surface with different gases and vapor. Carbon 1967; 5: 127–135.

Zaror CA. Enhanced oxidation of toxic effluents using simultaneous ozonation and activated carbon treatment. J Chem Technol Biotechnol 1997; 70: 21–28.

Zhang T, Walawender WP, Fan LT, Fan M, Daugaard D, Brown RC. Preparation of activated carbon from forest and agricultural residues through CO2 activation. Chem Eng J 2004; 105: 53–59.

Zhang H, Voroney RP, Price GW. Effects of temperature and processing conditions on biochar chemical properties and their influence on soil C and N transformations. Soil Biol Biochem 2015; 83: 19–28.

Zhang S, Chen T, Xiong Y, Dong Q. Effects of wet torrefaction on the physicochemical properties and pyrolysis product properties of rice husk. Energy Convers Manag 2017; 141: 403–409.

Zhong Z-Y, Yang Q, Li X-M, Luo K, Liu Y, Zeng G-M. Preparation of peanut hull-based activated carbon by microwave-induced phosphoric acid activation and its application in Remazol Brilliant Blue R adsorption. Ind Crops Prod 2012; 37: 178–185.

Zhou J-Y, Wang Z-W, Zuo R, Zhou Y, Cao X-M, Cheng K. The surface structure and chemical characters of activated carbon fibers modified by plasma. Asia-Pac J Chem Eng 2012; 7: S245–S252.

Zhuang Q, Kyotani T, Tomita A. Desorption behavior of surface oxygen complexes on carbon in an inert gas and in O2-gasification atmosphere. Energy Fuels 1996; 10: 169–172.